Univerzita Karlova v Praze
Matematicko-fyzikální fakulta

DIPLOMOVÁ PRÁCE

DIPLOMA THESIS

Martin Topinka

ZÁBLESKOVÉ ZDROJE GAMA: PŮVOD A KORELACE

GAMMA-RAY BURSTS: ORIGIN AND CORRELATION

Astronomický ústav UK

Vedoucí diplomové práce: RNDr. René Hudec.
Studijní program: fyzika
Studijní směr: astronomie a astrofyzika

Praha 2002

Rád bych touto cestou poděkoval René Hudcovi za cenné připomínky, rady, trpělivost a především za ochotu tuto práci vůbec zadat. Díky patří také celé katedře AÚ MFF UK, zvláště pak Attilovi Meszárosovi. Grazielle Pizzichini a Nicolovi Masettimu děkuji rovněz za cenné připomínky ohledně supernov a za vysvětlení nejasností v BATSE 4B katalogu. Vojtovi Šimonovi patří dík za připomínky týkající se barev dosvitů. Jsem taktéž velice vděčný Jiřímu Polcarovi a jeho excelentním znalostem Perlu, Matesovi za ochotu nabootovat do Woken a oskenovat mi převzaté fotografie a náčrty. Děkuji také OS Redhat Linux a především programům Perl, TeX, Gnuplot, Octave, R, ViM, Links, SSH a Pine za ochotu spolupracovat. Největší dík patří mámě, tátovi a Renatce.

M. T.

Prohlašuji, že jsem svoji diplomovou práci napsal samostatně a výhradně s použitím citovaných pramenů. Souhlasím se zapůjčováním práce.

V Praze dne 19. dubna 2002. Martin Topinka

Gamma-Ray Bursts - Origin and Correlation

Martin Topinka

April 17, 2002

Contents

Chapter 1

Introduction

1.1 Preface

Let me outline the purpose and the content of my work. At the very beginning besides this preface I write a list of used constant, terms, shortcuts and abbreviations.

In the second chapter I will introduce the state of the art of the up to date knowledge about gamma-ray bursts (hereafter GRBs). There is no monography on GRBs yet, and even not an extended and complete review. During the last years there were very few reviews which try to summarize observational and theoretical facts about GRBs. Although they have been often written by famous GRB experts all of them are either incomplete or too general. Authors usually omit the latest discoveries and nearly all unusual but interesting suggestions leaving the several years old state of GRB knowledge conserved. Partial reviews were made e.g. by (Paczyński 1999), a refreshed review from (Fishman 2000), followed by (Piro et al. 2000, Kulkarni 2000, Rees 1997, Piran 1999, Djorgovski 2001). I have done the hard work and I compiled, summarized, corrected, revised all the sources of information and I added my own notes to them. The result is that I have tried to create an almost complete review of the current state of GRB science.

In the third chapter I will discuss the afterglow phenomena. It could be confusing that there is a lot of general overview text and therefore it should be in fact included in the introduction chapter but I believed that the question of afterglows is worth to be described in the whole chapter. I also discuss two famous theoretical afterglow models (fireball and cannonball) and I compare them to my knowledge never done before. I suggest the experimental observation boundaries to distinguish which of these two models gives better predictions.

Also a question of jets which is directly related to the afterglows is discussed inside this chapter. I put stress on observational facts and their comparison with general theoretical predictions. I'll also constrain the rate of orphan afterglows.

In the fourth chapter I will introduce a new discovery of the GRB color diagrams behavior. I will explain some of their features. There I will come with a unique AGNs and QSOs color indices to GRBs correlation and I will discuss the similarity of GRBs to QSOs in the fifth chapter.

The purpose of the sixth chapter is searching for any correlation between supernova explosions and GRBs. I will outline a brief summary of up to date theoretical predictions and beliefs. I will also show the results of my search for a correlation between supernovae and poor-localized GRBs from the BATSE catalogue which covers my CNR Bologna work in November 2001.

In the seventh chapter I will open the question of GRB host galaxies and their properties. I will magnify occurrence of GRBs in star-forming regions. Then I will discuss the dust destruction process along the line of sight to the GRB as an explanation of the time and spectral evolution of GRB afterglows in the eighth chapter.

I cannot forget to notice the greatest potential of GRBs. In the nineth chapter I will mention cosmological effects involving in GRBs and a possibility of the scanning of inter-galactic medium through the GRB light curves and their spectra, a microlensing effect, known methods of deriving the redshift of GRBs, the rate of GRBs and a search for GRB remnants.

1.2 General notes

1.2.1 Abbreviations and shortcuts

In the following text I will use a lot of abbreviations or shortcuts. Here follows a brief list of the most frequent ones in the Table 1.2.1.

1.2.2 Frequently used constants and quantities

Frequently used constants and quantities are listed in the Table 1.2.2.

In this work I adopt the useful and space-saving convention for expressing the physical parameters: Q_x means $Q_x \times 10^x$, using cgs units (e.g. E_{52} means energy in units of 10^{52} ergs).

[1] BeppoSAX is named by Giuseppe Occhialini.

AG	Afterglow
AGN	Active galactic nuclei
BART	Burst Alert Robotic Telescope
BATSE	Burst and Transient Experiment
BeppoSAX	Satellite for Astronomica X[1]
BH	Black hole
CB	Cannonball
CGRO	Compton Gamma-ray Observatory
CMB	Cosmic microwave background
DM	Dark matter
FB	Fireball
GRB	Gamma-ray burst
GRBR	Gamma-ray burst remnant
HETE	High Energy Transient Explorer
HG	Host galaxy (usually of a GRB)
HVC	High velocity cloud
IPN	Inter-planetary network
ISM, IGN	Interstellar/galactic medium
LOS	Line of the sight
NS	Neutron star
OA	Optical afterglow
OT	Optical transient
PBH	Primordial black hole
QSO	Quasi-stellar object
ROSAT	Rontgen-Satellite
RXTE	Rossi X-ray Timing Explorer
RT	Radio afterglow or transient
SN	Supernova (pl. SNe)
SGR	Soft gamma repeater
SNR	Supernova remnant
SFR	Star-forming rate
WD	White dwarf
VLA	Very large array
VLBI	Very long baseline interferometry
XT	X-ray afterglow or transient

Table 1.1: Abbreviations and shortcuts.

Flux	erg s^{-1} cm^{-2}
Fluence	erg cm^{-2}
Gauss	1 G= 10^{-4} T
Energy	1 erg $= 10^{-7}$ W
Jansky	1 Jy= 10^{-26}Wm^{-2}Hz^{-1}
Parsec	1 pc $= 3.0856 \times 10^{16}$ m
Angstrom	1 A $= 1 \times 10^{-10}$ m
Solar mass	$M_{\odot} = 1.989 \times 10^{30}$ kg
Gravitational constant	$G = 6.6726 \pm 0.0009 \times 10^{-11}$ m^3 kg^{-1} s^{-2}
Planck's constant	$h = 2\pi \times 1.054572 \times 10^{-34}$ J s
Boltzmann's constant	$k = 1.3806 \times 10^{-23}$ J K^{-1}
Electron mass	$m_e = 9.109389 \times 10^{-31}$ kg
Proton mass	$m_p = 1.672623 \times 10^{-27}$ kg
Electron charge	$e = -1.602177 \times 10^{-19}$ C
Electron-volt	1 eV $= 1.602177 \times 10^{-19}$J $= 1.602177 \times 10^{-12}$ erg
Permeability of vacuum	$\mu_0 = 4\pi \times 10^{-7}$ N A^{-2}
Permitivity of vacuum	$\epsilon_0 = (c^2\mu_0)^{-1}$ F m^{-1}
dimensionless Hubble parameter	$h = H_0/100$ km s^{-1}Mpc^{-1}
Declaration parameter	$q_0 = 0.5$
Speed of light	$c = 2.99792458 \times 10^{10}$ cm s^{-1}
Thomson cross-section	$\sigma_T = e^4/(6\pi\epsilon_0^2 m_e^2 c^4) = 6.65246 \times 10^{-29}$
Lorentz factor	$\Gamma = (1-\beta^2)^{-1/2}$, where $\beta = v/c$

Table 1.2: Frequently used constants and quantities

Chapter 2

Gamma-ray bursts overview

2.1 Brief history of gamma-ray bursts

Tied 70s' of the last century and the strange times of the Cold war. The Vela satellites (designed to verify 1963 The Limited Nuclear Test Ban Treaty that prohibits nuclear test outside in Earth's atmosphere) discovered a peculiar and very strong γ-ray photon shower first in 1967. Photons caught by CsI scintillation counters didn't come from the Earth nor the Sun but from the Universe. The event discovery and measured data were postponed to astronomers much later in 1973 after 16 more γ-ray burst events (Klebesadel et al. 1973).

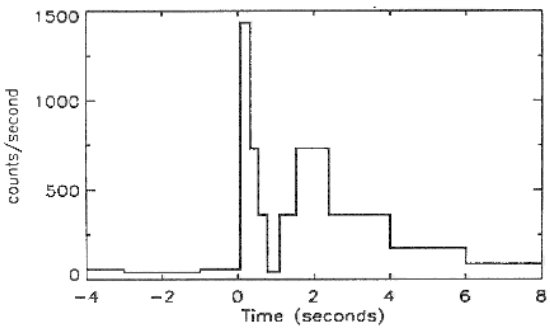

Figure 2.1: The time history of the first observed gamma-ray burst detected 2 July 1967 by Vela 4a satellite in the energy range from 0.3 to 1.5 MeV (Gorosabel 1999)

Since that time there have been thousands of gamma-ray bursts (GRBs) detected and these events became the most energetic and most mysterious phenomenon of high-energy astrophysics. There were suggested more than 150 theories of the GRBs explanation at a conference in 1976 (Fishman & Meegan 1995). Nowadays when studies of GRBs are one of the most active areas of research in astronomy (rate of GRB related publications and articles is about 500 per year) GRBs still remain the great puzzle of science. Where these bursts originate and how they come to have such incredible energies of 10^{53} ergs is a

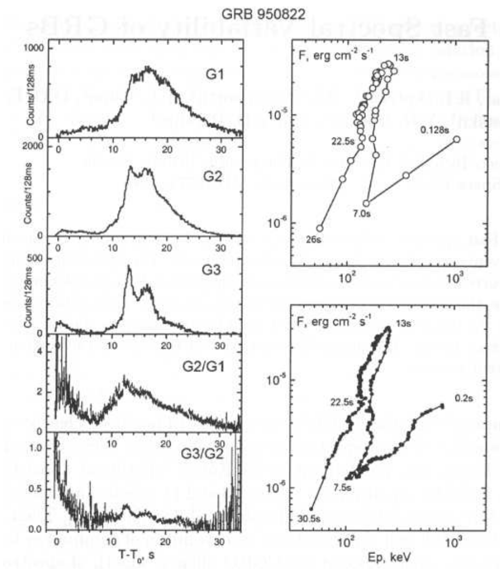

Figure 2.2: The time evolution of spectrum of GRB 950822, time histories and hardness ratio profile (left). Intensity - hardness correlation (right) (MAZETS ET AL. 1997).

mystery that scientists have been attacking for three decades.

GRBs are used to be catalogued in a format GRB yymmdd corresponding to the date of its discovery e.g. famous GRB 970228 was discovered by the Dutch-Italian satellite BeppoSAX on February 28, 1997. If more than one burst is detected in one day they put a letter after it in alphabetical order, e.g. the second burst on May 08 2000 has a name GRB 000508B.

2.2 Spectral properties and light curves of gamma-ray bursts

The spectra of GRBs are broad-band, hard, continuum, and typically a broken power-law suggesting a non-thermal (e.g. synchrotron) origin with a peak near $0.1 - 1$ MeV. Most of the power is emitted above 50 keV. Estimated γ-ray energies span the range $10^{51} - 10^{54}$ ergs $\sim 10^{-3} - 1 M_{\odot} c^2$, comparable to burning up the entire mass-energy of the sun in a few tens of seconds or to emitting over the same period of time as much energy as Milky way does in a hundred years. The lower end is comparable with energy release in supernovae and the death of massive stars. GRB with prompt X-ray emission or with an X-ray afteglow are valuable for much better localization of the event.

An empirical distribution of high energetic part of the typical peak energy spectrum as got from satellites designed for detecting GRBs is given as $N(E) \propto E^{\alpha}$, where $\alpha \sim 1$ at low energies or α greater at the higher frequencies.

GRBs duration ranges from 0.001 to 1000 s. Distribution of T_{90} (the time in which counts from 5% to 95% of the total counts are detected) for 2704 GRBs

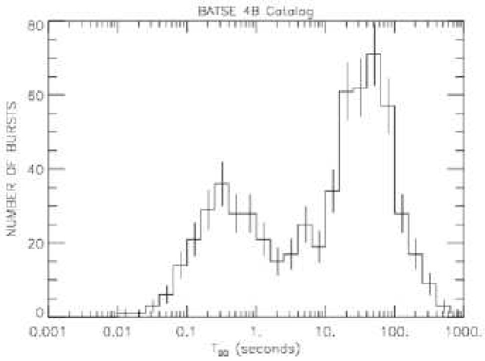

Figure 2.3: The bimodality of the time duration of 2704 BATSE gamma-ray bursts (BATSE WEB SITE)

detected by BATSE shows bimodality: the short events (< 2 s), with peak about 0.2 s and the longer ones (> 2 s), with the peak at about 30 s (KOUVELIOTOU ET AL. 1993). This implies that there are at least two different possibilities of the GRB origin.

There is a suspicion that there is a third class of GRBs of intermediate duration with a small peak about 5 s (HORVÁTH ET AL. 1998, MUKHERJEE ET AL. 1998).

The duration is anti-correlated with the spectral hardness. The short bursts are harder than the long ones (KOUVELIOTOU ET AL. 1993). Statistically faint GRB should originate at a higher distance and should be redshifted (softened) to X-ray and the duration is expected to be prolonged due to cosmological time dilation. Burst class properties must be identified and separated from the cosmological effects, so that the burst physical parameters can be accurately modeled and understood. However, cosmological effects cannot change power law spectral indices e.g. X-ray spectral index α and γ-ray index β.

Systematic differences between α and β and the peak energy E_{peak} (the peak in the νF_ν plot) could be related to intrinsic burst properties. In general the bursts do exhibit a shift of E_{peak} to lower values at fainter peak fluxes and corresponding softening of hard-to-soft ratio of the channel 3 to the channel 2 (HR32) and HR321 of the BATSE satellite[1] which is consistent with a cosmological redshift signature.

The light curve variability on time scales of milliseconds indicates that a characteristic spatial scale of the GRB event is $L = c\delta t \sim 3 \times 10^7$ cm. It could originate from a compact object such as very dense stellar remnants e.g. neutron stars (NSs) or black holes (BHs).

The time histories are very chaotic with single or multiple peaks, smooth or not, and very different each from other. Peaks of some bursts show the fast rise and exponential decay (FRED). This might be useful for the distinction of the GRBs into several classes according to the morphological structure of their time histories as suggested by (FISHMAN & MEEGAN 1995).

[1]The channels 1, 2, 3 and 4 of fluences cover the energy ranges $20 - 50$ keV, $50 - 100$ keV, $100 - 300$ keV, and $E > 300$ keV respectively. The peak flux energy range is 50-300 keV, coinciding with the energy range of the nominal BATSE on-board burst trigger.

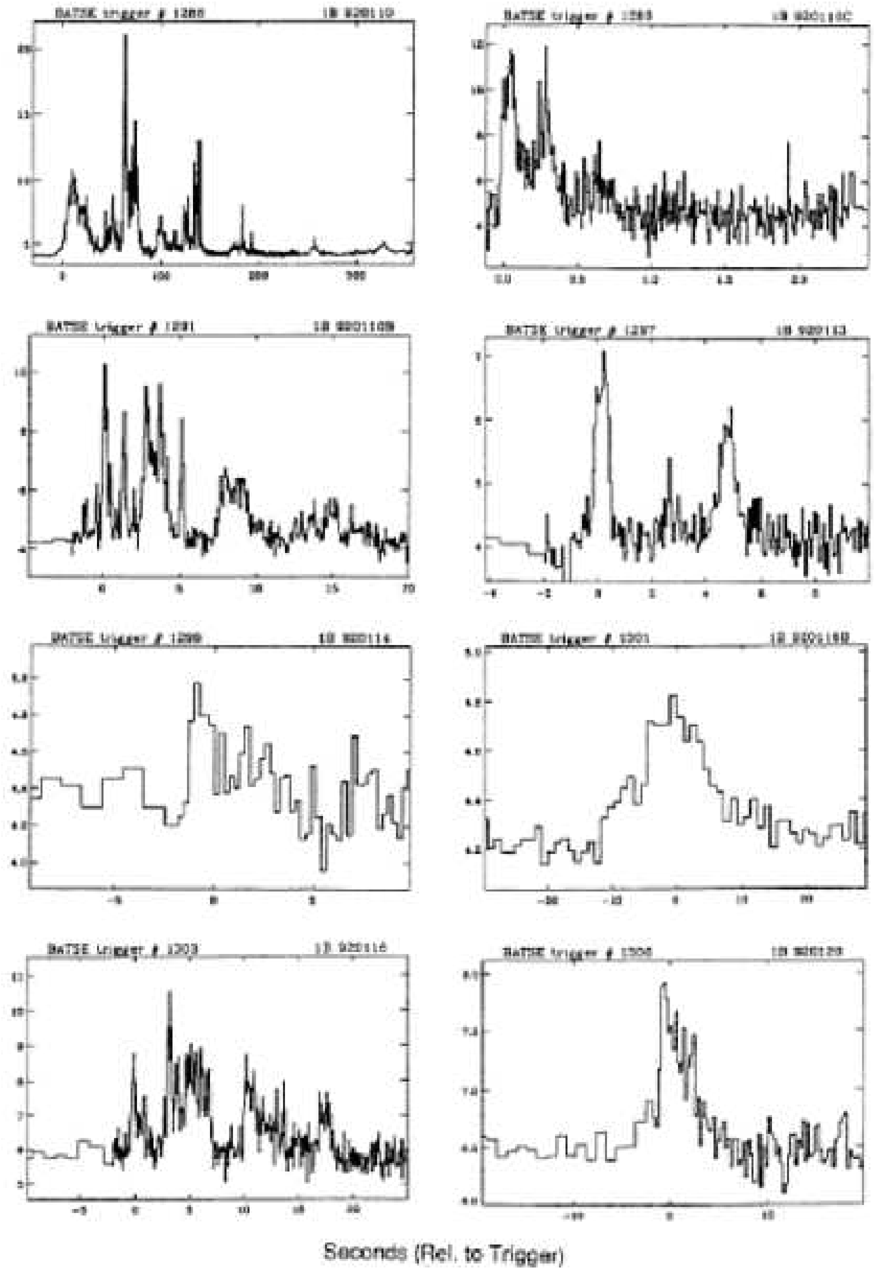

Figure 2.4: The GRB time histories divided by morphological structure: single peaked, multi-peaked, separated emissions, irregular (Fishman & Meegan 1995)

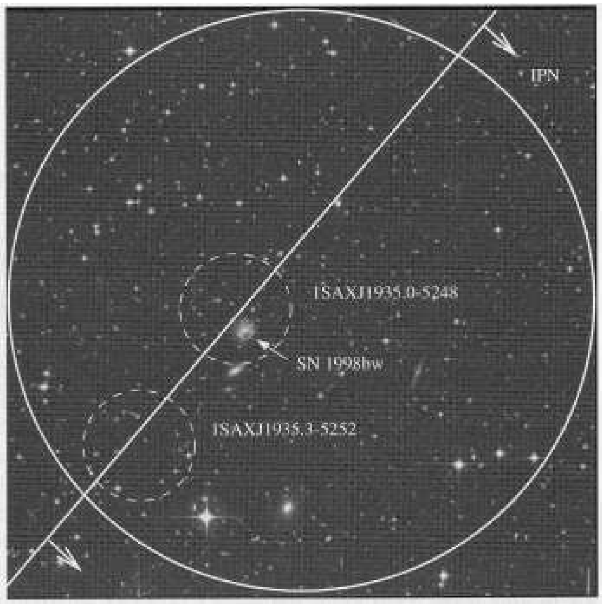

Figure 2.5: A typical error box of GRB 980228 from BATSE (the large one is of 8' radius) corrected by BeppoSAX and IPN (Galama 1999)

The peak flux, fluence, duration, spectral hardness and the number of peaks implies that GRBs are not standard candles.

2.3 GRBs angular distribution on the sky and GRBs distribution in space

2.3.1 Direct measurement of GRBs angular distribution and their rate

The Burst and Transient Source Experiment (BATSE) on-board the Compton Gamma-ray Observatory (CGRO) observed GRBs at a mean effective rate of $\sim 10^3$ per year, this corresponds to $\sim 10^{-6}$ per galaxy. But one may expect many more fainter bursts. Note that the expected rate of neutron star mergers is also $\sim 10^{-6}$ per year per galaxy (Galama 1999).

The precise localization of a GRB is really not an easy task. The majority of the first decade GRB detectors was unable to provide localizeation. A few of the experiments has used a principle of triangulation measuring the time difference between triggering gamma photons believed to belong to one gamma-ray burst shower at different parts of detectors. A typical error box of BATSE instrument is about 5 deg radius. A set of satellites which belongs to the Inter-Planetary Network (IPN) allows better localization of order of 10 arcmin so many GRBs have been confirmed and their positions have been specified more accurately unfortunately at much later times. Thus an identification of GRB with an already known deep sky object was extremely hard.

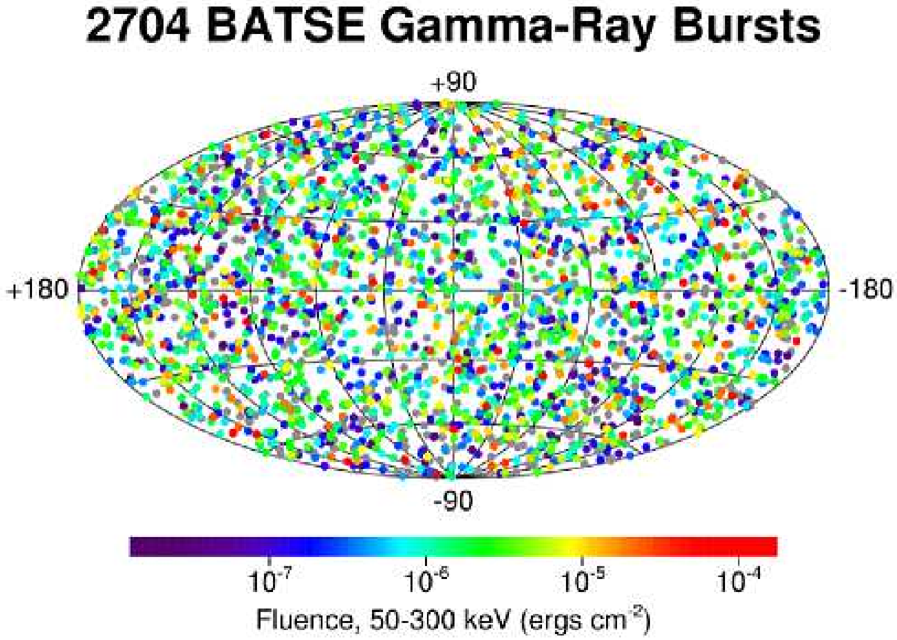

Figure 2.6: All sky view of 2704 BATSE GRBs in galactic coordinates (BATSE WEB SITE)

The angular distribution of GRB sources on the sky corrected for the sensitivity of the detectors and for the proper motions is highly isotropic all over the sky in the meaning of significant level 3σ. This implies that they origin in a halo-like structure close around the observer or cosmological distance of sources. Even after distracting all known corrections there is a space for a little anisotropy in order of magnitude of 10^{-2}. The main reason for this anisotropy is that the distribution of the intermediate duration subclass of the bursts has an intrinsic nonrandomness on the 96.4% confidence level (MÉSZÁROS ET AL. 2000). However GRBs cumulate nor to the galactic plane neither to the close galaxies so most authors believed that the distribution of GRBs is isotropic at all.

The GRBs are not recurrent events with exception of one four times repeated burst. Repeatedly occurring gamma-ray events with a sign of periodicity are believed to be rather so-called soft gamma repeaters (SGR) which probably belong to other distinct class of objects from GRBs.

2.3.2 The $log(N > P) - log(P)$ and the $\langle V/V_{max}\rangle$ indirect tests for isotropy of the gamma-ray burst sample

Two methods for obtaining GRB rates and peak luminosities that are formally equivalent are to use the distribution of V/V_{max} or, alternatively, the cumulative distribution of received fluxes $N(> F)$.

Let suppose that GRBs are standard candles uniformly distributed in homo-

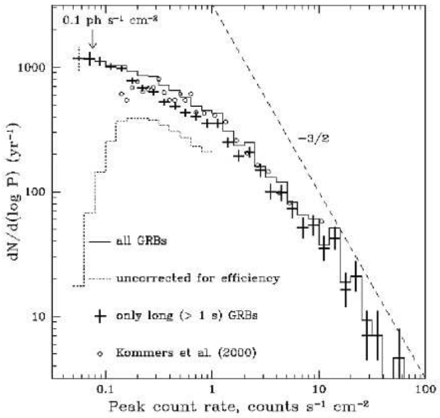

Figure 2.7: The $log(N > P) - log(P)$ diagram with a $-3/2$ slope (NORRIS 1995)

geneous and isotropic Euclidean universe. A burst in a distance d is observed with a peak flux $P \sim d^{-2}$. The more distant burst is statistically fainter than a close one. The cumulative rate of bursts in case of constant burst density is proportional to volume $V \sim d^3$, yielding a $log(N > P) - log(P)$ graph with a slope curve $-3/2$. BATSE bursts peak flux distribution shows a deviation from this slope in faint events. It could be easily explained by cosmological expansion effects (NORRIS 1995) as are redshift and time dilation. This argument was also used in the great debate on a cosmological origin of GRBs. Unfortunately, also alternative explanations for this exist, mostly instrumental ones.

After the discovery of afterglows, host galaxies and having estimated redshifts we are now sure that GRBs originate in cosmological distance up to suggested $z \sim 10$ reaching the earliest phases of galaxy formation.

The other method of estimation the homogenity of the GRB distribution is so-called $\langle V/V_{max}\rangle$ test. This method introduced by (SCHMIDT 1968) was used to study space distribution of a complete sample of radio quasars from the 3CR catalogue. If we expect Euclidean geometry, uniformly distributed sources and limiting flux P_{max} of the survey then two volumes correspond to every object in the sample, the volume enclosed at the distance of object $V(r) = \frac{4}{3}\pi r^3$ and the maximum accessible volume $V_{max} = \frac{4}{3}\pi r^3_{max}$ where r is the radial distance to the object and $r_{max} = (\frac{L}{4\pi P_{max}})^{1/2}$ is the limiting distance at which the flux of an object with luminosity L reduces to the luminosity volume F_{max}. For $r > r_{max}$ the object would no longer be a part of the sample (its flux would be reduced to a level below the flux limit). If object population is distributed uniformly it is equally likely to find an object anywhere in the accessible volume, so V/V_{max} is uniformly distributed in an interval $[0,1]$ with a mean value $\langle V/V_{max}\rangle = 1/2$, $\langle (V/V_{max})^2\rangle = 1/3$ and $\sigma(V/V_{max}) = 1/\sqrt{12}$:

$$\langle V/V_{max}\rangle = \frac{\int_{L_{min}}^{L_{max}} dL\Phi(L) \int_0^{r_{max}(L)} (V/V_{max}) 4\pi r^2 \rho_0 dr}{\int_{L_{min}}^{L_{max}} dL\Phi(L) \int_0^{r_{max}(L)} 4\pi r^2 \rho_0 dr}$$

where ρ_0 is the uniform density. V/V_{max} is insensitive to fluctuations in background or instrumental sensitivity, since the minimum flux and hence V/V_{max} is recorded individually for each object.

In expanding universe we've got luminosity L, redshift z of objects and the limiting flux of the detector P_{min}, we define volumes $V(z)$ and $V(z_{max})$

$$\langle V/V_{max}\rangle = \frac{\int_{L_{min}}^{L_{max}} dL \int_0^{z_{max}} (V/V_{max})\Phi(L,z)dV(z)}{\int_{L_{min}}^{L_{max}} dL \int_0^{z_{max}} \Phi(L,z)dV(z)}$$

If the luminosity function is independent of z then $\langle V/V_{max}\rangle = 1/2$ and if Φ is independent of z then the number of objects per unit comoving volume is the same everywhere in the accessible volume, so V/V_{max} drops to interval $[0,1]$ with the mean value $\langle V/V_{max}\rangle = 1/2$.

In this case of GRB from BATSE sample we use $\langle V/V_{max}\rangle \equiv (C_{max}/C_{min})^{-3/2}$, where C_{max} is the count rate at the maximum amplitude of the bursts and C_{min} is a detector threshold (minimum detectable count rate for the same burst). The $\langle V/V_{max}\rangle$ value of 0.334 ± 0.008 was obtained (Schmidt 2001).

In order to estimate the GRB rate in a given galaxy (e.g. Milky Way) we avoid the practice of dividing the derived cosmic rate by the total number of galaxies per unit volume derived from luminosity function. This division gives the rate per galaxy of mean luminosity not per L^*_{gal} galaxy as usually quoted. The mean galaxy luminosity can be much smaller than L^*_{gal} depending on the slope and the cutoff of the low-luminosity portion of the adopted luminosity function.

The early estimates of GRB rates and mean peak luminosities or energies assumed that all GRBs had the same luminosity – standard candle. The growing catalogue of GRBs with known redshift shows that L_{peak} spans $3-4$ orders of magnitude even omitting sub-energetic SN1998bw/GRB980425 and thus the standard candle model is hence questionable.

2.4 Fuzzy logic

I think that when comparing GRB properties it would be more suitable to use the complex multi-dimensional space than comparing only two properties alone in one test. I recommend using a fuzzy methods and AI[2] computing methods based on fuzzy logic which allows to see the whole burst as a set of many properties simultaneously. The fuzzy logic assumes that an object has all the properties each weightiness by a given probability function. This approach might find new valuable relations in the future. A theory of neural sites is recommended. Unfortunately nobody has worked it out. It is a challenge for an eventual Ph.D. thesis.

2.5 Detectors, satellites and telescopes

As you will see in the next section GRBs are usually followed by an afterglow – a manifestation of this event in other spectral bands, from radio to X-ray. That's why other than gamma satellites and telescopes are also very valuable.

[2] Artificial intelligence (AI)

2.5.1 X-ray and gamma-ray satellites

Since the times of Vela 5 and Vela 6 a plenty of gamma-ray satellites or systems of satellites which monitor parts of celestial sphere has entered the scene.

- BATSE on the board on CGRO launched in 1991 has already finished its mission April 2001 with more than 2704 bursts detected and localized. The only complete data set available nowadays is the 4B GRB catalogue also available on the www (BATSE WEB SITE). There exists the current GRB catalogue too but it's ever changing.

- RXTE (Rossi X-ray Transient Explorer) a satellite that observes black holes, neutron stars, X-ray pulsars and bursts of X-rays (RXTE WEB SITE)

- Dutch-Italian BeppoSAX detects only the GRBs with $T_{90} > 2$ s due to the instrumental effect. The sample of detected afterglows corresponding to the BeppoSAX triggers is hence not a fully representative. Sensitivity of BeppoSAX is in the range of $0.1 - 300$ keV (BEPPOSAX WEB SITE).

- IPN (Interplanetary Network) is very useful for refining GRB positions but because of large distance of involved satellites from the Earth the respond time is usually too long for afterglow hunting. However, many burst triggers detected by BATSE have been corrected later by IPN IPN WEB SITE.

- HETE, HETE-2 the current GRB monitoring satellite. Most of the last detected GRBs have been detected by HETE. The rate of well localized GRBs is about 16 GRBs per year (HETE WEB SITE).

- Newton XMM an ESA X-ray satellite (XMM WEB SITE).

- Chandra, also an X-ray satellite (USA) that could detect "softer brothers" of gamma-ray bursts producing main energy peak in X-rays. It can detect X-ray afterglows of regular GRBs as well (CHANDRA WEB SITE).

2.5.2 Ground-based observation of gamma-ray burst afterglows

Since 1997 there exists a fast respond message system. When a burst is detected by any satellite a note is immediately send to all subscribers and to all ground-based telescopes ready to observe the suspicious sky destination for hunting a possible optical counterpart of the burst. Brief summary of results and reports are shared via Internet in so-called GCN Circular. Besides the large ground optical telescopes there are smaller but much more flexible telescopes reacting to the GRB alert note. They are e.g. ROTSE, LOTIS, TAROT, BOOTES 1 and 2 and BART in Ondřejov[3].

[3]The author is an active member of the BART team

Figure 2.8: The Ondřejov BART (Burst Alert Robotic Telescope) (BART WEB SITE)

2.5.3 Close future outview

- INTEGRAL - This satellite will investigate the high energy universe using gamma-ray, X-ray and optical monitors and a gamma-ray spectrometer. Among black holes, active galactic nuclei it will study GRBs too. There are scientists and developers from more than 13 countries in the ESA INTEGRAL team including Czech republic. INTEGRAL mission is about to start on October 2002 (INTEGRAL WEB SITE).

- Swift is about to start in 2003, expecting nearly 300 well localized GRBs per year. Gamma-ray, X-ray and optical detector on the board enable to start observing within a minute since the burst trigger at the quality of localization of arc-seconds (SWIFT WEB SITE).

- XEUS - an X-ray telescope. The start is planned in 2012 (XEUS WEB SITE).

- Lobster eye all-sky X-ray telescope enables monitoring of high energy photons with high sensitivity, nowadays in development (LOBSTER EYE WEB SITE).

2.6 Progenitors

What could cause such a tremendous energy output as indicated by recent GRBs? How to get energy reservoir strong enough? After a continuous stream of more than 100 theoretical models two mainstream theories (with little modification of course) have been established.

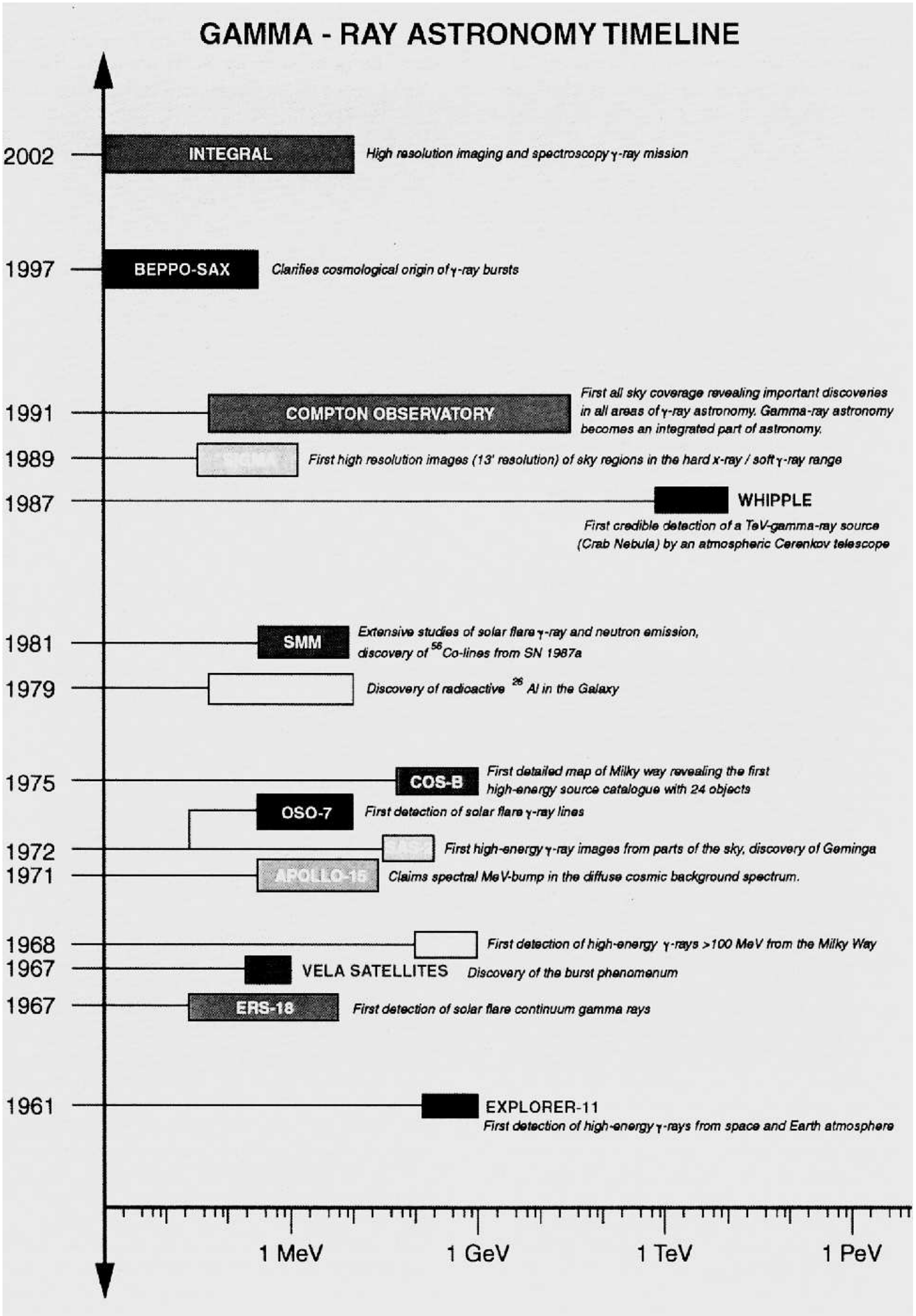

Figure 2.9: Gamma-ray astronomy timeline (ESA 2000)

- A collapse of a very massive star with $\geq 30 M_{\odot}$, also called a collapsar, a supranova, a failed supernova or hypernova. The terminology differs (Paczyński 1998, Woosley & MacFayden 1999).

- Mergers of compact stellar remnants (NS-BH, NS binaries, WD-NS) (Meszaros 1998). As we can get from estimation $\frac{GM_{\odot}^2}{R_{NS}} \sim 10^{53}$ erg where R_{NS} is a typical NS radius. While total rest mass of solar mass star $M_{\odot}c^2 \sim 10^{54}$ implies very high efficiency of transformation of energy.

  The gravitational energy would be primarily released via the production of neutrino-anti-neutrino pairs, a small proportion of which would interact to produce electron-positron pairs, which would in turn annihilate generating a gamma-ray fireball.

- Modification of both where a strong magnetic field is added which could be easily amplified to $\sim 10^{15}$ G. For a distinct class of Soft Gamma-ray Repeaters the model based on highly magnetized neutron star of up to $\sim 10^{15}$ G has been established. These object are called magnetars (Kouveliotou et al. 1998).

- (Vietri & Stella 1998, 1999) conclude the third way: not only NS or supernova but both. The iron detected millions of kilometers from the source suggests that gamma-ray bursts result from star that explode in two phases. Very massive, rapidly rotating spinning star explodes as a supernova, leaving behind a rapidly spinning neutron star. Due to energy loss (for instance, due to magnetic dipole radiation, or gravitational waves) the neutron star collapses into a black hole, creating a gamma-ray burst that lights up the older supernova shell. The supernova explodes twice. This scenario solves the baryon pollution problem. A GRB environment is swept up by the first explosion and the latter explosion is not polluted by baryons. That is in agreement with observable GRBs spectra in which we don't see any absorption lines.

- Completely strange and more bizarre variants of dark matter (90% of all gravitationally attracting matter in the Universe is hidden in the non-luminous (or too faint) state - "dark"), anti-matter matter annihilation, PBH interaction or Hawking's BH evaporation etc. The mass loss rate of a BH is $\frac{d\dot{M}}{dt} \propto \frac{1}{M^2}$ (Hawking 1976). But BH vaporation scenario is unlikely because a black hole has only few quantities as its mass, (angular spin moment and charge are neglible in a small mini-BH in the last phase of evaporation) and GRBs shows wide range of properties.

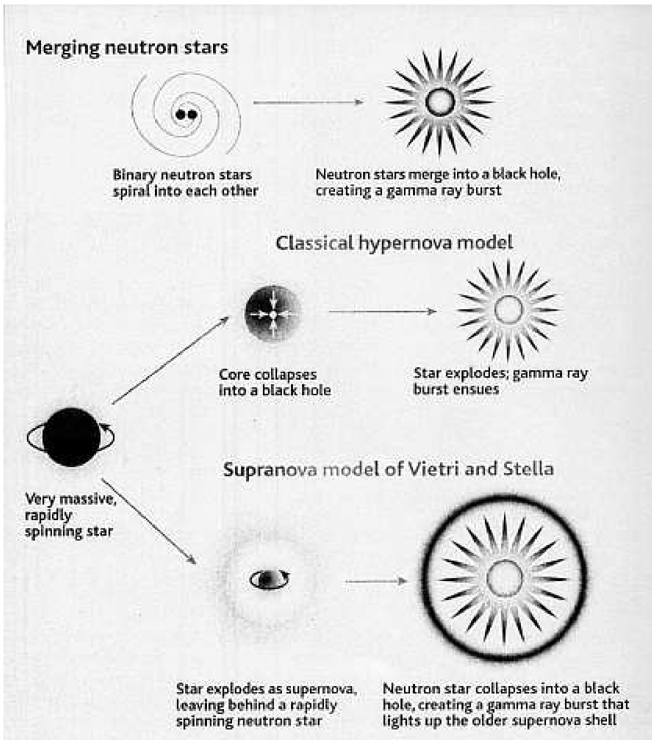

Figure 2.10: Three possible most pushed scenarios of the origin of GRBs (Science web site 2000)

Chapter 3

Gamma-ray burst afterglow theory

3.1 Introduction

Our understanding of GRBs has been revolutionary improved by the BeppoSAX discovery of GRB afterglows. While GRBs last seconds or minutes the afterglow lasts days, weeks or even months. The most famous 80 seconds long GRB 970228 was followed with X-ray afterglow (Costa et al. 1997). The first transient optical counterpart [1] was found (van Paradijs et al. 1997) in a faint galaxy with $\sim 0.8''$ diameter.

Considering that the gamma-ray and the observed X-ray, UV, optical, IR and radio afterglow emission is only the different manifestation of one violent astrophysical event, a self-consistent model is needed. In the afterglow model the emission depends on

- the initial energy of the GRB (or its energy per solid angle).
- the collimation of the GRB outflow and (or) on the viewing angle.
- the density of the external, decelerating medium.
- the microphysical parameters pertaining to the shock acceleration of electrons and the generation of magnetic fields.
- the used model!

[1] There is no clear division when using these terms. Here I call an afterglow a delayed slowly decaying optical emission which starts from minutes to days after the trigger and lasts more than several days up to several weeks. Under optical transient is meant a prompt shorter optical emission which counterparts the gamma-ray burst and decreases more rapidly. These two events might have a different physical purpose and an origin. Notice that many authors are used to call the optical transient (OT) in the meaning of the optical afterglow (OA) or simply the afterglow (AG). It could be confusing.

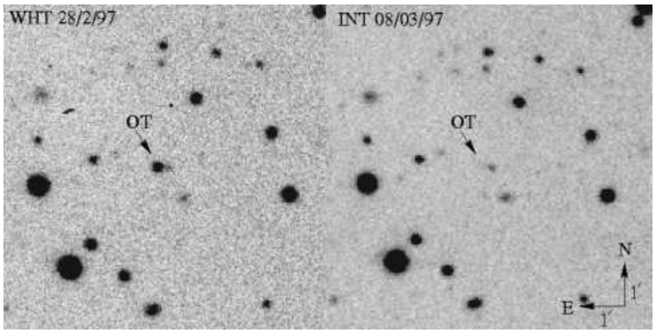

Figure 3.1: The optical transient (afterglow) of GRB 970228 (Bloom 1998).

3.2 Baryon overloading and compactness problem

Assuming that high energetic GRB photons as observed from a GRB spectra are released in a small volume of linear dimension $R \sim c\delta t$ where $\delta t \sim 10^{-3}$ s is a time variability of the spectra that gives $R \sim 300$ km. If so a high energy photon E_1 may (and will) interact with lower energy E_2 photon and thermalize via creating electron positron pair $\gamma\gamma \rightarrow e^{\pm}$, when fulfill the condition

$$E_1 E_2 (1 - \cos\theta_{12}) \geq (2m_e c^2)^2$$

where $\theta_{1,2}$ is the angle between the directions of these two photons. Typical energy of the burst is $\sim 10^{52}$ ergs. Under these conditions the optical depth $\tau_{\gamma\gamma} \sim 10^{15} \gg 1$. However the observed spectrum is obviously non-thermal.

The solution is in assuming a relativistic motion of the ejecta. Photons with an observed frequency ν_{obs} are blue-shifted and their energy in an ejecta rest frame is lower by Lorentz factor of the outflow $\sim \frac{h\nu}{\Gamma}$. Also the radius where the radiation is emitted is larger by factor Γ^2 and relativistic motion beams the radiation on the average within an angle equal to Γ^{-1}. All these effects reduce significantly the optical depth when $\Gamma \geq 100$. The baryonic load remains small only until the outflow remains relativistic.

The radius of transparency of the ejecta is (Soderberg & Ramirez-Ruiz 2002)

$$R_\tau = \left(\frac{\sigma_T E_{iso}}{4\pi m_p c^3 \Gamma_0}\right)^{1/2} \sim 10^{12} - 10^{13}\mathrm{cm}$$

where E_{iso} is the isotropic equivalent energy and σ_T is the Thompson cross-section.

However an explosion e.g. of a SN is contaminated by baryons and therefore a conversion of radiation energy to kinetic takes place.

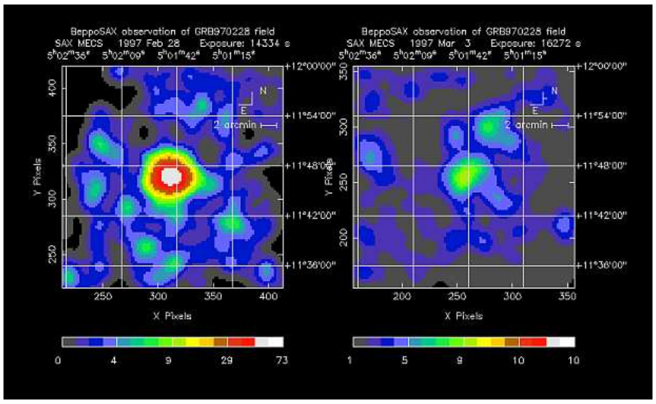

Figure 3.2: The X-ray counterpart (afterglow) of GRB 970228 (BeppoSAX web site).

3.3 Radiative processes

3.3.1 Synchrotron emission

The motion of a charged particle in a magnetic field $\vec{B}$ is described in the classical electrodynamics by the Lorentz equation

$$\frac{d}{dt}(\gamma m\vec{v}) = \frac{e}{c}(\vec{v} \times \vec{B})$$

where Lorentz factor $\gamma = (1-\beta^2)^{-1/2}$ and $\beta = v/c$ are defined as usually. Since there is no force in the magnetic field direction and the magnitude of $||v||$ is constant the particle moves in a helix with the gyration frequency

$$\nu_g = \frac{eB}{2\pi\gamma mc}$$

The power is emitted in a narrow cone of opening angle $\theta \sim \gamma^{-1}$. The total emitted power averaging over the angles between the current velocity and the magnetic field is

$$F = \frac{4}{3}\sigma_T c\beta^2\gamma^2\frac{B^2}{8\pi}$$

and the Doppler factor $\delta = \Gamma(1-\beta\cos\theta)$

The frequency spectrum of this radiation consists of series of spikes at ν_g Doppler affected due to the motion of the charged relativistic particle around the magnetic field. The pulse width acts as γ^{-3} thus for a large γ and an ensemble of particles the spectrum appears to be continuous with a maximum at the so-called critical frequency

$$\nu_c = \frac{3eB\sin\alpha}{4\pi mc}\left(\frac{E}{mc^2}\right)^2 = 16.1 \times \left(\frac{B_\perp}{1\mu G}\right)\left(\frac{E}{1GeV}\right)^2 \text{MHz}$$

The observed energy distribution is $\frac{dN}{dE} \propto E^{-p}$ or, in terms of flux, $\nu F_\nu \propto \nu^{-p}$ (Kembhavi & Narlikar 1999).

3.3.2 Synchrotron self absorption

In the presence of a magnetic field an electron can absorb a photon and make a transition to a higher energy state. Photons in a particular quantum mechanical state can stimulate further emission of photons into the same state. Both these processes are proportional to frequency and luminosity:

$$F(\nu) \propto \nu^{-\alpha}, \nu > \nu_a$$
$$F(\nu) \propto \nu^{5/2}, \nu < \nu_a$$

where ν_a is the frequency at which the optical depth $\tau_\nu \sim 1$, below that a given source would be optically thick (Kembhavi & Narlikar 1999).

3.3.3 Fermi's acceleration mechanism

Even ultra high-energy cosmic rays (UHECRs) of $E \geq 10^{18.5}$ eV might be accelerated in the relativistic fireball jet (Vietri 1995). In Fermi's mechanism particles are deflected elastically (due to scattering on magnetic field) in the local fluid frame on either side of the shock, so that upon recrossing upstream after an excursion downstream after multi scatters they will have a net average energy gain. For ultra relativistic particles of Lorentz factor $\gamma \gg \Gamma_{sh} \gg 1$ the ratio of gained Fermi's energy to initial energy is

$$\frac{E_f}{E_i} = \Gamma_{rel}^2(1 - \beta_{rel}\cos\theta_i)(1 + \beta_{rel}\cos\theta'_f)$$

where $\Gamma_{rel} \approx \Gamma_{sh}/\sqrt{2}$ is the relative Lorentz factor of the upstream and downstream medium, $\theta_{i,f}$ is the angle between particle velocity at shock crossing and the shock normal vector and primed and unprimed quantities are respectively measured in downstream and upstream frames.

Because of kinematics $(1 - \beta_{rel}\cos\theta_i) > 0$ and the initial shock crossing angle θ_i is isotropically distributed so $\frac{E_f}{E_i} \sim \Gamma_{rel}^2$ (Longair 1992).

3.4 GRB afterglow models

Nowadays there are two basic (and controversial) models of the needed transformation between the kinetic energy of exploding baryons back into the observed radiation. A fireball model gives one possible explanation of it. There is also a cannonball model that doesn't assume light explosion (called fireball) and doesn't have to solve problem of baryonic overloading. Both models try to explain observation data, including light curves of the afterglows in different spectral bands.

3.4.1 Fireball

Introduction

In a fireball model the afterglow is the result of a blast wave propagating into the surrounding matter (ISM). The γ-emission arises either after the fireball becomes optically thin, in shocks occurring when the ejecta run into an external medium (where it develops a blast wave moving into ISM and a reverse wave

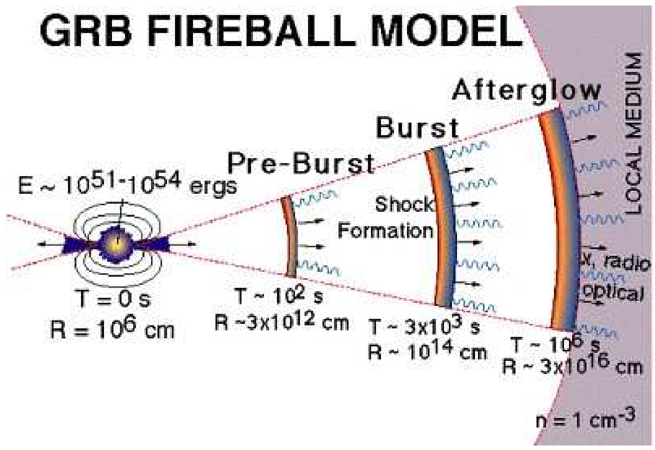

Figure 3.3: Internal and external shock in fireball model (GALAMA 1999)

moving into the ejecta) or because internal shocks occurring in a relativistic wind.

Thus it is useful to distinguish between four areas: the cold unshocked shell (denoted with index 1), shocked shell (2), shocked ISM (3) and cold unshocked ISM (4). The detailed relativistic computation of propagating blast-wave was made and it is called BM by (BLANDFORD & MCKEE 1976), I will use slightly rewritten and modified version from (SARI, PIRAN & NARAYAN 1996, MESZAROS & REES 1997).

Relativistic blast wave formalism

A cold shell is formed and expands with approximately uniform Lorentz factor $\Gamma = \eta$. The interaction between the outward moving shell and the ISM take place in the form of two shocks. A forward shock that propagates into the ISM and a reverse shock that propagates back into the relativistic shell.

For a strong shock we have

$$n_2^{'} = 4\Gamma n_1$$

$$\gamma_1 = \sqrt{2}\Gamma$$

where prime denotes comoving frame, $n_{1,2}$ is particle density, $\gamma_{1,2} = \sqrt{1/(1-\beta_{1,2}^2)}$ Lorentz factors and $\gamma_2 = \Gamma$. The contact discontinuity (the boundary between the shocked shell and the shocked ISM) moves with a Lorentz factor Γ and the forward shock with $\sqrt{2}\Gamma$. The width of the shocked ISM shell is

$$\Delta r = \Delta\beta ct = (1/4\Gamma^2)ct = (1/4\Gamma^2)r$$

where $r = ct$ is the shell radius. In a comoving frame an observer sees ISM approaching with Lorentz factor Γ. The dominant kinetic energy is in the nucleons, $\Gamma m_p c^2$. Let assume that all this energy is thermalized in a strong shock and hence the comoving energy density

$$e_2' = n_2' E_{therm}' = 4n_1\Gamma^2 m_p c^2$$

where E_{therm}' is the thermal energy per particle. The total energy contained in the shell

$$E_{tot}' = 4\pi r^2 \Delta r' e_2'$$

We observe this energy blue-shifted, hence

$$E_{tot} = 4\pi r^3 \Gamma^2 n_1 m_p c^2 = 3M_{swept}\Gamma^2 c^2$$

where M_{swept} is the swept-up ISM mass. We can obtain an estimate of the deceleration radius r_{dec}, the point where the energy in the hot, swept-up interstellar material equals that in the original explosion, by assuming that at this early stage decelerating does not yet strongly influences the evolution of the blast wave and so $\Gamma = \eta =$ constant. Here $\eta = E/M_0c^2$ is the ratio of initial energy in the explosion to the rest mass energy of the baryons (mass M_0) entrained in it. We derive

$$r_{dec} = (E/(4\pi\eta^2 n m_p c^2)^{1/3} = 1.81 \times 10^{16}(E_{52}/n)^{1/3}\eta_{300}^{-2/3} cm$$

The point of deceleration corresponds to $M_{swept} = (1/3\eta)M_0$

We can relate the last equation to the time in the observer's frame by

$$\delta t_{obs} = \frac{\delta r}{2\Gamma^2 c}$$

and using $\Gamma = \eta =$ constant we find for the deceleration time scale

$$t_{dec} = r_{dec}/2\eta^2 c = 3.35(E_{52}/n)^{1/3}\eta_{300}^{-8/3} s$$

The time scale of interaction of the blast wave with the ISM is of the order of seconds and it occurs at a rather large radius of 10^{16} cm, i.e., if GRBs are produced by the interaction of the blast wave with the ISM, the radiation can be non-thermal.

For the case of an adiabatically expanding blast wave we have $E_{tot} \sim$ constant and so the blast wave resolves as $\Gamma \propto r^{-3/2}$. Using the equations above we find

$$r = r_{dec}(t_{obs}/t_{dec})^{1/4}$$
$$\Gamma = \eta(t_{obs}/t_{dec})^{-3/8}$$

Low energy emission at late times - the afterglow

Fireball shock model in which relativistic electrons radiate via synchrotron mechanism, predicted that detectable optical and radio emission can be seen over a period of days to weeks after GRB event. This late-time softer radiation is called afterglow.

The observational characteristics of GRB afterglows can be derived from classical synchrotron spectrum and taking into account synchrotron cooling at high frequencies and synchrotron self absorption at low frequencies. The electrons are assumed to be accelerated in a strong shock, to a power-law distribution of electron Lorentz factors, $N(\gamma_e) \sim \gamma_e^{-p}$, with some minimum Lorentz factor γ_m. In the following we assume slow cooling (the bulk of electrons do not radiate a significant fraction of their own energy and the evolution is adiabatic); these conditions appear applicable to some observed GRB afterglows at late times. Then, the synchrotron spectrum of such a distribution of electrons is a power law with $F_\nu \sim \nu^{1/3}$ up to a maximum F_m, at the peak frequency ν_m (corresponding to the minimum Lorentz factor γ_m).

Above ν_m it is a power law, $F_\nu \propto \nu^{-(p-1)/2}$ up to the cooling frequency, ν_c. Electrons with energies $\gamma_e m_e c^2 > \gamma_c m_e c^2$, where γ_c is the electron Lorentz factor associated with the cooling frequency, radiate a significant fraction of their energy and thereby deplete the high-energy part of the electron distribution and correspondingly, the synchrotron spectrum above ν_c. Cooling causes a spectral transition; above ν_c we have $F_\nu \propto \nu^{-p/2}$. Synchrotron self absorption causes a steep cutoff of the spectrum at low frequencies, $\nu < \nu_a$, so $F_\nu \propto \nu^2$ for $\nu_a < \nu_m$, where ν_a is the synchrotron self absorption frequency.

Thus, the spectrum consists of four distinct power-laws, separated by three break frequencies:

- the self absorption frequency ν_a
- the peak frequency ν_m
- the cooling frequency ν_c

For the synchrotron peak frequency in the comoving frame we have

$$\nu' \propto B_2' \gamma_m'^2$$

where B_2' is the magnetic field strength in the shocked ISM shell. We assume that a constant fraction E_e of the shock energy goes to the electrons. Then

$$\gamma_m = \frac{2}{1+X}\frac{m_p}{m_e}\frac{p-2}{p-1}E_e\Gamma = \kappa_1\Gamma$$

where X is the usual hydrogen mass fraction (often taken as $X = 1$), m_e is the mass of the electron. We also assume that the magnetic energy density $B_2'^2/8\pi$ is the constant fraction E_B, of the shock nucleon energy density e_2', it means

$$B_2' = \sqrt{32\pi n_0 m_p}\Gamma c = \kappa_2\Gamma$$

Thus

$$\nu_m = \Gamma\nu_m' \propto \Gamma^4 \propto t_{obs}^{-3/2}$$

The complete set of remaining scaling is shown in the section dedicated to beaming both for the jetted and the spherical case.

External vs internal shocks

If burst duration is determined by the timescale for the outflow ejection and by processes that convert kinetic energy of the ejecta into gamma-rays. If the outflow energy is dissipated through the interaction with circumburst medium, GRBs of long duration can be obtained even if the initial ejection is impulsive. The GRBs itself are internal not external shocks, and hence the GRB duration is a direct measure of the time the "central engine" is active.

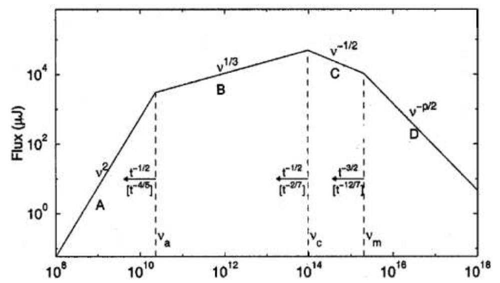

Figure 3.4: The synchrotron spectrum of a relativistic shock with a power-law electron distribution for the case of slow cooling. The spectrum consists of four segments, break frequencies decrease with time as indicated (Sari, Piran & Narayan 1998)

If GRBs originate in binary NS or in BH-NS, such GRBs are expected to last less than 1 s. Thus these progenitors are likely to produce short GRBs.

The relativistic single shell expands outwards by single energy release during the collapse/merging. The shell becomes gamma-ray active due to the interactions with external interstellar matter.

The shell coasts in a gamma-ray quite multiple shells (wind).

The cosmological origin of GRBs established as a result of optical and X-ray follow-up observations of fading GRB counterparts requires an extraordinarily large amount of energy to flood the entire photon-photon attenuation of high energy of photons implies substantial bulk relativistic motion of Lorentz factor $\Gamma_{sh} = (1-\beta^2)^{-1/2} \sim 10^{2-3}$.

3.4.2 Beaming alias jets

Introduction

However the original fireball model as supposed by (Mézsáros & Rees 1993, Paczyński 1998, Sari & Piran 1999) doesn't fit all the observation data well. Moreover, there is a direct evidence that many of astrophysical explosions could be aspherical when their energy of explosion is collimated into a small angled jet.

By a jet I mean a tightly collimated stream of fluid, gas or plasma. It typically carries kinetic and internal energy and linear momentum, and if it is set spinning about its direction of motion by some mean, it can carry angular momentum as well.

Various examples of relativistic astrophysical jets in the Universe of different origin are e.g.:

- Radio galaxies ($\Gamma \leq 20$) and quasars with luminosity $\geq 10^{46}$ erg s^{-1}. The plasma in these jets contains high energy photons, trapped in magnetic field, that emit primarily radio synchrotron radiation. It is believed that in a center of each active galactic nuclei there is a massive or supermassive black hole ($\sim 10^6 - 10^{10} M_\odot$) where an accretion on it powers the jets.

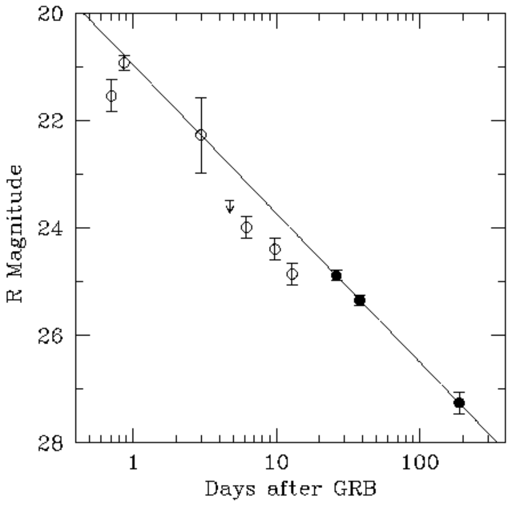

Figure 3.5: Single power law fit of R-band light curve of GRB 970228 (Greiner web site)

- Microquasars, the X-ray binaries where a BH ($\sim 10 M_\odot$) or NS ($\sim 1.4 M_\odot$) works as a central engine. In the case of BH $\Gamma \geq 2.5$. Because the timescale of accretion of these objects is proposed to be related to their mass and the physics seems to be similar for QSO and microquasars we can study their evolution and make implications to AGN (and perhaps even GRB) astrophysics (Mirabel 2000, Blandford & Znajek 1977).

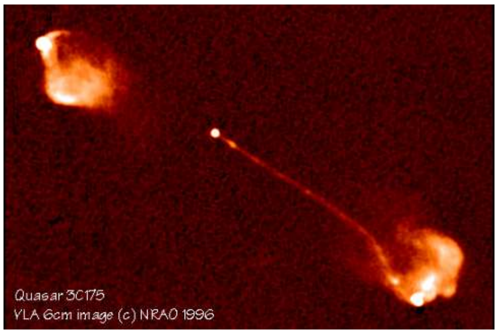

Figure 3.6: The evidence for jets in quasar 3C175. Two lobes point where the outflowing material decelerates in the collision with surrounding ISM (HST web site)

- Supernovae. HST image of SN 1987a shows two hot spots opposite to each other that could be interpreted as a deceleration of outflow from ISM or pre-explosion wind. Another direct evidence is a polarization of the light observed from supernova explosion. Also the latest research at a supernova field and their modeling shows that a supernova explosion could be strongly aspherical (GRANOT & PIRAN 2000)

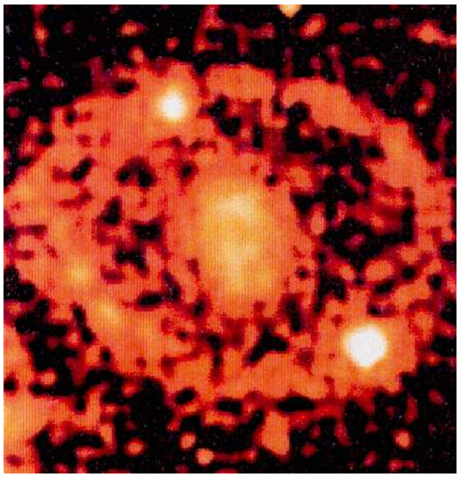

Figure 3.7: The evidence for jets in supernova explosion - HST image of center region of SN 1987a (HST WEB SITE)

- Gamma-ray bursts? So why GRBs could not to be collimated when they are assumed to originate during a supermassive supernova explosion or the final stage of merging two very compact objects. If the burst is spherically symmetric the polarization will be small because there is no preferred position angle. Jets break the symmetry and when observing not directly in the axes of the jet there is a preferred direction (the polarization could be parallel or perpendicular to it).

  Angular moment of the torus or two merging components defines rotating axes as a preferable direction of collimation. The magnetic field should be added too. Note that in a case of a BH the angular momentum and the magnetic dipole axes tend to unify into one axes during the first phase of BH evolution.

  It would also help to solve the energy reservoir problem. Present data requires isotropic equivalent energy exceeding 10^{54} ergs in γ-ray for the most energetic burst. This could lead to energy crisis for some progenitor models. The collimation decreases this energy by factor $\Omega/4\pi$. A conical GRB will not light up the full celestial sphere but a fraction defined by beaming factor

  $$f_b \equiv (1 - \cos\theta) \sim \theta^2/2$$

  which is equivalent to the $\Omega/4\pi$ factor. Thus the true energy release is smaller than E_{iso} by this factor $E_\gamma = f_b E_{iso}(\gamma)$

  If assuming that an additional break in spectra of suspicious OAs is caused by the jet spreading the $\langle E_{iso}(\gamma)\rangle$ about 110×10^{51} ergs while E_γ is clustered around 5×10^{51} ergs. True total energy $E_0 \equiv E_\gamma/\eta_\gamma \propto n^{1/4}\eta^{-3/4}$ implies restrictions on n and η_γ estimation $\eta_\gamma \sim 0.2$ and derived $E_0 \sim 3\times10^{51}$ ergs (only little higher than typical SN release) (FRAIL ET AL. 2001).

Also the GRB rate would be increased by the same value $4\pi/\Omega$, thus it could be comparable to the mean SN rate. Since conical fireballs are visible to only a fraction f_b of observers, the true GRB rate $R = \langle f_b^{-1} \rangle R_{obs}$. Estimated mean opening angle and $\langle f_b \rangle \sim 500$ with the mean error of 200%.

Thus the rate of observed GRB events $R_{obs}(z = 0) = 0.5$ Gpc^{-3} yr^{-1} is increased to the total rate of $R(z = 0) \sim 250$ Gpc^{-3} yr^{-1} which is comparable to NS-NS mergers rate $R_{NS} \sim 80$ Gpc^{-3} yr^{-1} estimated by (PHINNEY 1991) and the SN type Ib/c rate $R_{Ib/c} \sim 6 \times 10^4$ Gpc^{-3} yr^{-1} estimated by (SCHMIDT ET AL. 2000).

Jet formalism

Many authors (e.g. SARI ET AL. 1999, GRANOT, PIRAN & SARI 1999, 2000) have slightly modified the existing fireball model formalism and consider the jets.

Unfortunately considering the geometry of beaming introduces another free parameter, the opening angle of the jet θ.

Doppler factor

$$\delta = \frac{1}{\Gamma(1 - \beta \cos\theta)}$$

where θ is the viewing angle between the jet flow direction and the observer's LOS is added to the equations. For $v \ll c$ it comes to a standard Doppler effect $\delta \sim 1 + \frac{v}{c}\cos\theta$.

A jet emitting at a single spectral color would appear at a frequency δ times higher and into a solid angle δ^2 times smaller, thus a combined factor of δ^3 times brighter if moving toward us.

If the baryon loading in the jet was higher ("dirty fireball") we would expect Lorentz factor only $1 \ll \Gamma \ll 100$. It would produce optical-ray burst instead of in gamma-rays. As mentioned bursts have a light curve with variability 10^{-3} s and have non-thermal spectrum usually described by broken power-laws. This implies that the gamma-ray must come from an optically thin region to avoid being thermalized. We could also expect high energy density in a static source model (assuming optical depth $\tau_{\gamma\gamma} \gg 1$ for $\gamma + \gamma \rightarrow e^{\pm}$). The solution could be a relativity in motion. Variabilities of an approaching matter at $V/c \sim 1$ appear more rapid and the pair creation optical depth is lower because in ejecta comoving frame the energy is below 511 keV.

The signature of conical geometry manifests itself as a broad band break in the power-law decay of the afterglow emission, which declines more rapidly relative to that of a spherical case. This break happens for two reasons

- an edge effect that occurs at time t_j when the bulk Lorentz factor of the blast wave Γ has slowed down to $\Gamma < \theta^{-1}$
- the lateral spreading of the jet. The ejecta encountering more matter of surrounding ISM decelerate faster than in a spherical case.

$$\theta = 0.057 \left(\frac{t_j}{1\text{day}}\right)^{3/8} \left(\frac{1+z}{2}\right)^{-3/8} \left[\frac{E_{iso}(\gamma)}{10^{53} ergs}\right]^{-1/8} \left(\frac{\eta_\gamma}{0.2}\right)^{1/8} \left(\frac{n}{0.1cm^{-3}}\right)^{1/8}$$

η_γ efficiency of the fireball in converting the kinetic energy of ejecta into gamma-rays and n is the mean circumburst density.

According to the relativistic fireball model, the emission from a spherically expanding shell and a jet would be rather similar to each other as long as we are along the jet's axis and the Lorentz factor γ is large compared to the inverse of the angular width of the jet θ_0. When γ drops below θ_0^{-1}, the jet's material begins to spread sideways, and we expect a break in the light curve of the afterglow at this stage.

One physically plausible way to account for the early break from steep decay to shallower decay at early times is to suppose that the early ($\leq 10^{-2}$ days), rapidly fading optical flash (OT) arises in the reverse shock that propagates from the fireball interstellar medium (ISM) boundary back into the ejecta material, while the more slowly fading optical emission seen on timescales of a few hours (OA) arises in the forward shock propagating into the ISM (Sari & Piran 1999a, 1999b). A possibility for a break to a steeper power law at late times is the spread of the opening angle of a strongly beamed (or jet-dominated) flow (Rhoads 1997, Piran et al. 1999). This occurs when the fireball material has decelerated to $\Gamma \sim \theta^{-1}$, where θ is the opening angle of the beam and the motion starts to be non-relativistic.

However, even if the relativistic ejecta is beamed, as long as the Lorentz factor γ of the relativistic motion satisfies $\gamma > \theta_0^{-1}$, the hydrodynamics of the jet will not be influenced by the fact that it has a finite angular size. The matter does not have enough time (in its own rest frame) to expand sideways.

The light curve from a jet differs strongly from the light curve of a spherical evolution.

The typical frequency synchrotron frequency at the observer frame is

$$\nu_m = \frac{eB}{m_e c}\gamma_e^2\gamma \propto \gamma^4 \propto \begin{cases} t^{-3/2}, & spherical \\ t^{-2}, & jet \end{cases}$$

The cooling frequency is given by

$$\nu_c = \frac{36\pi^2 e m_e c}{\gamma B^3 t^2} \propto \gamma^{-4} t^{-2} \propto \begin{cases} t^{-1/2}, & spherical \\ t^0 (constant), & jet \end{cases}$$

Let $N_{e,j}$ be the total number of electrons radiating toward the observer i.e. those located in a cone of opening angle γ^{-1}. First approximation gives $N_{e,j} = 4\pi\gamma^{-2}R^3 n/3$. The total energy per unit time per unit frequency emitted by these electrons $\sigma_T m_e c^2 N_{e,j} B\gamma/6\pi e$ is distributed over area of $\pi\gamma^{-2}d^2$ at a distance d from the source. The observed peak flux density is therefore

$$F_{\nu,max} = \frac{2\sigma_T m_e c^2}{\pi e}\frac{R^3 n B\gamma}{d^2} \propto R^3\gamma^2 \propto \begin{cases} t^0 (constant), & spherical \\ t^{-1}, & jet \end{cases}$$

The self-absorption frequency can be estimated as

$$\nu_a \propto R^{3/5}\gamma^{2/5} \propto \begin{cases} t^0 (constant), & spherical \\ t^{-1/5}, & jet \end{cases}$$

The light curve and corresponding fluxes are

$$F_{\nu<\nu_a} \propto (\frac{\nu}{\nu_a})^2(\frac{\nu_a}{\nu_m})^{1/3}F_{\nu,max} \propto R^2 \propto \begin{cases} t^{1/2}, & spherical \\ t^0 (constant), & jet \end{cases}$$

$$F_{\nu_a<\nu<\nu_m} = (\frac{\nu}{\nu_m})^{1/3}F_{\nu,max} \propto R^3\gamma^{2/3} \propto \begin{cases} t^{1/2}, & spherical \\ t^{-1/3}, & jet \end{cases}$$

$$F_{\nu_m<\nu<\nu_c} = F_{\nu_m}(\frac{\nu}{\nu_m})^{-(p-1)/2} \propto R^3\gamma^{2p} \propto \begin{cases} t^{-3(p-1)/4}, & spherical \\ t^{-p}, & jet \end{cases}$$

$$F_{\nu_m<\nu_c<\nu} = F_{\nu_m}(\frac{\nu_c}{\nu_m})^{-(p-1)/2}(\frac{\nu}{\nu_c})^{-p/2} \propto R^3\gamma^{2p-2}t^{-1} \propto \begin{cases} t^{-3p/4+1/2}, & spherical \\ t^{-p}, & jet \end{cases}$$

For a spreading jet, the light curve decay index (but not the spectrum) is independent of whether $\nu > \nu_c$ or $\nu < \nu_c$. This is because of the fact that ν_c is constant in time in the case of a spreading jet. Since p determines both the light curve and spectrum, a parameter-free relation between the temporal decay index α and the spectral index β (defined by $F(t) \propto t^{-\alpha}\nu^{-\beta}$) can be given.

The model was successfully used in describing GRB 990123 radio afterglow. Another break was observed in light curves of GRB 990123, GRB 990510 (Stanek et al. 1999), GRB 000301C (Masetti et al. 2000) and GRB 991216 (Halpern et al. 2000) apart from the predicted breaks from breaking frequencies of the broken power-laws of the fireball model. On the contrary an evident absence of the break has been shown for GRB 970508 (Rhoads et al. 1999). Another fine example of the break is GRB 000301C (Rhoads & Fruchter 2000).

GRB 000301C - an excellent example of beaming

I will just show the presence of the additional break in the light curve of GRB 000301C in more details. This GRB was detected independently by the All-Sky Monitor on the RXTE (Rossi X-Ray Timing Explorer) and by two spacecrafts (Ulysses and NEAR) of the current IPN (Interplanetary Network) on 2000 March 1.4108 UT.

The K' filter (2.1 μm) light curve shows a well-sampled break in the decay slope at $t \sim 3.5$ days after the burst. Comparison with the optical (R-band) light curve shows marginally significant differences, especially in the early time decay slope (which is steeper in the optical) and the break time (which occurs later in the optical). This is contrary to the general expectation that light-curve breaks should either be achromatic (e.g., for breaks due to collimation effects) or should occur later at longer wavelengths (for most other breaks). By combining the IR-optical-UV data with millimeter and radio fluxes, we are able to constrain the locations of the self-absorption break and cooling break and to infer the location of the spectral peak at t = 3 days, $f_\nu \sim 3.4$ mJy at $\nu \sim 10^{12} Hz$.

Using the multiwavelength spectral energy distribution, we are able to constrain the blast wave energy, which was $E \geq 3 \times 10^{53}$ ergs if the explosion was isotropic.

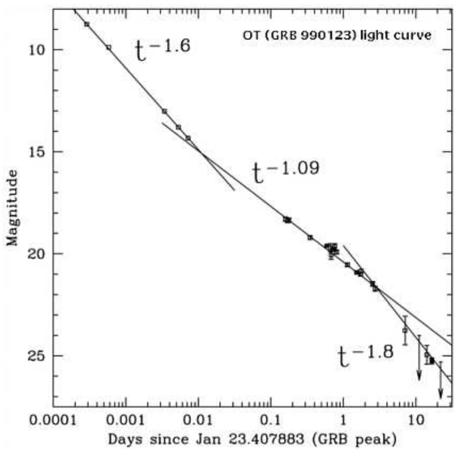

Figure 3.8: Evidence for the jet break in the light curve of GRB 990123 (Frail 2001)

Broken power laws is usually empirically fitted by a function of the form

$$f = f_0[(t/t_b)^{\alpha_1\beta} + (t/t_b)^{\alpha_2\beta}]^{-1/\beta}$$

with $\alpha_1 < \alpha_2$ and $\beta > 0$, this function describes a light curve falling as $t^{-\alpha}$ at $t \ll t_b$ and $t^{-\alpha_2}$ at $t \gg t_b$. β controls the sharpness of the break, with larger β implying a sharper break. In terms of magnitudes I get

$$m = m_b + \frac{2.5}{\beta}(log_{10}[(t/t_b)^{\alpha_1\beta} + (t/t_b)^{\alpha_2\beta}] - log_{10}(2))$$

where m_b is the magnitude at time t_b

Orphan afterglows

Assuming the jet-like geometry of the event I have to mention the case in which the observer is off the axes out of the angle Ω_γ but still inside the angle Ω_{OA}. If I assume that a beamed gamma-ray emission points to a small fraction of the sky and later more spherical optical emission to a larger fraction of the sky occurs it is possible to estimate the beaming factor from a simple equation in which angles are related to the rates as (Rhoads et al. 2001)

$$\frac{\Omega_{OA}}{\Omega_\gamma} = \frac{\dot{N}_{GRB}}{\dot{N}_{OA}}$$

Thus there would be expected many of so-called orphan afterglows - OAs with no detected GRB emission, according to the ratio of the opening angles.

Statistics of orphan afterglows can lead to guess the mean collimation angle of GRB sample. Not only optical but X-ray an radio afterglows. X-ray orphan afterglow search was made (Greiner 1999) and 23 sources have been found however none of them is thought to be the orphan afterglow.

I suggest the search for radio transients as well but there is the possibility that radio afterglows being confused with radio supernovae of SN type II (they

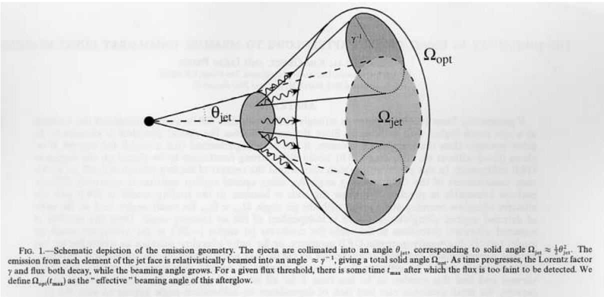

Figure 3.9: Schematic geometry of the jetted afterglow emission (DALAL ET AL. 2002)

follows the same radiating mechanism, and the expansion is non-relativistic in later times), Properties of SN type I are uncertain and radio loud AGNs show rapid variability. The optical counterpart of these AGN are easily detectable by HST deep field survey and so it would be easy to exclude these sources from radio afterglows.

3.4.3 Cannonball

Introduction

However there is an alternative to a classical fireball model or to its fire-cone modification in a case of assuming collimated beaming jets. The authors (DAR & DE RÚJULA 2000A, 2000B, DADO, DAR & DE RÚJULA 2001, 2002) criticize the fireball scenario and suggest a new model.

As already mentioned in the previous section many astrophysical systems, such as radio galaxies, quasars and microquasars, in which period of intense accretion onto a compact massive object occurs emit highly collimated relativistic jets of plasma. The Lorentz factor of the outflow $\gamma = \sqrt{1 - v^2/c^2}$ of these jets covers a wide ranges from mildly relativistic $\gamma \sim 2.55$ (GRS 1915+105) to $\gamma \sim 10$ for typical quasars, even to highly relativistic $\gamma \sim 10^3$ (QSO PKS0405-385). These jets don't continuously stream a matter but consist of individual blobs "cannonballs". Unfortunately the exact mechanism of this fueling is not known.

Cannonball formalism

A star core-collapses in SN explosion, a fraction of the parent star material falls back in a time very roughly of the order of one day and settles an accretion disk around a compact rest object. Then it is ejected through discrete bulbs (cannonballs) in jets until the accreting matter is exhausted. The emitted CBs initially expands in the SN rest frame at a speed $\beta c/\gamma$, with βc presumably of the same order as the speed of sound in relativistic plasma $\beta_{exp} = 1/\sqrt{3}$, or smaller.

The collision of the CB with the SN shell heats the CB to a surface temperature $\sim$ 150 eV, further decreasing as the CB travels. The resulting CB surface radiation, Doppler shifted in energy and forward collimated by the CB

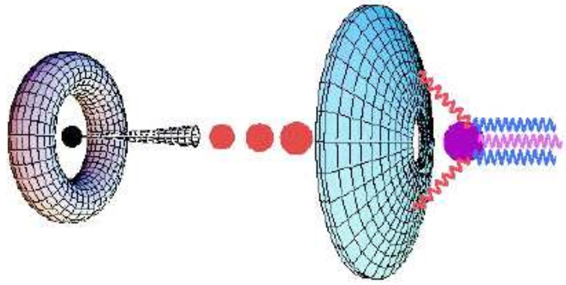

Figure 3.10: Cannonball model of γ-ray emission mechanism and cannonball model geometry (Dado, Dar & de Rujula 2001)

motion makes a single GRB pulse. The GRB is a set of such pulses, overlapping each other. Unlike the fireball model the GRB is not produced by synchrotron emission.

Thus the observed radiation is composed of three component: ejected CBs, SN explosion and constant host galaxy.

The free-fall time of previously exploded outer parts of the star of radius R and mass M falling back onto the newly born compact object is

$$t_{fall} = \pi \left(\frac{R}{8GM}\right)^{1/2} \sim 1 \text{ day} R_{12}^{3/2} \left(\frac{1.4 M_{\odot}}{M}\right)^{1/2}$$

If the parent star rotates the t_{fall} will be longer.

In the time after the collapse $t_{fall} \sim 1$ day the SN shell will have a radius $R_{sh} \sim 2.6 \times 10^{14}$ cm for a typical velocity $\sim 0.1c$ of the ejecta.

The rest frame of CB and SN shell is Doppler-shifted to the observer after the cosmological redshift correction $\nu_{CB} = \nu_{SN}\delta^{-1}$ and $\nu_{SN} = (1+z)\nu_{obs}$. Doppler shift δ is defined as usually

$$\delta \equiv \frac{1}{\gamma(1-\beta\cos\theta)} \simeq \frac{2\gamma}{(1+\theta^2\gamma^2)}$$

if $\theta \ll 1$ and $\gamma \gg 1$. The fluence is also affected by Doppler-shifted geometry by factor $\delta^{3+\alpha}$.

The collision of the CB nuclei (of energy $\sim$ TeV) with those in the SN shell produce hadronic cascades. The SN shell and the CB are transparent to the neutrinos but opaque to photons. A fraction of the energy not carried out by neutrinos heats the shell that radiates as a black body. As heated CB expands it becomes transparent and emits γ-rays collimated and boosted by the CB motion. A local observer at angles θ to the axes of the jet sees the energy distribution into an angle Ω

$$\frac{dE}{d\Omega} \simeq \frac{\beta_{exp}^2}{\gamma^{3/2}} \left(\frac{2\gamma}{(1+\gamma^2\theta^2)}\right)^3 \left(\frac{4\pi R^2}{3\sigma_T}\right)^{1/2} \frac{\sqrt{2m_p M}c^2}{24\pi}$$

assuming the most likely $\theta \sim \gamma^{-1} \sim 10^{-3}$ gives

$$E_{iso} \simeq 6.4 \left(\frac{\beta_{exp}}{0.1}\right)^2 \times 10^{53}\text{erg}$$

assuming n_{CB} cannonballs increases the energy to $n_{CB}E_{iso}$.

The duration of a single CB pulse corrseponds to the light crossing time of the CB when it becomes transparent to its radiation $\sim \frac{R_{CB}}{c}$ in the rest frame or for the observer

$$t_{obs} \sim \left(\frac{3M_{CB}\sigma_T}{4\pi m_p}\right)^{1/2} \frac{1+\theta^2\gamma^2}{2\gamma c}(1+z)$$

Although a supernova explosions are definitely not standard candles the authors set the SN 1988bw supernova explosion (at $z = 0.0085$) connected to GRB 980326 to be a standard in energy and a shape of the light curve. Let define a SN 1998bw scaling for all SN

$$F_{SN} = \frac{1+z}{1+z_{1998bw}} \frac{D_L^2(z_{1998bw})}{D_L^2(z)} F_{1998bw}[\nu\frac{1+z}{1+z_{1998bw}}, t\frac{1+z_{1998bw}}{1+z}]A(\nu,z)$$

$A(\nu, z)$ is the extinction along the LOS, the authors adopted $E(B-V) = 0.148$.

When an expanding CB becomes transparent to its enclosed radiation, it loses its internal radiation pressure. CB encloses a magnetic field maze, as the observed ejections from quasars and microquasars do. The ISM previously ionized by gamma-ray radiation and by the entering CB. The early X-ray afterglow is dominated by thermal bremsstrahlung from cooling CBs, ionized ISM particles are multiply scattered by the CBs' turbulent magnetic fields and looses energy by synchrotron radiation. The CB's emission is strongly relativistically aberrant.

The unextincted late time contribution of a CB to the GRB afterglow is given as

$$F_{CB} \propto \gamma(t)^{3\alpha-1}\delta(t)^{3+\alpha}\nu^{-\alpha}$$

where $\alpha \sim 1.1$ is the spectral index of the synchrotron radiation mainly from Fermi-accelerated electrons in the CB and Lorentz factor γ is a function of observer's time

$$\gamma = \gamma(\gamma_0, \theta, x_\infty, t) = \frac{1}{B}[\theta^2 + C\theta^4 + \frac{1}{C}]$$

where

$$C \equiv [\frac{2}{B^2 + 2\theta^6 + B\sqrt{B^2+4\theta^6}}]^{1/3}$$

$$B \equiv \frac{1}{\gamma_0^3} + \frac{3\theta^2}{\gamma_0} + \frac{6ct}{(1+z)x_\infty}$$

where $\gamma_0 = \gamma(0)$ and

$$x_\infty \equiv \frac{N_{CB}}{\pi R_{max}^2 n_p}$$

characterizes the CB's slow down in terms of its baryon number N_{CB} and R_{max} the radius exponential decrease (it takes a distance x_∞/γ for CB to slow down to half its initial $\gamma(0)$.)

In the CB model the GRB emission in gamma-rays is (mainly) of thermal origin (although the spectrum is apparently non-thermal) and it decreases exponentially with time. After the GRB pulses quite complicate consequence of processes begin. While mixing in collision of CB and ISM originally ionized material recombines into H and emits on Lyman lines (at radio band in CB rest-frame) and Doppler-blue-shifted to optical afterglow. The radiated optical band is shifted to X-ray etc. The radio emission is similarly to quasar jets produced by bremsstrahlung. The synchrotron emission originates while electrons of ISM enter the CB. The radiation is highly isotropic in CB rest frame but collimated in observer frame.

The authors have more or less successfully explained light curves of beside GRB 980326 more than 18 GRBs with known redshift including famous GRB 990123, GRB 980425, GRB 970228, GRB 000301C and the newest GRB 010921. Surprisingly GRB 000301C was not interpreted as gravitationally lensed, on the other hand the authors guessed that GRB 970508 was lensed.

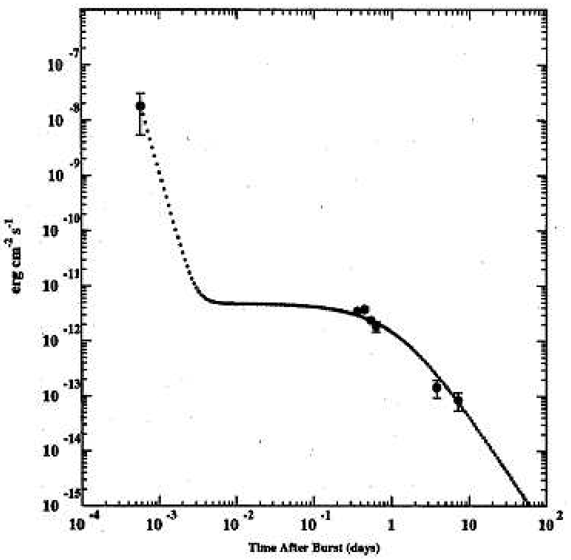

Figure 3.11: The X-ray afterglow of GRB 970228 (left) and GRB 990510 (right) fitted to a cannonball model. The light curves were taken from (Dado, Dar & De Rujula 2001 and references therein).

3.4.4 Fireball vs cannonball model

Introduction

Although these two models (fireball and cannonball) stay aside each other for more than a year no one has ever tried to compare them before. Unfortunately both groups of FB and CB model advocates don't communicate with each other and give no explanation of anything that would break their models. As one can see none of them fits the observational data clearly and with no exception.

For and against the cannonball model

- **SN 1998bw candle:** Why to take so unusual supernova 1998bw as the standard? SN 1998bw has extremely low isotropic energy equivalent, it

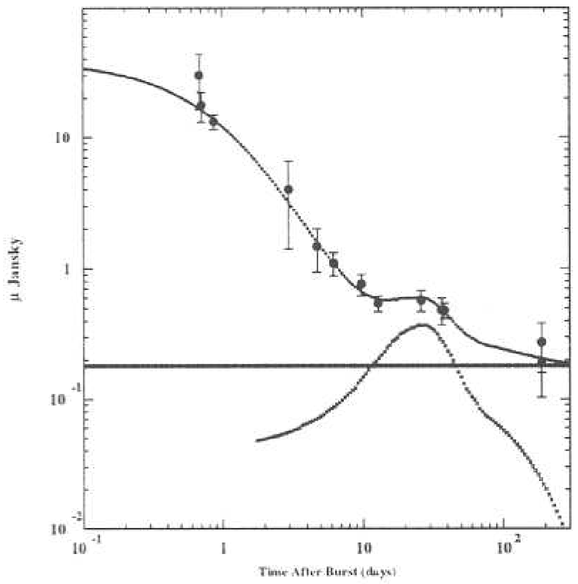

Figure 3.12: The R-band afterglow fit for GRB 970228. The contribution of the light curve of SN1998bw-like SN placed at GRB's redshift is shown (Dado, Dar & De Rujula 2001).

is extremely close and extremely faint. But the spatial and temporal GRB/SN coincidence by chance was much less than 10^{-4} for this case (this value was computed for the original large uncorrected errorbox) (Galama 1998).

- **Ball compactness:** Another often discussed question is the compactness problem of each plasma ball of the cannonball. But it could be easily solved when we assume the Lorentz factor $\Gamma \sim 10^2$, or higher. The plasma ball will not have enough time to spread out. The problem enters the scene after the slow down, when e.g. the radio afterglow would show different behavior than X-ray or optical afterglow. Unfortunately no radio afterglow data have been used to fit the cannonball model. Very complicated studies try to compute the influence of the pressure of ISM on the plasma ball and the results are unclear.

- **Common jets:** The jet-like behavior is very common in astrophysics. There is a direct evidence that at least some supernovae show jet-like structures. But no one has seen the jets directly in GRB events even in the case of the very close SN 1998bw. The jets could be considered through the late radio observation and the scintillation, from measurement of polarization or via other indirect way such is an indirect measurement of superluminal motion in supernovae and GRBs explosion. There is no evidence of strong polarization in SN 1998bw.

- **Stochastic accretion modeling:** If I assume the discrete accretion on a black hole mechanism and the time between the pulses in gamma-ray time profile I would expect stochastic behavior of it. The modeling of it through the stochastic Poisson process should be made.

- **UV bump-like contribution:** If there is a torus or a disk-like structure around the GRB progenitor I suggest to try to find and distinguish its own contribution to the emission probably in the first phase of the burst similarly to the UV observed in the spectrum of many QSOs. These bump could be cosmologically redshifted to lower frequencies even to the optical bands and it could be responsible for optical transient event in the time of the burst. To prove or disprove this idea a better sort of data would be needed and shorter delay between the gamma-ray trigger with better and faster localization and following (or simultaneous) optical observation.

- **Bad fits:** The data which doesn't fit the model well are excluded or another explanation is given e.g. gravitational microlensing or unusual reddening.

- **Underlying SN:** Many of GRBs indicate the presence of underlying supernova light curve. Also the rate of SNe and GRBs when we assume a non-negligible degree of collimation is comparable. But a non-negligible fraction of GRB afterglows show no evidence for it.

- **Blueshifted lines:** I suppose that there should be hydrogen Lyman α lines blueshifted from UV to X-ray spectrum due to the CB motion propagating through the ISM. It's never been proved through any observation.

- **Superluminal motion:** Viewing angle is an important factor omitted in the fireball model, due to the geometry I suggest to try to observe a superluminal motion in close GRB and/or SN events.

  A relation for superluminal motion could be given as

$$v_T = \frac{\beta \sin\theta}{1-\beta\cos\theta} c \simeq \frac{2\gamma^2\theta}{1+\gamma^2\theta^2} c$$

  for $\gamma \gg 1$, $\theta \ll 1$ and $\gamma\theta \sim 1$ (Kembhavi & Narlikar 1999).

  Thus a transversal velocity is obtained by direct integration

$$D = \int v_T(\gamma(t))$$

  and assuming later phase of the afterglow $\gamma < \theta^{-1}$ or according to the time of the afterglow peak $t \gg t_{max}$

$$v_T \sim 2\gamma^2\theta c$$

  A transverse superluminal distance between the bulks

$$D \simeq \frac{2ct_p}{\theta} \left(\frac{t}{t_p}\right)^{1/3}$$

- The host galaxy contribution to the spectrum is added and calculated.

- A long duration tail of γ-ray emission is expected if the emission is pseudo-thermal. At least the tail from the last pulse should be observable but no evidence has been given yet.

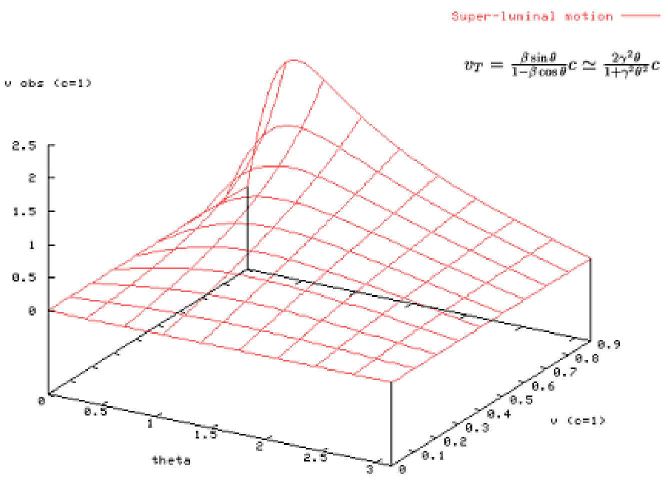

Figure 3.13: The plot of the superluminal motion

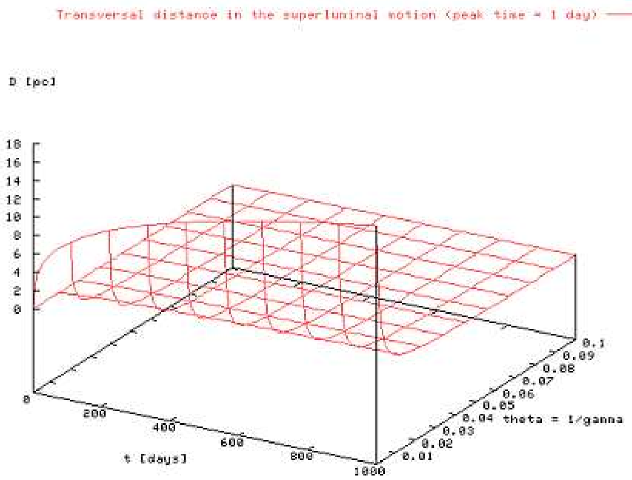

Figure 3.14: The transversal distance in the case of superluminal motion in the small angle and high γ assumption

For and against the fireball model

- **Elegance:** One elegant model of relativistic shock wave interacting with ISM explains all the GRB and AG attributes.

- **Bad fits:** There are too few data not to be fitted by a four times broken power law (three breaking frequencies plus one break due to the jet yielding to be relativistic) relatively well. Is the light curve too smooth to predict the break? Any deviations from the model are explained by other effects e.g. the gravitational microlensing.

- **Observed breaks:** The predicted breaks in the spectra of several GRB OAs have been observed.

- **Undetectable break frequencies:** The maximum frequency and the maximum of the flux beam happens very soon after the gamma-ray emission is nearly impossible to detect.

- **Wind:** There are difficulties in modeling various exploding shells (wind) with different initial velocities responsible for internal shocks believed to be the origin of the gamma-ray emission.

Conclusion

It is impossible to get the right conclusion without additional data and further observations. Extremely important is a direct early multi spectral observation immediately after the burst where the light curves differ in the cannonball and fireball model. The best way would be to observe by chance a pre-γ-ray emission, pointing to the direct mechanism.

Also suggested stochastic modeling of accretion as an energy reservoir for cannonball model would be valuable. Also a search for the presence of optical transient in GRB and pre-GRB phase corresponding to the accretion process is suggested.

The cannonball model assumes an underlying supernova responsible for a bump in the light curve opposed to the fireball in which the supernova is not included directly in the model.

Of course a possible Delphi's solution is that a fraction of GRBs with underlying SN is produced via discrete cannonball model and the rest by the fireball model assuming failed SN fueling continuously (over the duration of the burst) or all in once energy output.

Although nearly spherical fireball idea is almost dead now it would be valuable to compare CB with jetted FB model viewed under angle δ and add a Doppler factor to it.

3.5 Dark bursts and orphans

Whatever afterglow model is closer to reality two mysteries persist in that topic. Only 40% of observed well and promptly localized GRBs revealed an optical afterglow. They others are called "dark burst". The "orphans" and the failure of searching for them were discussed in the previous section. Very narrow openning angles could be responsible for this. Assuming that the cone has not enough time to spread before it drops under the limit observing magnitude and therefore the ratio of $\Omega_\gamma/\Omega_{OA} \sim 1$ could be a reason.

As I will show in one of the next chapters a dust extinction (as an indirect evidence for SFR) could obscure the GRB afterglow. The IR observation of IR afterglows following-up GRB 990705, GRB 000418 were successfully detected even before than being confirmed at optical wavelengths. There is still not any detection of an IR afterglow without an optical counterpart which would suggest that the emission was absorbed and scattered on dust grains and reemited at lower frequencies. But again the observation of extinction in X-ray spectra seems to reveal a very low gas to dust ratio (LAZZATI ET AL. 2000).

3.6 X-ray, radio and other wavelength band afterglows

3.6.1 X-ray afterglows

X-ray afterglows (COSTA ET AL. 1997) are used to localize more precisely the GRB position and through the comparing of X-ray and optical extinction it is possible to estimate inter-galactic reddening. Also strong Fe K lines at ~ 6.55 keV and Fe absorption edge ~ 9.28 keV could arise from the X-ray illumination of a pre-ejected shell (e.g. supernova remnant) or from the X-ray radiation colliding with the outer stellar envelope and they have been detected in X-ray spectrum of the afterglow implying high abundance of iron in the circumburst medium.

3.6.2 Radio afterglow scintillation

The radio observations of radio afterglows (FRAIL ET AL. 1997) could be used indirectly for estimating the size and initial velocity of the explosion (caused either through the cannonball or fireball scenario). The used method is called the scintillations. The BM self similar solution is derived with the assumption $\gamma \sim \Gamma \gg 1$. These assumption breaks down when the shock sweeps out a volume $\sim r_{dec}^3$ of ISM and its motion becomes non-relativistic. At radius r_{dec} the Sedov-Taylor solution is a good approximation.

In the radio afterglow regime the velocity of the jet is non-relativistic but Newtonian. As the source of radiation and its surface is small the multi-scattering on the dust of ISM causes high fluctuation in intensity. When the surface grows up the fluctuation from ISM scattering modulation will average up and the difference in the intensity will be smaller. A presumption of that the wavelength of the radiation is comparable to the dust drain or to the molecular hydrogen scale is made. This behavior has been observed in the radio flare of GRB 990123 and more obviously in the case of GRB 970508.

Radio observations of the afterglow of the gamma-ray burst GRB 970508 provide unique new constraints on afterglow models. The quenching of diffractive scintillation at ~ 4 weeks delay provides the first direct estimation of the source size and the expansion rate. It implies an apparent size $R \sim 10^{17}$ cm and an expansion at a speed comparable to that of light at $t \sim 4$ weeks, in agreement with the fireball model prediction,

$$R = 10^{16}\left(\frac{1+z}{2}\right)^{-5/8}\left(\frac{E_{52}}{n_0}\right)^{1/8}(\mathrm{t/week})^{5/8}\mathrm{cm}$$

The radio flux and its dependence on time and frequency at 15 weeks delay are in agreement with the model and imply a fireball energy (assuming spherical symmetry) $\sim 10^{52}$ ergs, consistent with the value inferred from observations at shorter delay. The observed radio behavior deviates from model predictions at delays greater than 5 weeks. This is expected, since at this delay the fireball is in transition from highly relativistic to sub-relativistic expansion, with Lorentz factor ~ 2. Deviation may result from a change in the physical processes associated with the shock wave as it becomes sub-relativistic (e.g., a decrease in the fraction of energy carried by the magnetic field) or from the fireball being a cone of opening angle $1/\gamma \sim 1/2$.

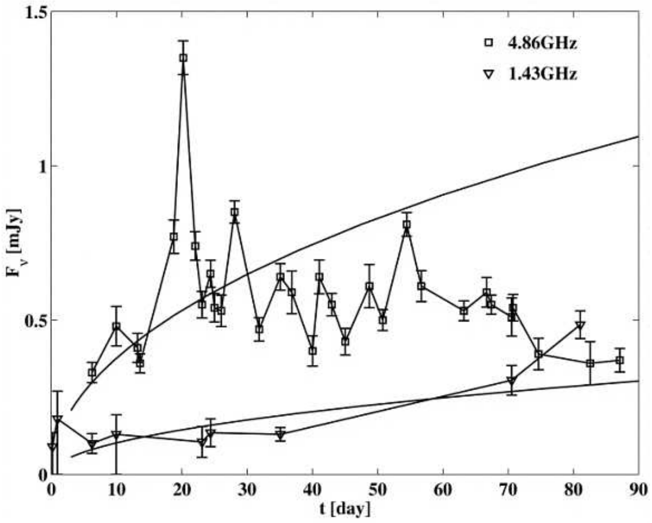

Figure 3.15: The scintillation due to ISM scattering modulation in the light curve of GRB 990123 radio afterglow (WAXMAN, FRAIL & KULKARNI 1998)

The UV and IR GRB afterglows will play a crucial role in proving the dust destruction and in the interactions between the radiation and ISM generally.

Chapter 4

Color indices of GRB afterglows

4.1 Introduction

A new and very interesting method of studying GRB afterglows through their color indices was suggested by (Šimon et al. 2001). A data analysis of multicolor photometrical data for all available GRB afterglows of the total number of 16 was made. The data came from (Greiner web site, GCN Circulars). It revealed a surprising discovery.

4.2 Time evolution of color indices and color diagrams

There is a cummulation of the color indices in the well defined belt when plotted as a function of time during $t - T_0$ less than 10 days. The concentration in well defined regions $(R - I)_0 = 0.46 \pm 0.18$, $(V - R)_0 = 0.40 \pm 0.13$, $(B - V)_0 = 0.47 \pm 0.17$ is obvious. Thus the color indices evolve in a very narrow band less than 0.4 magnitude wide in time for 10 days since their detection. The $(U - B)_0$ color index shows greater variability. The 10 days horizon has been chosen because there were no more suitable data available for further times. So the color evolution is negligible during the time interval of 10 days.

There is also shown that most of 16 afterglows appear to concentrate in the well-localized region. The mean color indices with computed standard deviations are $(R-I)_0 = 0.46 \pm 0.18$, $(V - R)_0 = 0.40 \pm 0.13$ $(B - V)_0 = 0.47 \pm 0.17$. OAs therefore appear quite red.

Also the recently discovered afterglow of GRB 011211 falls into the region well with its values enriching the sample to the number of 17.

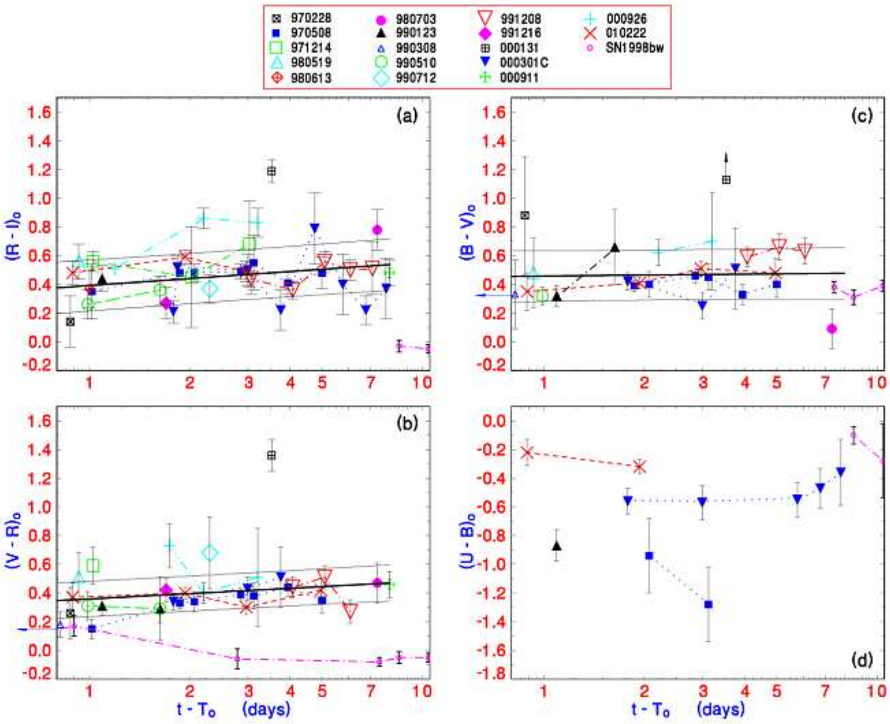

Figure 4.1: The time evolution of color indices of 17 GRB afterglows (Šimon et al. 2001)

4.3 Discussion and conclusion

4.3.1 GRB 00131

The peculiar GRB 000131 that is out of the region can be explained in the way that Lyman spectral lines or a Lyman break is redshifted into the optical pass-band because the redshift of this burst was very large ($z = 4.5$). As will be clear from the histogram of redshifts of GRBs this is not a typical GRB.

4.3.2 Powerful search toolkit

Knowing that color indices of OAs concentrate in such a small regions and the fact that this region is different from stellar objects could be used as a strategy for prompt searches for GRB afterglows. For GRBs closer than $z \leq 2$ where no Lyman α break or other lines or cutoff normally observed in UV disrupts in the OA spectra using the color-color selection seems to be a very valuable hint. The more higher redshift of the GRB more longer wavelength pass-band to the IR end of the spectrum we should use. It was already used by (Gorosabel 2001) to post-priori detect GRB afterglow from a CCD image. $J - K_S$ vs $R - K_S$ color diagram was used.

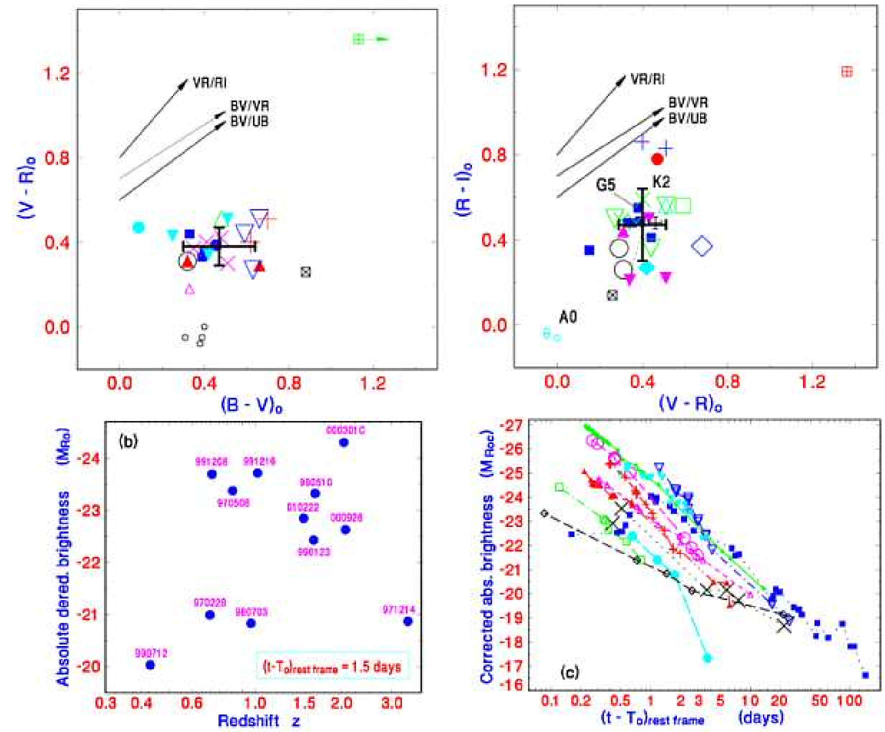

Figure 4.2: Color diagrams (upper part), SN 1998bw is included for comparing (not included in the calculation of the mean value), (lower part) (Šimon et al. 2001)

4.3.3 Reddening

Nearly all the OAs analysed by (Šimon et al. 2001) show very similar value of extinction. If I adopt the empirical relation (Predehl & Schmitt 1995)

$$E(B-V) = 0.3^m, A_V = 3.1 \times E(B-V)$$

or in terms of the column density

$$N_H = 1.79 \times 10^{21} A_V \text{ cm}^{-2}$$

resp.

$$A_V = 0.56 \times N_H 10^{21} \text{ cm}^{-2}$$

Also the reddening is very small. It would imply that we see only these bursts which are closer to us not to be obscured by dust clouds or deep in the circumburst medium. If we see bursts from different depths of circumburst medium we would observe all the range of reddening due to the selection effect. I will discuss this fact later in the next section while determining the average dust destruction.

4.3.4 Redshift determination derived from absolute magnitudes slopes

As one can see the time evolution of the absolute magnitudes calculated from the luminosity distance and corrected for the time dilation to the rest frame have similar slopes for all the GRB OAs. There were several attempts to estimate the redshift of the burst considering these slopes.

Unfortunately it is, according to my analyses and considerations, impossible. Absolute R-band magnitudes corrected for cosmological time dilation and computed in the rest-frame R-band of afterglows span nearly 4 magnitudes in one time, it means a factor of ~ 40 in luminosities. Thus GRBs and their afterglows cannot be considered as standard candles at all. The K-correction is different for each OA and thus no serious computation of the redshift can be obtained because we need scaling in both axes of the M_{abs} vs $t - t_0$ graph. We can only derive statistically the another form of $\log(N > P) - \log(P)$ diagram (noticed in the chapter 2). On the contrary the slope value is independent on redshift and a similar slope only indicates similar fading of OA and that this behavior is in a good agreement with the fireball model of the afterglows.

Chapter 5

Quasi-stellar objects and gamma-ray bursts correlation

5.1 Introduction

Quasi-stellar objects, quasars (QSOs) are the most luminous subclass of AGNs, with nuclear magnitudes $M_B < -21.5 + 5 \log h_0$. A small minority of these sources are the strong radio sources that originally defined the quasar class. Quasars are distinguished from Seifert galaxies in that in general they are spatially unresolved on e.g. Palomar Sky Survey photographs (angular sizes smaller than $\sim 7''$). Many of these sources are surrounded by a low surface brightness halo, some of them show observable jets.

As suggested the jets originate due to disk of debris accreting on a very massive black hole in a center of a distant galaxy. Relativistic electrons from the jet produce synchrotron radiation which we observe. Also a fraction of disk radiation known as a UV bump is observable in the other way non-thermal spectrum of quasars.

Quasars are very distant objects, with mean redshift $z \sim 2$. A better understanding of AGNs and QSOs could help to solve the GRB puzzle. Clearly both these astrophysical events belongs to high energy astrophysics and GRB collimation idea predicts that GRBs produce jets in the similar way to AGN. No doubt that both QSOs and GRBs are far objects at cosmological distance with a high redshift. In both cases it is believed that compact object such as a very massive black hole plays an important role as a progenitor. If the accretion model of fueling GRBs is valid then GRBs could be a smaller and faster manifestation of the same physics.

5.2 Spatial QSOs and GRBs correlation

A detailed search for QSO and GRB spatial angular sky coincidence was made for 344 GRBs and more than 11500 QSO sources from the 7$^{\text{th}}$ Veron catalogue of quasars and active galactic nuclei (Veron-Cetty & Veron 1996) with an unsuccessful result that there is no evidence for correlation above the significant level between these objects (GOROSABEL 1999). On the other hand, QSOs have been found to be located inside some (small) GRB error boxes e.g. GRB 960720 (VRBA ET. AL 1999).

No Evidence for GRBs and Abell Clusters or GRBs and radio-quiet QSOs correlations was found (HURLEY ET AL. 1999)

Also the redshift distribution of QSOs and GRBs doesn't show any significant correlation but I note that the sample of GRBs with known redshift is about 24 only and only of the long-duration GRB subclass.

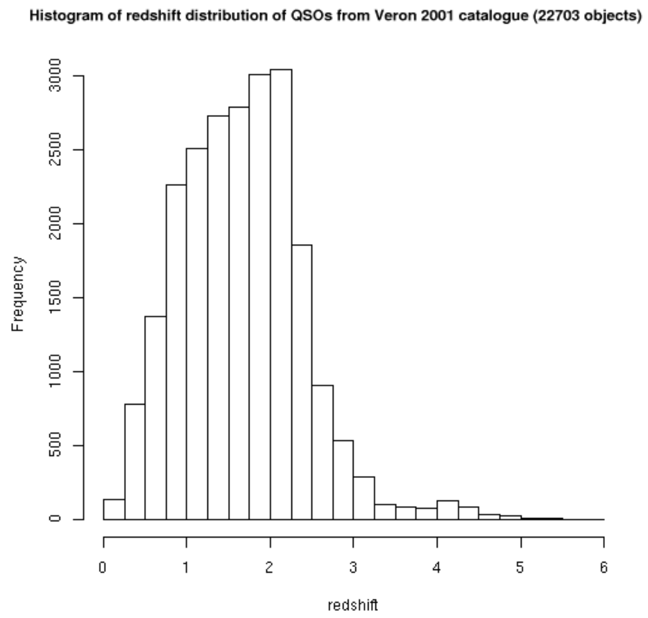

Figure 5.1: The histogram of QSOs' redshifts

5.3 QSO color-color diagrams

5.3.1 Introduction

According to the specific and well defined AG color indices it would be useful to compare these with color indices of QSOs. The related work was hard because there is not any public catalogue of QSOs with all the needed data together. Moreover many of sky surveys covers only a part of the sky.

5.3.2 $(U-B)_0$ vs $(B-V)_0$ color diagram

This is the most complete graph because the used data have been got from the famous (VERON-CETTY & VERON CATALOGUE OF QSOS AND AGNS 2001). 1097 objects are known with both $(U-B)_0$ and $(B-V)_0$ color indices. The mean

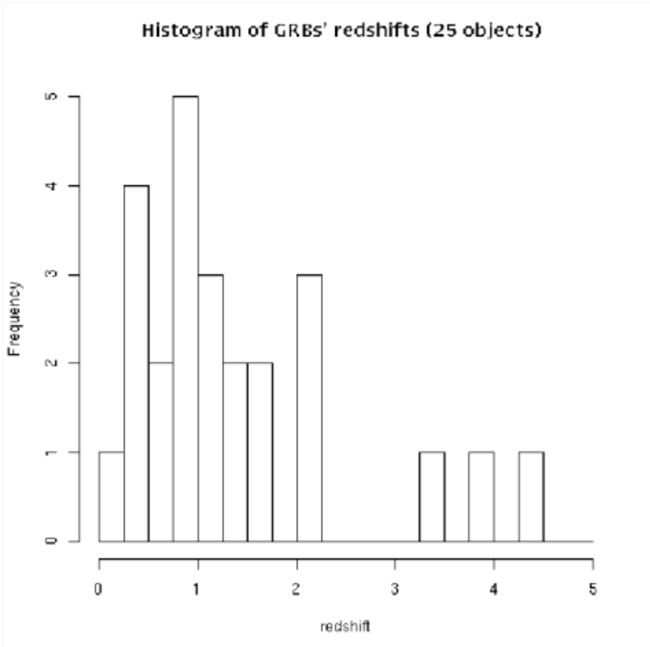

Figure 5.2: The histogram of GRBs' redshifts

value of $(U-B)_0$ is 0.23 ± 0.31 and the mean value of $(B-V)_0$ is -0.49 ± 0.53. The large standard deviation is caused by less than 7% of "excentric" objects.

5.3.3 $(B-V)_0$ vs $(V-R)_0$ color diagram

Data of 174 QSOs have been compiled from several sources (Lehman et al. 2001, Barger et al. 2001, Schreier et al. 2001). Because the objects have different catalogue names in each catalogue objects were sorted by their names inside each catalogue and than matched by sky position (RA, dec) using a Perl script. Then they have been plotted into the $(B-V)_0$ vs $(V-R)_0$ color diagram. The mean value of $(B-V)_0$ is (0.43 ± 0.36) and the mean value of $(V-R)_0$ is (0.42 ± 0.24). The large standard deviation is caused mainly by less than 5% of "excentric" values.

5.3.4 $(V-R)_0$ vs $(R-I)_0$ color diagram

Data of 174 QSOs have been compiled again from several sources (Lehman et al. 2001, Barger et al. 2001, Hornchmeier et al. 2001, Schreier et al. 2001). Because the problem with different catalogue names persists the objects were sorted by their names inside each catalogue and than matched by sky position (RA, dec) using a Perl script were plotted into the $(V-R)_0$ vs $(R-I)_0$ color diagram. The mean value of $(V-R)_0$ is (0.42 ± 0.21) and the mean value of $(R-I)_0$ is (0.50 ± 0.24). The difference between the $(V-R)_0$ here versus $(R-I)_0$ and versus $(B-V)_0$ is caused due to the different sample of QSOs because of some B or V and R or I photometry data missing. The error

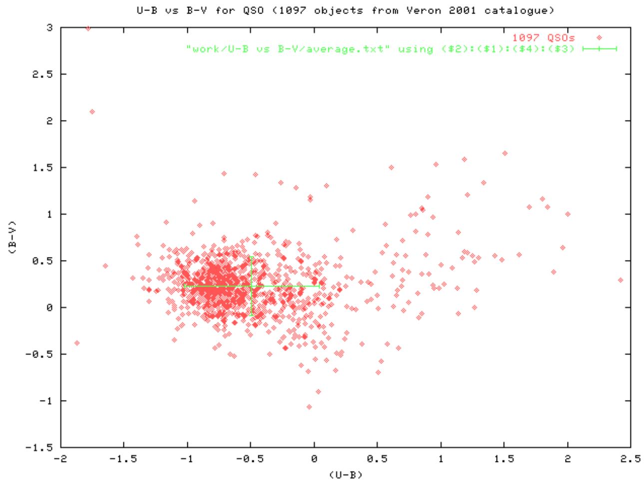

Figure 5.3: $(U-B)_0$ vs $(B-V)_0$ color diagram

is negligible and with a good agreement with the computed standard deviation. The large standard deviation is caused mainly by less than 5% of "excentric" values.

5.3.5 Discussion

I have found that more than 90% objects of QSOs' (B-V) vs (V-R) and (V-R) vs (R-I) color diagrammes shows very similar behavior to the GRB AGs. Because of large difference between the number of objects in the samples I cannot use a more robust Kolmogorov-Smirnoff test. I use a Student t-test for checking the similarity of two sets of distribution[1] (Press et al. 1993)

$$t = \frac{\overline{X_A} - \overline{X_B}}{S_D}$$

where S_D is the standard error of the difference of the means

$$S_D = \sqrt{\frac{\sum_{i\in A}(X_i - \overline{X_A})^2 + \sum_{i\in B}(X_i - \overline{X_B})^2}{N_A + N_B - 2}\left(\frac{1}{N_A} + \frac{1}{N_B}\right)}$$

The significance of this value of t for Student's distribution with $N_A - N_B - 2$ degrees of freedom is a number between zero and one, and is the probability that $|t|$ could be this large or larger by chance, for distributions with equal means. Therefore, a small numerical value of the significance (0.05 or 0.01) means that the observed difference is "very significant".

[1] I thank Attila Meszaros very much for fruitful discussion and for help about statistics.

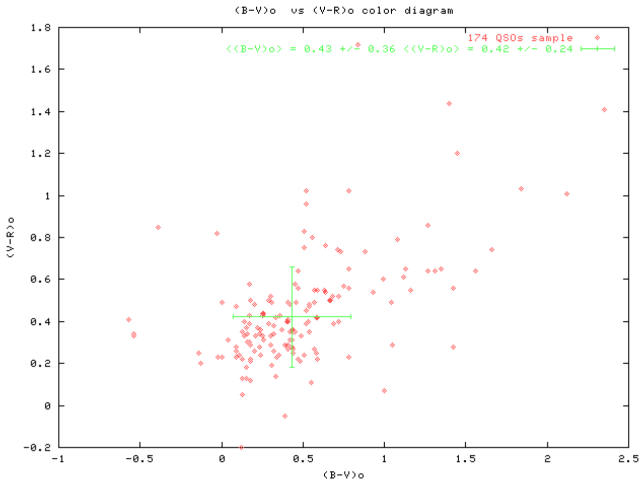

Figure 5.4: The $(B-V)_0$ vs $(V-R)_0$ color diagram

Color index	$\lvert t \rvert$
$(U-B)_0$	-
$(B-V)_0$	0.20
$(V-R)_0$	0.33
$(R-I)_0$	0.56

Table 5.1: Student t-test for the OAs and QSO color indices sample

In all cases the $|t| < 1$ so the differences are not significant. In the worst case of $(R-I)_0$ the probability that two distributions are the same is still much higher than 50% (even $|t| \leq 0.67$ for the probability higher than 50%).

The expected AGN – QSOs surface densities are $\sim 10-37$ deg^{-2} with limiting magnitude B and V about 20.5 and about 100 deg^2 for limiting magnitude B ~ 22.6 (Hudec 1999 and references therein). The probability of that the object with suspicious color indices is a QSO is $\sim 0.16 - 0.55$ for a typical errorbox ~ 10 arcmin^2 but for smaller errorbox it is less.

The analyse of correlation of colors of OAs and of QSOs-AGNs is important for two reasons.

- The typical colors of OAs according to (Šimon et al. 2001), are believed to be significant for searches for OAs even on single CCD images. However, the fact that also the QSOs and AGNs may exhibit not very different colors indicates that the analyses based on this must be much more careful and should take this into consideration. This also confirms that for independent optical searches for OAs related to (undetected) GRBs (orphan afterglows) the color data must be accompanied by (fading) time profile to be able to reliably confirm the true nature of the source.

- The searches for optical emission before the BeppoSAX era have revealed few cases where (historical) OTs have been detected at positions close

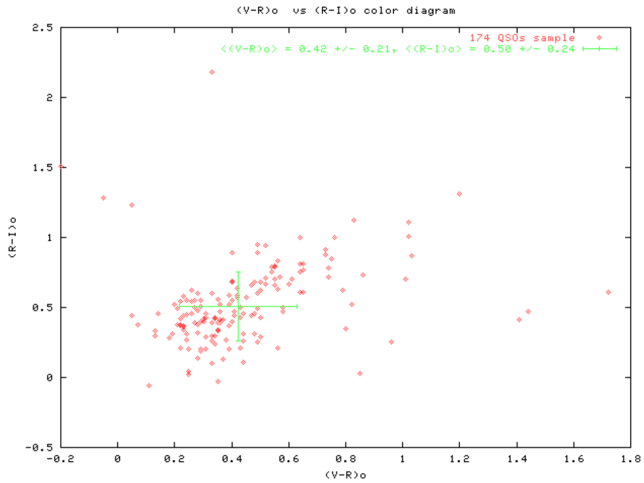

Figure 5.5: The $(V-R)_0$ vs $(R-I)_0$ color diagram

to the positions of known GRBs (Hudec et al. 1990). The detailed analyses of positions of these OTs with large CCD telescopes have then confirmed the presence of faint underlying objects with colors resembling those of QSOs-AGNs (Vrba et al. 1994, Motch, Hudec and Christian 1990), e.g. historical OT within the BeppoSAX errorbox for GRB 960720 the available color indices were $(U-B)_0 = -0.31 \pm 0.08$, $(B-V)_0 = 1.21 \pm 0.05$ and $(V-I)_0 = 1.36 \pm 0.02$ which fits to the QSO sample very well or OT 1809+31 $(U-B)_0 = -0.9$ and $(B-V)_0 = 0.0$ which at the boundary of the region. This has lead to the opinion that the QSOs-AGNs may exhibit very large amplitude optical flares with magnitudes exceeding mag 10. The comparison of colors of these objects with the colors of recent OAs and of host galaxies of GRBs has been never done. At least some of the sources found in the detailed search for orphan optical afterglows on the photographic plates (Levinson et al. 2002) made could have been misinterpreted. An example of misinterpretation is variable AGN SDSS J124602.54+011318.8 (probably the BL Lac object) thougth to be an orphan afterglow by mistake. Subsequent SDSS[2] imaging and spectroscopy showed that the point source declined or disappeared, revealing an underlying host galaxy at redsfift $z = 0.385$ (Gal-Yam et al. 2002).

- The emission mechanism may also have analogous physical processes ivolved as well as the influence of local environment (however much more effort would be necessary to confirm this and to discuss this in more details).

- GRBs and QSOs have a power-law spectrum dominating as expected. GRBs and QSOs so might have similar progenitor process and they differ in scaling only. It support the idea of an existence of a jet in GRB system.

[2]Sloan Digital Sky Survey (SDSS)

- The further studying the QSO with respect to GRBs could be very valuable.

5.3.6 Conclusion

The colors of the faint underlying objects found at the positions of the two historical OTs are as follows. For OT 1905, $(B-V)_0 = 0.40$ and $(U-B)_0 = -0.77$ (Vrba et al. 1994) and for OT 1946, $(B-V)_0 = 0.0$ and $(U-B)_0 = -0.9$ (Motch, Hudec and Christian 1990). These colors are consistent with colors of AGNs – QSOs but, at the same time, are not in contrast with the typical colors of OAs of GRBs as found by (Šimon et al. 2001). One can conclude that the colors of OAs are in agreement with colors of faint underlying objects at positions of historical OTs detected on archival astronomical plates and reaching amplitudes exceeding mag 10.

I discuss color indices of the host galaxies of GRBs in the chapter dedicated to host galaxies and star-forming regions.

Chapter 6

The supernova - gamma-ray burst connection

6.1 Brief introduction to supernovae

Introduction

Literally, a supernova is an exploding star. The star explodes in a massive explosion, resulting in an extremely bright and short-lived object that emits vast amounts of energy, typically as much as an entire galaxy. As well as visible light (i.e. optical radiation), supernovae emit huge amounts of various types of radiation: X-rays, ultraviolet, infrared, gamma rays, neutrinos, cosmic rays and radio waves. The remains of the matter that is exploded away from the star during the supernova is known as a supernova remnant. Supernovae were first proposed as a distinct class of objects in 1934 by the astronomers Fritz Zwicky and Walter Baade.

6.1.1 Supernovae taxonomy

Introduction

The taxonomy of supernovae is quite complicated. Astronomers use observational criteria, not theoretical criteria, to type supernovae. Type 1 supernovae do not have hydrogen lines in their spectral, but Type II do. Each Type is broken down into further subclasses, depending on their light curves, progenitors and location - type I into types 1a, 1b and 1c, and type II into types IIL and IIP (Cappellaro & Turatto 2000). But as with most other classifications, there are exceptions.

The majority of type II supernovae are split into II-L (linear) or II-P (plateau) subclasses, depending on their light curves.

Type I supernovae

Type Ia supernovae occur in a binary system, where one component is a white dwarf. The gravitational attraction of the white dwarf is so intense that it is capable of siphoning off material from its companion star. This causes the star

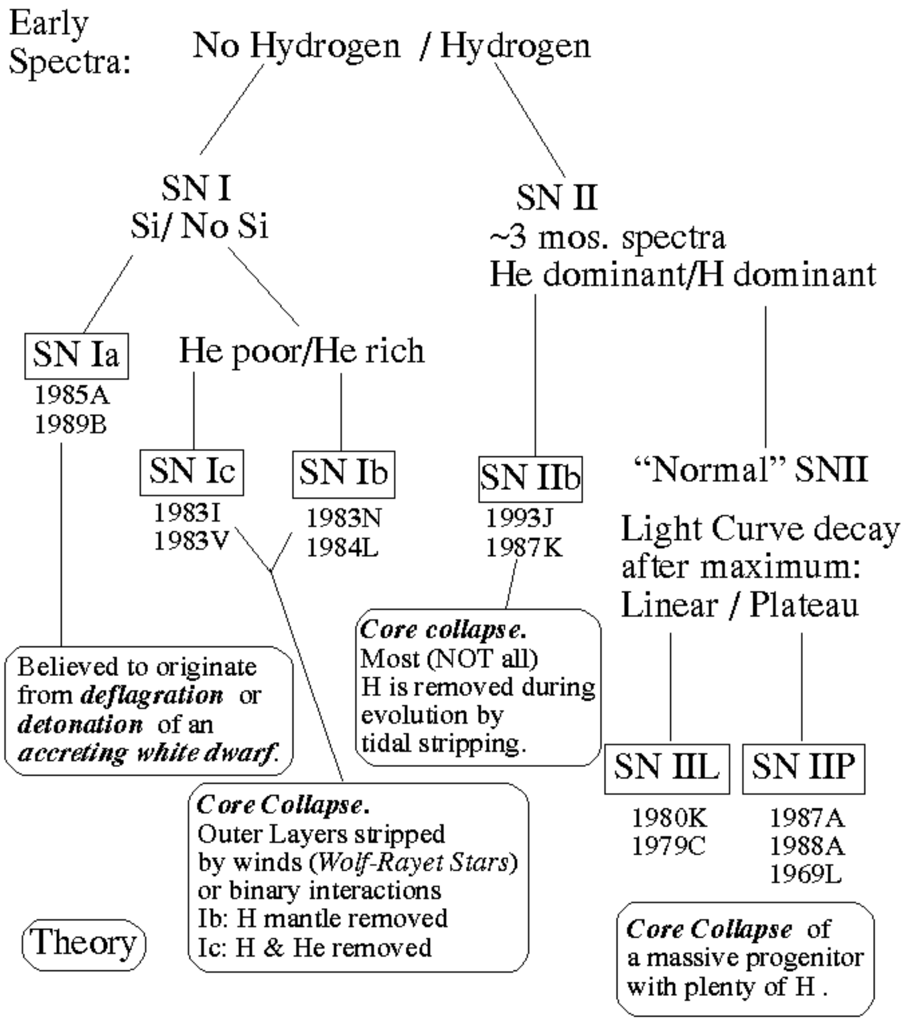

Figure 6.1: The supernovae taxonomy (List of SNe pages web site)

to exceed its limit of stability - the Chandrasekhar limit $1.4 M_{\odot}$ - causing it to go into thermonuclear instability. At this point, the thermonuclear incineration of the white dwarf ensues, although how exactly this occurs is unclear. Whatever the exact mechanics, however, the result is a massive explosion that produces an extremely massive outburst of energy, some 10^{51} ergs, with an absolute magnitude of about -19.5 (SAHA ET AL. 1997). The star blows itself, leaving nothing behind except a rapidly expanding remnant.

Type Ib and Ic supernovae are actually similar to type II supernovae (the type was named before astronomers better understood what these SNe were).

Type II supernovae

These occur when a high mass star ($\geq 8 M_{\odot}$) has no longer enough fuel for the fusion process in the core of the star to create the outward pressure which combats the inward gravitational pull of the star's great mass. When this occurs, the star will swell into a red supergiant ... at least on the outside. On the inside, the core yields to gravity and begins shrinking. As it shrinks, it grows progressively hotter and denser. This allows a new series of nuclear reactions to occur, forming new elements which in turn fuse to form further new elements, and so on. As these new reactions take place, the structure of the star becomes similar to an onion - there are shells of progressively less heavy chemical elements surrounding the core.

The silicon fuses into iron is the last exothermic reaction. Further converting of iron into i an endothermic reaction, which requires approximately 2 MeV per Nucleon. Thus, fusion halts, the core starts to rapidly collapse. Different parts of the core collapse at different rates, with the result that the inner core decouples from the outer core, leaving it behind. During the collapse, speeds can reach $7,000$ km s^{-1} in the outer core. This collapse of the inner iron core continues until the density there exceeds approximately $\sim \times 10^{15}$ g cm^{-3}. At this point, the material that now makes up the inner core stiffens (as a result of the nuclei of the atoms present becoming repelled by each other), and rebounds, sending pressure waves outwards into the infalling material of the outer core. These pressure waves, when they reach the local speed of sound, form a shock wave that starts moving outwards.

If the iron core is massive enough, the shock stalls, becoming nearly stationary, with infalling material now accreting onto it. At this point, the neutrinos now streaming from the core (due to the conversion of the iron core into essentially a neutron core) superheat the material beneath the shock wave; the resulting plumes of hot material push the shock wave outwards and allow it to continue its march toward the surface, driving all before it (as the shock). The total energy in the expanding material is in the order of 10^{51} ergs (or less). Vast amounts of photons are released, resulting in a spectacular optical display, giving an absolute magnitude of about -18. Due to the radioactive decay of heavy elements produced in the explosion, it then starts to slowly fade, at a rate of approximately six to eight magnitudes each year.

Type II supernovae are not as luminous as Type Ia supernovae, by a factor of at least three. The mechanics of this type of supernovae are dealt with in detail by (BETHE 1993, WALLERSTEIN ET AL. 1997, MEZZACAPPA 2000 AND LIEBENDOERFER ET AL. 2001).

If the mass of the core remnant is beneath about three solar masses, it will

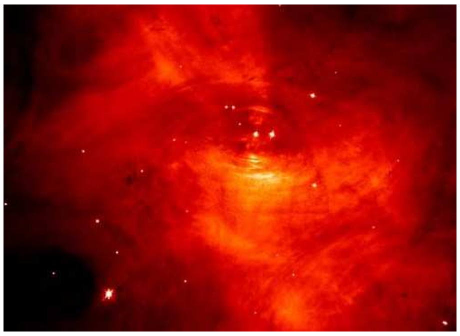

Figure 6.2: The pulsar in the center of Crab Nebula with a pulsation period of 0.0331 s. (HST WEB SITE)

become a neutron star (or a rapidly rotating neutron stars known as pulsars). If it exceeds about three solar masses, it continues to contract and collapses into a black hole (BALBERG & SHAPIRO 2001) accompanied by a tremendous production of neutrinos, the majority of which escape into space with a total energy of $\sim 3 \times 10^{53}$ ergs.

6.1.2 SN remnants

There are three generally accepted types of SNRs (PEEBLES 1997):

- **Shell-type remnants:** As the shock wave from the supernova explosion ploughs through space, it heats and stirs up any ISM it encounters, thus producing a big shell of hot material in space. A ring like structure in this type of remnant is seen because at the edge of the shell there is more hot gas in our line of sight than in the middle. The majority of SNRs are of this type.

- **Crab-like remnants:** These remnants, also known as "plerions"[1] are similar to the Crab Nebula. They are similar to shell-type remnants, except that they contain a pulsar in the middle that blows out jets of very fast moving material. These remnants look more like a "blob" than a "ring."

- **Composite Remnants:** These remnants are a between the shell-type remnants and crab-like remnants. They appear shell-like, crab-like or both depending on in what part of the electromagnetic spectrum one is observing them. There are two kinds of composite remnants – thermal and plerionic. Thermal composites appear shell-type in the radio wave band (synchrotron radiation). In X-ray wavelengths, however, they appear crab-like, but unlike the true crab-like remnants their X-ray spectra have spectral lines, indicative of hot gas. Plerionic composites appear crab-like in both radio and X-ray wave bands, however they also have shells.

[1]The term plerions was first suggested by (WEILER & PANAGIA 1978), and comes from the Greek word meaning "full".

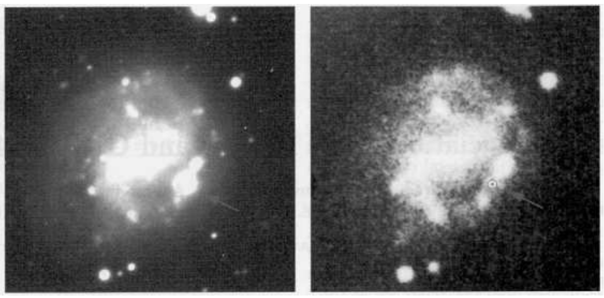

Figure 6.3: Left: NTT image (May 1998) of SN 1998 bw in the barred spiral galaxy ESO 184-G82. Right: Pre-discovery image from 1976 (UK Schmidt telescope, Australia) (Ramirez-Ruiz et al. 2000).

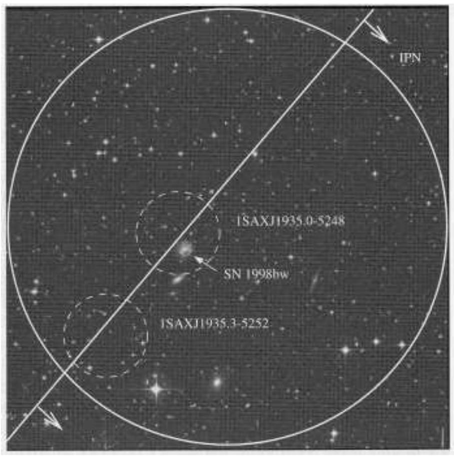

Figure 6.4: DSS image of the WFC error box of GRB 980425 (large circle with radius $8'$) (Galama 1999)

Their X-ray spectra in the center do not show spectral lines, but the X-ray spectra near the shell do have spectral lines.

6.2 Evidence for GRBs and SNe correlation

The first coincidence both in time and space between GRB and SN was the one of famous GRB 980425 and famous SN 1998 bw (Galama et al. 1998). It would imply that a subclass of GRBs is a hot candidate of a SN origin. But GRB 980425 was 100 times dimmer than typical GRBs. The characteristic scale derived from the variability of the gamma-ray time profile evolution is comparable to the size of the NS as well as the SN remnants. If I consider beaming than both the rate of GRBs and GRB energy reservoir is of the same order of magnitude. Also several GRBs show that the light curve of underlying SN could be fitted into the light curves of their afterglows.

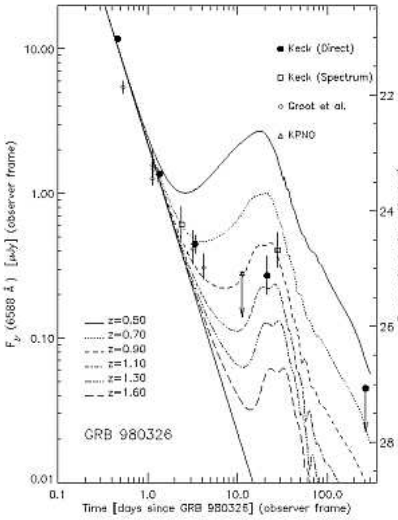

Figure 6.5: The R-band light curve of GRB 980326 (the sum of initial power-law decay with SN Ic light curve for redshift range $0.50 < z < 1.60$). The best fit for the SN is $z \sim 0.95$ and it is consistent with the observed spectrum of the burst. (GREINER WEB SITE)

Another reason for speculation that GRBs and SNe correlate is that possible identification of K Fe lines in the X-ray afterglow spectrum occurred. But in direct collapse of the central region of a very massive star to a black hole "hypernova", when an accretion disk is formed and an ultra-relativistic jet launched $0.5M_\odot$ of radioactive Ni is ejected. No evidence for Ni abundance was found, however.

Despite the lack of the exact understanding of the "normal" core collapse SNe and the mechanism which results into the ejection of the envelope there is an evidence that SN explosion could also be aspherical. As already mentioned in the previous chapter the direct evidence is polarization, HST image of SN 1997a, pulsar-like behavior of some SNRs, the discovery of magnetars (KOUVELIOTOU ET AL. 1998) a and theoretical modeling supports the correlation between jetted GRBs and SNe.

Both spectral data and light curves of SNII, SNIb/c suggest the core collapse with successively smaller H and He envelopes, but one cannot be sure about geometry of the expanding envelope. The unique tool to explore the asymmetry is polarization. The linear polarization of $\sim 1\%$ is typical for SN II. There is a trend for the observed polarization to increase in core collapse supernovae with decreasing envelope mass e.g. from SN II to SN c.

For the core collapse events type II and type Ib/c, all such events are polarized at about 1% level. The smaller the hydrogen envelope, the larger the observed polarization. As an example: SN 1987a with $10M_\odot$ envelope had a polarization of about 0.5%, SN 1993j or sn 1996cb with small hydrogen envelopes 0.1 $M_\odot$ were polarized at 1-2% level and type Ic SN 1997x which showed no

SN	Lines	Ejecta mass $[M_\odot]$	Polariz. [%]
1987a	H	10	0.5
1993j	H	0.1	1.5
1998bw	Si, Ca, H, K	2.0	0.5
1997x	no H little or no He (SN Ic)	?	several percent

Table 6.1: SN polarization level (HOFLICH ET AL. 2000)

hydrogen or helium was polarized at greater than 3% level (HOFLICH ET AL. 2000).

As we will see in the next chapter GRBs are supposed to be related to active star-forming regions (as well as SNe) mainly due to high extinction and reddening along LOS, supposed high column densities, blue broad-band colors of host galaxies and [OII] lines and an evidence for molecular hydrogen H_2 in the AG spectra. But color indices strongly suggest low density environment unlike to be expected in star-forming regions. There is no baryonic load in the GRB explosion. Moreover, there is no direct coincidence between well-localized SNe type II (believed to be a progenitor of at least one GRB class) and GRBs. SN 1998bw resembled type Ic in the sense that there was no obvious evidence for H and He, but it was different than the canonical type Ic SN. It was very energetic with 10^{52} erg and bright, it showed very large shell velocities $\Gamma \geq 2$ and it had a very bright radio source. Also Si II and Ca H K lines found in its spectrum were 30% to 50% higher at maximum light than in other SNe of this kind. The accidental alignment coincidence by chance probability is much less than 10^{-4}. In nebular spectra of SN 1998bw there are [OI] and [FeII] lines found comparable to the normal type Ic.

Not only GRB 980425 but also e.g. the light curve of GRB 980326 afterglow shows evidence for GRB/SN connection and a host galaxy of R-band magnitude 27^m was found (BLOOM ET AL. 1999). The redshift derived from the host galaxy spectrum is $z = 0.0085$, the reddening $A_V = 0.2$ mag if $H_0 = 70$ km s^{-1} Mpc^{-1}.

6.3 Well-localized gamma-ray bursts and supernovae correlations

(KIPPEN ET AL. 1999, HUDEC, HROCH & REZEK 1999) found no positive correlation evidence for time and space connection between SNe and any of precisely well-localized GRBs by BeppoSAX and RXTE with typical errorbox 4' derived from (GREINER WEB SITE) according to Asiago Padova SN catalogue (except the SN 1998bw case). 20 GRBs show non-isotropic distribution (mainly caused by non-isotropic monitoring of the sky by BeppoSAX satellite) were compared to 1443 SNe detected since 1885 with the precision of localization better than $1'$.

Since 1990 the systematic SN searches using modern instruments usually small and fast telescopes, covering a wide field or deep search in a small field with large (4m class) telescopes were conducted, there are more than 2000 SNe discovered.

Angular distribution of SNe is definitely not homogeneous because it is affected by galactic extinction and preferable directions where the observations are made with the expectation that SNe would origin at high rate in star-forming regions of close galaxies (HUDEC, HUDCOVÁ & HROCH 1999).

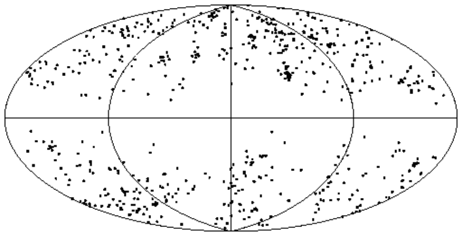

Figure 6.6: Angular distribution of historical supernovae in galactic coordinates

Two groups investigated the radial distribution of well localized gamma-ray bursts and type Ib/c supernovae in host galaxies with two completely different results. (TSVETKOV, BLINNIKOV, PAVLYUK 2000) found no correlations in the term of Kolmogorov-Smirnoff test.

6.4 Poor-localized gamma-ray bursts and supernovae correlations - Bologna work

6.4.1 Introduction

The sample of preciously localized afterglows is much smaller than number of all known GRBs. Thus I realized[2] to search for less accurately localized GRBs vs SNe correlation and take a look at the suspicious SNe and GRBs if they have some unique or common properties. Previous space-time correlation was started by (HUDEC, HUDCOVÁ & HROCH 1999) although not emphasizing the properties of the found SNe and GRBs. I can assume for a while that the found SNe and GRBs are possibly connected and they share their properties (e.g. none of BATSE GRBs has a known redshift but I can assume that the redshift of this GRB is the same as of the connected SN.)

6.4.2 Search for space-time correlation

The search for time - space correlation between the GRBs from 4B BATSE catalogue and SNe from Asiago Padova, UIC and SAI catalogue has been made. Time interval of ± 1 months (60 days) and 3σ criterium of determining whether a SN falls into a BATSE localization errorbox have been applied. The following 19 correlations have been found:

- **SN 1991x**
  $V \sim 13.8$ mag at the time of discovery (May 5, 1991), spectrum type Ia, around maximum on 1991 May 6, $z = 0.0088$, possibly related to

[2]Here I have to thank Graziella Pizzichini and Nicola Masetti from T.E.S.R.E, CNR in Bologna for help

GRB910423. (IAUC 5258, 5263; ApJS 92, 219)

- **SN 1991bg**
  $B \sim 14.75$ and $V = 13.96$ at the time of maximum (Dec 14, 1991), spectrum type peculiar Ia, $z = 0.0034$, possibly related to GRB911125. (MNRAS 283, 1; ApJS 92, 219)

- **SN 1992al**
  $B = 14.59$ and $V = 14.64$ at the time of maximum (Aug 3, 1992), spectrum type Ia, $z = 0.0145$, possibly related to GRB920708. (IAUC 5569; lightcurve reported in AJ 112, 2048)

- **SN 1993r** $R \sim 17$ mag at the time of discovery (Jun 2, 1993), spectrum type peculiar Ia (Iac), at an advanced stage on 1993 Jun 19 and probably near maximum at the time of discovery, $z = 0.0055$, weakly related to GRB930524. (IAUC 5812, 5818; A&AS 130, 333)

- **SN 1993w**
  $V \sim 18.5$ mag at the time of detection (Aug 18, 1993), spectrum type II, $z = 0.018$, near maximum on 1993 Aug 20, possibly related to GRB930807. (IAUC 5848, 5859)

- **SN 1993y**
  IIIa-J magnitude about 17 at the time of discovery (Sep 18, 1993); spectral type Ia, unknown redshift, 3 weeks past maximum on Sep 22, 1993 ; weakly associated to GRB9307025 (IAUC 5870)

- **SN 1993aa**
  $V = 17.5 - 18$ at the time of discovery (Sep 19, 1993); spectral type Ia, unknown redshift, 1 month past maximum on Sep 25, 1993; possibly associated to GRB930807. (IAUC 5871)

- **SN 1994g**
  $I \sim 21.8$ at the time of discovery (Feb 13, 1994), spectrum type Ia, about a week past maximum light on Mar 9-10, 1994, $z = 0.425$, possibly related to GRB940214 but SN was already exploded at least 1 day before this GRB. (IAUC 5956)

- **SN 1996bx**
  $R \sim 19.2$ at the time of detection (Nov 18, 1996), spectrum type Ia 3-4 weeks after maximum around Dec 10, 1996, $z = 0.058$, possibly related to GRB961029. (IAUC 6517)

- **SN 1997b**
  Unfiltred ~ 16.5 at the time of detection (Jan 13, 1997), spectrum type Ic, about 10 days after maximum on Jan 14, 1997, $z = 0.011$, possibly related to GRB961218. (IAUC 6535)

- **SN1997bz**
  $V \sim 17.5$ at the time of detection (Apr 27, 1997), spectrum type Ia, slightly more than one week after maximum on May 2, 1997, $z = 0.03$; possibly related to GRB970407 or GRB970408. (IAUC 6641)

- **SN 1997dq**
  Unfiltred ~ 15.0 at the time of detection (Nov 2, 1997), spectrum type Ib, near maximum on Nov 5, 1997, $z = 0.003$, possibly related to GRB971013. (IAUC 6770)

- **SN 1998bw**
  $V \sim 13.79$ mag at the time of maximum (May 13, 1998), spectrum type Ic, $z = 0.0085$, likely related to GRB980425. (Nat 395, 670)

- **SN 1999dg**
  Unfiltered mag. ~ 16.7 at the tme of discovery (Jul 23, 1999), spectral type Ia, within about 1 week after maximum on Aug 9, 1999 in UGC 9758, $z = 0.0218$, possibly associated to GRB990719. (IAUC 7229, 7239, AJ 107, 1629)

- **SN 1999dn**
  Unfiltered mag. ~ 16.0 at the time of discovery (Aug 19, 1999), spectral type Ib/c, shortly after maximum on Aug 21, 1999, $z = 0.0093$, in NGC 7714, possibly associated to GRB990810a, but SN might have exploded 1 week before the GRB. (IAUC 7245)

- **SN 1999ds**
  Magnitude $g' = 22.4$ at the time of discovery (Sep 6, 1999), spectral type II (uncertain), likely around maximum light at the time of discovery, $z = 0.350$, possibly associated to GRB990810a. (IAUC 7258)

- **SN 2000bu**
  $V = 19.4$ at the time of discovery (Mar 31, 2000), spectral type II (uncertain), near maximum at the time of discovery, $z = 0.05$, possibly related to GRB000319. (IAUC 7404)

- **SN 2000by**
  $V = 19.3$ at the time of discovery (Apr 7, 2000), spectral tpye Ia, near maximum at the time of doscovery, $z = 0.10$, possibly related to GRB000319.

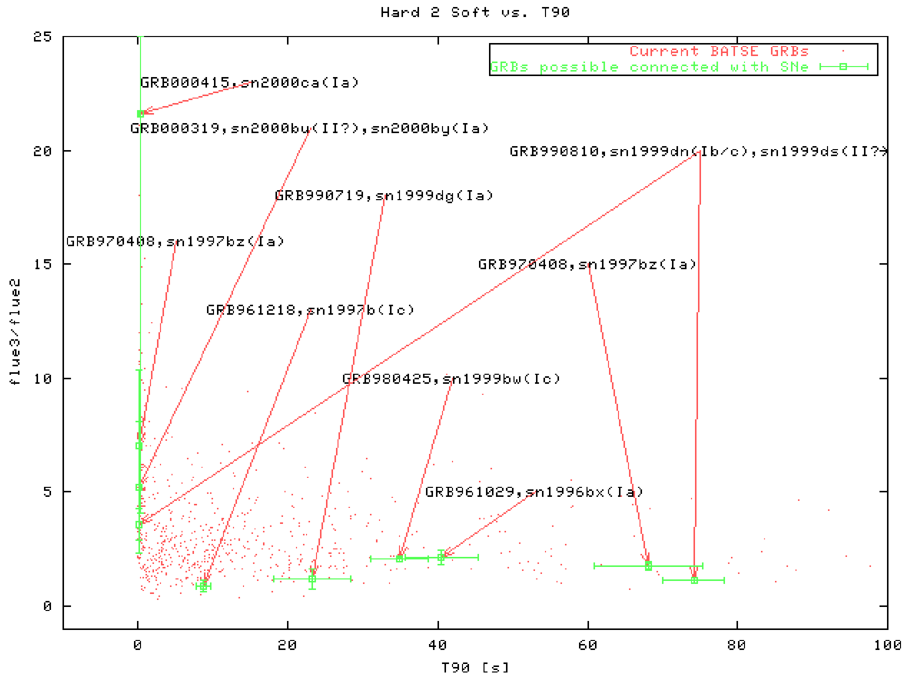

Figure 6.7: Hard to soft ratio vs T_{90} of suspicious (named) GRBs correlation.

(IAUC 7404)

- **SN 2000ca**
  B = 15.91, V = 15.99 one day after discovery (Apr 29, 2000), spectral type Ia, near maximum on Apr 29, 2000, in ESO 383-32, $z = 0.024$, possibly associated to GRB000415. (IAUC 7409, 7413)

6.4.3 Hard to soft vs T_{90}

The BATSE channel 3 and channel 2 were used as usually. T_{90} is defined as usual. All the data are taken from BATSE 4B catalogue. Distribution of T_{90} is an a good agreement with expected bimodal distribution of all BATSE GRBs, the only deviation is that there are few more longer bursts, but a sample of 10 GRBs possibly connected to SNe is not statistically reliable[3]. The cumulative distributive function (cdf) shows that there are more shorter than longer bursts among the suspicious GRBs.

Hard to soft ratio of selected bursts is also divided into two groups according to known anti-correlation between spectral hardness and burst duration with no significant deviation from the rest of the BATSE GRBs sample. The long GRBs possibly connected to SNe are generally softer than the majority of all of the long bursts from BATSE catalogue.

[3]The is a number of SNe which fall into one GRB errorbox

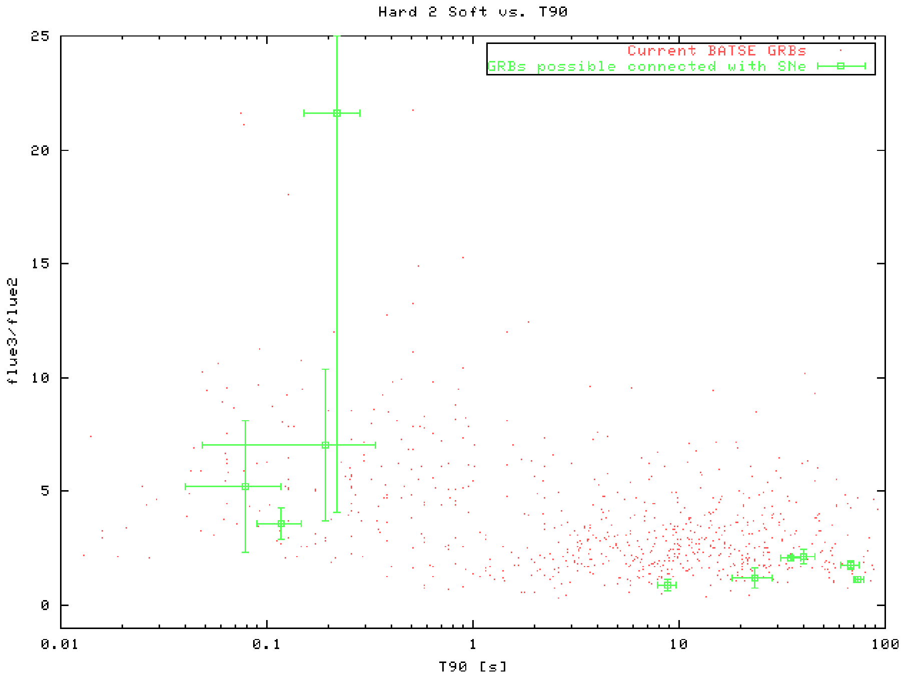

Figure 6.8: Hard to soft ratio vs T_{90} of suspicious GRBs correlation in log-scale.

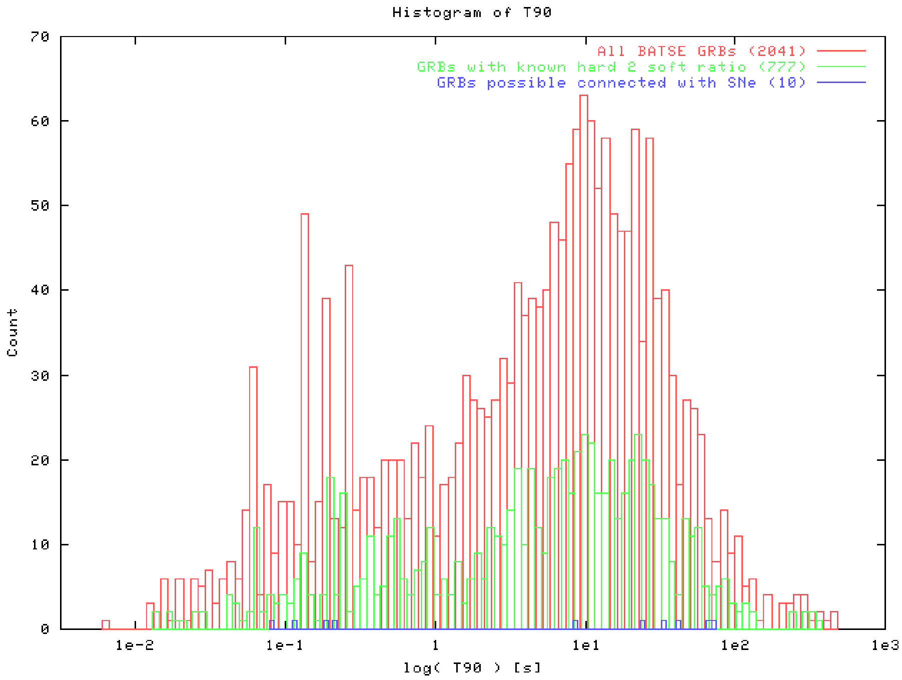

Figure 6.9: The histogram of T_{90} of suspicious GRBs.

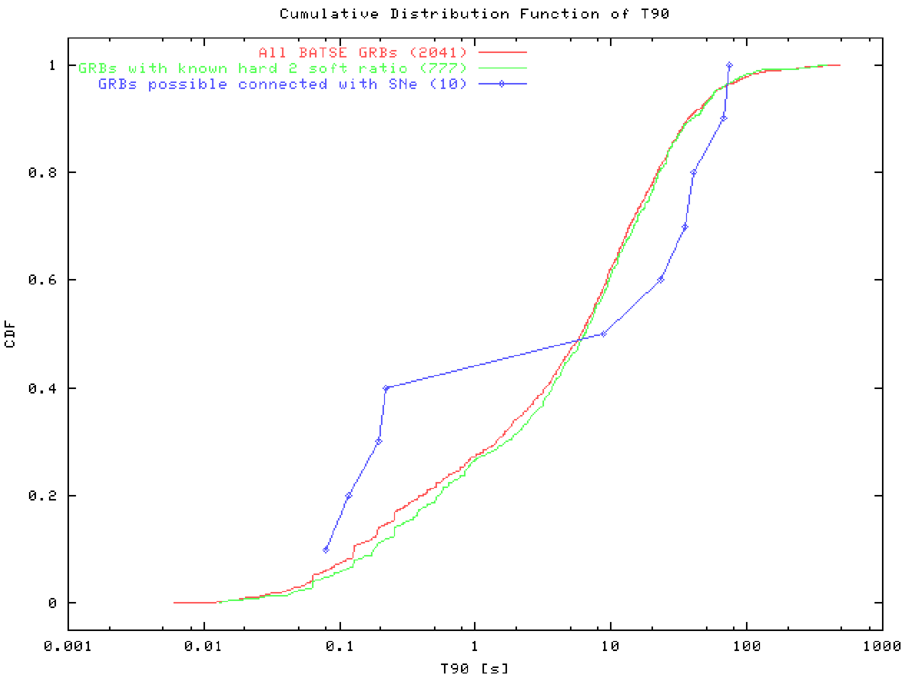

Figure 6.10: Hard to soft ratio vs T_{90} of suspicious GRBs cumulative distribution function.

6.4.4 Offset distribution

Because the redshift is not negligible in the following I compute a luminosity distance (WEINBERG 1972)

$$D_L = \frac{c}{H_0 q_0^2}[zq_0 + (q_0 - 1)(-1 + \sqrt{2q_0 z + 1})]$$

and I adopt the usual cosmological frame-work of standard model with $H_0 = 70$ km s^{-1}Mpc^{-1} and the deceleration parameter $q_0 = 0.5$. The result is not significantly sensitive on the chosen cosmological framework.

As will be clearly seen in the next chapter the offset distribution (i.e. the distribution of distances between the objects and the corresponding host galaxy centers) could strongly constrain the possibilities of GRB origin and location. Comparing it to the known distribution of offset typical for SNe I didn't find the suspicious SNe different from the rest. Because I don't know the inclination of the host galaxy I compute the projected radius only. These SNe are concentrated in the offset projection range of 1 to 3 kpc from the center.

A search for correlation of the peak flux of GRBs integrated over 1024 ms bins and the offset projection from the center of their (SN) host galaxies has been made.

Neither the plot of redshift vs offset projection of pinched out SNe shows any deviation from the rest of the sample of SNe.

The histogram of absolute magnitude of SNe implies that these SNe are not more or less energetic and hence more or less luminous than the rest of the sample.

The most interesting diagram is that of correlation between an isotropic energy calculated as

$$E_{iso} = \frac{4\pi D_L^2 F_\gamma}{1+z}$$

vs offset projection of the SN to the host galaxy. There seems to be an indication that SNe which are closer to the center are possibly connected with more energetic GRBs.

6.4.5 SN statistics

It could be useful to compare a fraction of SNe with a known type with the total fraction from the whole SN catalogue.

Total SNe with known types (TK): 897
Total SNe (TL) : 2051
Total SNe vs GRBs KNOWN[4] : 15

The total rate of type II/Ib/Ic SN estimated from their observed rate in the local Universe and the star formation rate as a function of redshift $R_{SN} = 2 \pm 5$ s^{-1} $\sim 3.8 \times 10^8$ y^{-1} in the observable Universe. The observed rate of GRBs is $R_{GRB} \sim 10^3$ y^{-1} (LAMB 2001).

[4](LEE 2000)

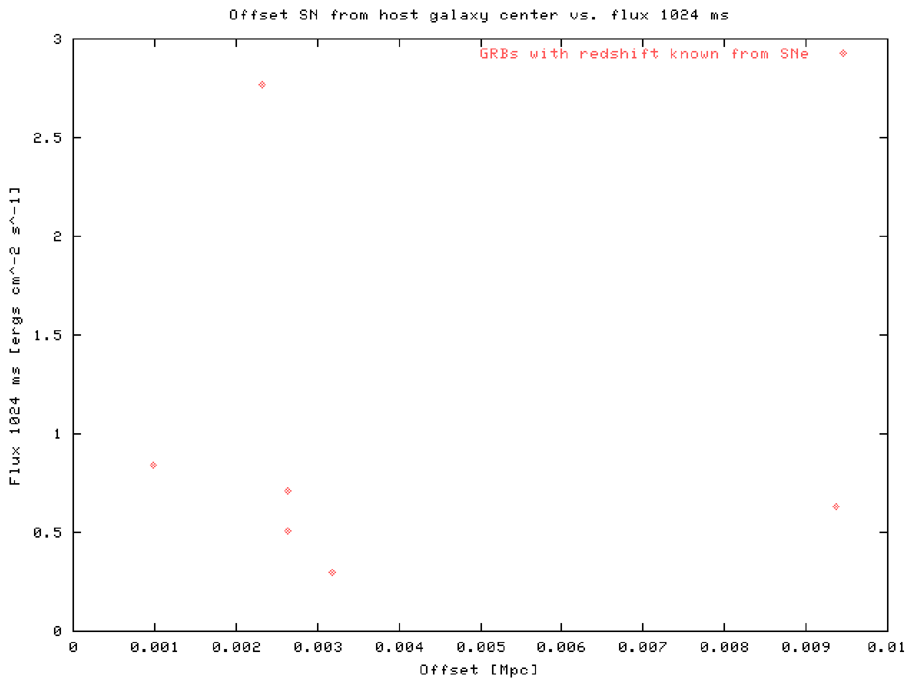

Figure 6.11: The BATSE GRBs Flux vs Padova SNe offset.

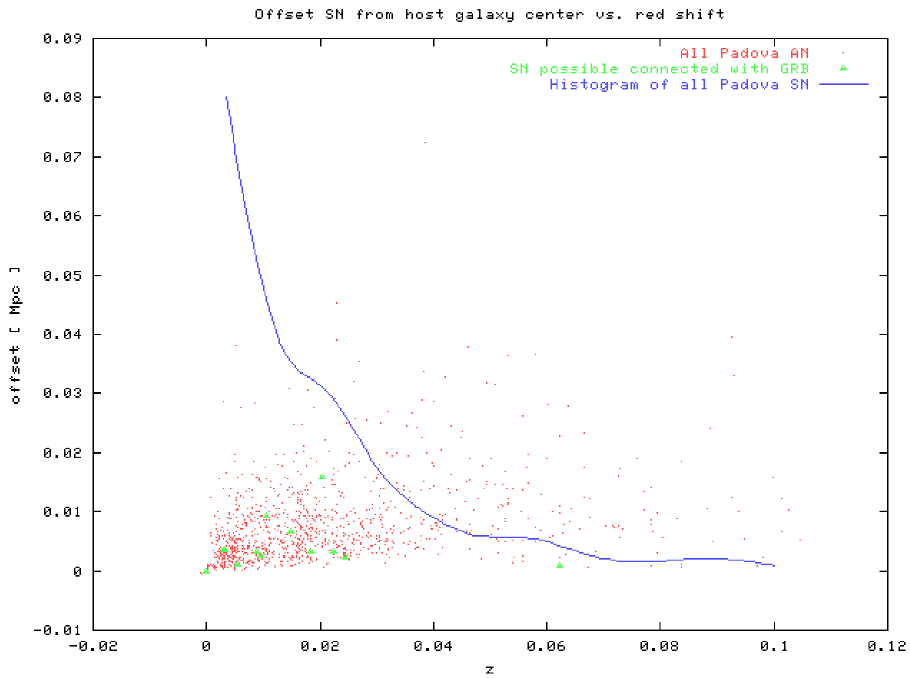

Figure 6.12: The redshift vs offset of SNe possibly correlated to GRBs

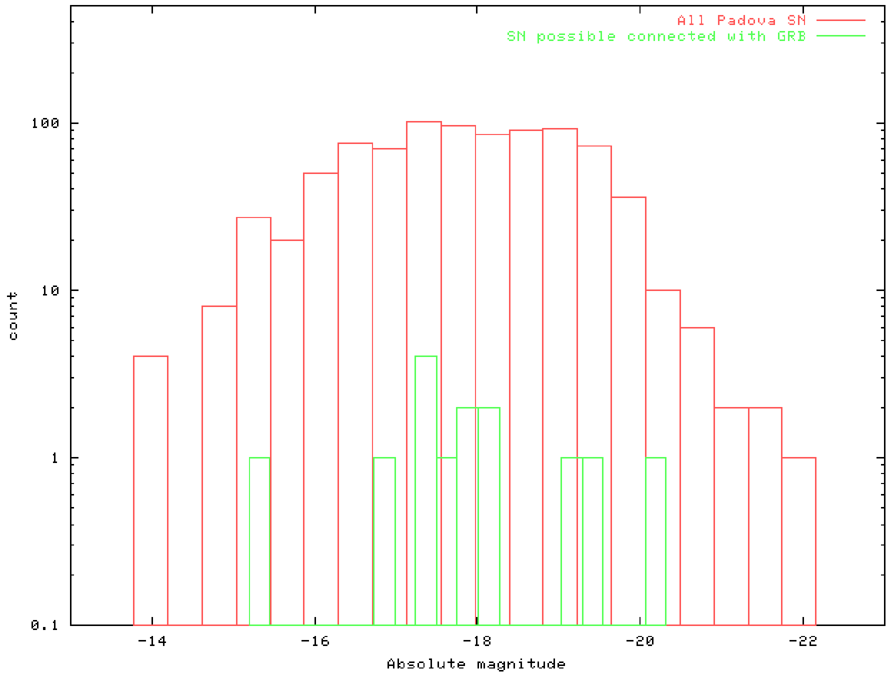

Figure 6.13: The histogram of absolute magnitudes of SNe possibly related to GRBs.

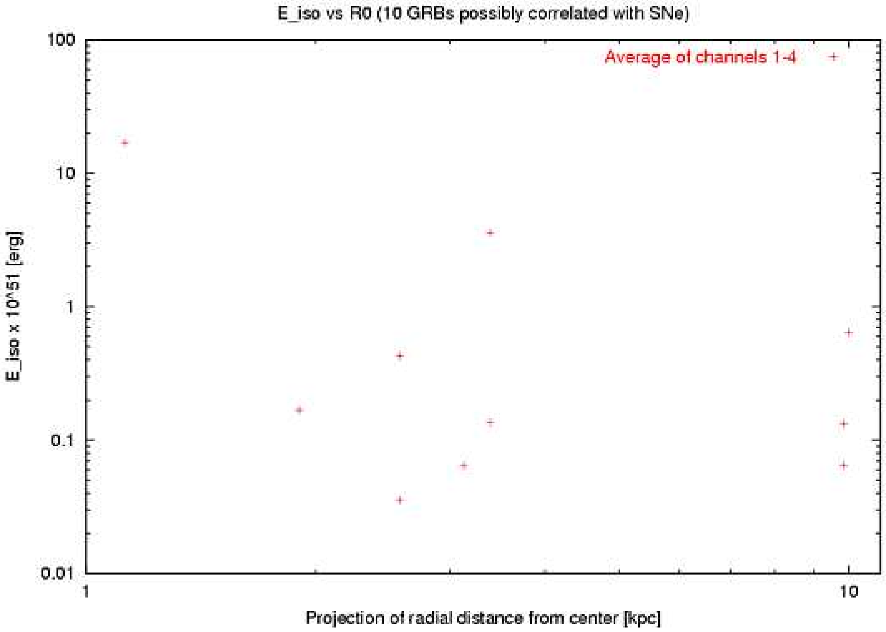

Figure 6.14: The correlation between an isotropic energy of GRBs and a projection of radial distance of SNe to the centers of their host galaxies.

SN types	**type**	**N**	**N/TK**	**N/TK***	**n**	**n/TK**
Ia, Ia?, Iap	Ia	503	0.561	0.50	7	0.467
Ic, Ic?	Ic	34	0.038	N/A	3	0.200
Ia/b, Ia, Ia?, Ib, Ib?	Ib/c	59	0.066	0.06	2	0.133
II, II:, II?	II	252	0.281	0.27	3	0.200
I*	I	583	0.650	0.66	N/A	N/A

Table 6.2: SN statistics of types

6.5 Conclusion

Remember that these SNe are only possibly connected to the GRBs. If I assume that the surface distribution of SNe from the catalogues is uniform (i.e. ignoring the observation preferences and lack of SNe in the galactic plane due to the galactic extinction) the probability of space correlation by chance is given by Poisson distribution

$$P_i = 1 - \exp(-\alpha_i)$$

where

$$\alpha_i = \pi r_i^2 \sigma(\leq m_i)$$

is the expected number of galaxies in a circle with an effective radius, $r_i = max[R_0, 3\sigma_{R_0}]$ and $\sigma(\leq m_i)$ the mean surface density of SNe up to the limiting magnitude m_i. In this case I study all the SNe from the catalogue regardless to their magnitudes, the dependence on a size of the errorbox is shown.

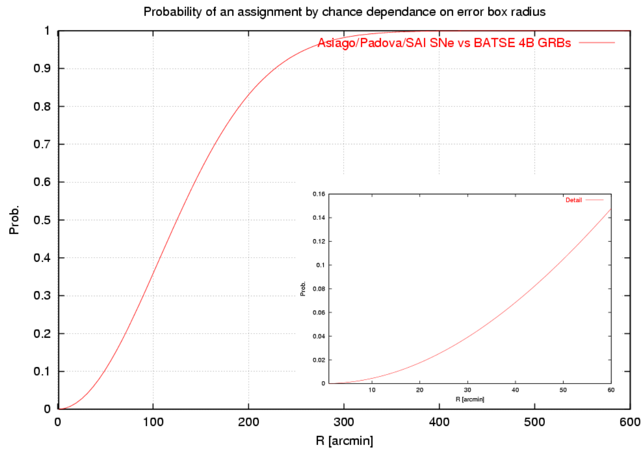

Figure 6.15: The probability of space coincidence by chance against the size (radius) of an effective errorbox.

The probability of space-time coincidence by chance over the time period of 30 days if assuming the typical BATSE of tens of arcmin, assuming the ratio of observed SN rate to GRB rate and the total number of GRBs and SNe in 4B BATSE catalogue and SAI and Padova/Asiago catalogues and integrated over the desired time period. I got the probability of $\sim 1.5\%$ that the space-time coincidence is correlated only by chance in an individual case. The number of found possibly related pairs is in an agreement with this value.

It means that only a fraction of all suspicious GRBs might be connected to suspicious SNe and vice versa. Thus the only possible way to prove an existing correlation if any is through the parameters. Unfortunately the whole sample of possibly correlated events is small so excluding one or two values from the set would break all the predictions and empirical laws.

Further progress of examining the parameters of possibly correlated SNe and GRBs seems to be worth and valuable especially after the launch of the Swift satellite in 2004 as well as further studying of a SN explosion mechanism. The Swift baseline fascinating predicted capabilities are (SWIFT WEB SITE):

- $\sim$ 1000 GRBs studied over a three year period
- 0.3–2.5 arcsec positions for each GRB
- Multiwavelength observatory (gamma, X-ray, UV and optical)
- 20–70 s reaction time
- Five times more sensitive than BATSE
- Spectroscopy from 0.2–150 keV
- Six colors covering 170–650nm

- Capability to directly measure redshift
- Results publically distributed within seconds

Analogues analyses may be much more important for the future evolution of (numerous and accurate) Swift GRBs.

The offset of AGs from HG centers suggest that there are two sub-groups: GRBs/SNe originating close to the galaxy center (1–2 kpc) and the second of about 10 kpc. The general believe that both GRBs and SNe are more often occurring in regions of active star-forming is with an agreement with this.

The result is that any of current 19 or less (when data are missing) SNe correlation with GRBs is not evidential.

The statistics of SN types shows several deviation from the sample of all SN but it is a statistics of small numbers in each group so one or two more values could break any debate.

Chapter 7

Host galaxies of GRBs

7.1 Introduction

The crucial upheaval came shortly after the detection of GRB 970228 by BeppoSAX which allows to localize the position of the burst to a 3 arcmin (radius). A fading X-ray (Costa et al. 1997) and optical (van Paradijs et al. 1997) counterpart was discovered. Ground-based observers also detected a faint nebulosity in the vicinity of the optical afterglow. Hubble Space Telescope (HST) imaging showed a presence of a distant galaxy ($z = 0.695$). More host galaxies (HGs) were found for further GRBs localizzed by BeppoSAX. Naturally the question that arises is whether are these often anonymous host galaxies of GRBs unusual or some way different from other galaxies. Note that BeppoSAX only detect a softer and long-duration subclass of GRBs (66%).

Generally a majority of known GRB redshifts so far comes from the spectroscopy of host galaxies, and some are based on the absorption line system seen in the spectra of the afterglows (which are otherwise featureless power-law continua). In some cases no OT is detected but a combination of X-ray and radio transient pinpoints the host galaxy. The X-ray spectroscopy uses redshifted Fe K line at ~ 6.55 keV or Fe absorption edge at 9.28 keV.

7.2 Color indices of host galaxies of GRBs

7.2.1 Introduction

The task is, similarly to the case of correlation between color indices of GRB OAs and AGNs/QSOs, to investigate color indices of GRB HGs. Unfortunately there is much less data than for QSOs because only a fraction of GRBs has a HG found and only a tiny fraction of these is observed in more than one or two filters (different from R-band).

I adopt a comprehensive collection of photometry data from (Chary et al. 1999). For comparing to GRB AG and AGN color indices there are only $(B-V)_0$ vs $(V-R)_0$ and $(V-R)_0$ vs $(R-I)_0$ available.

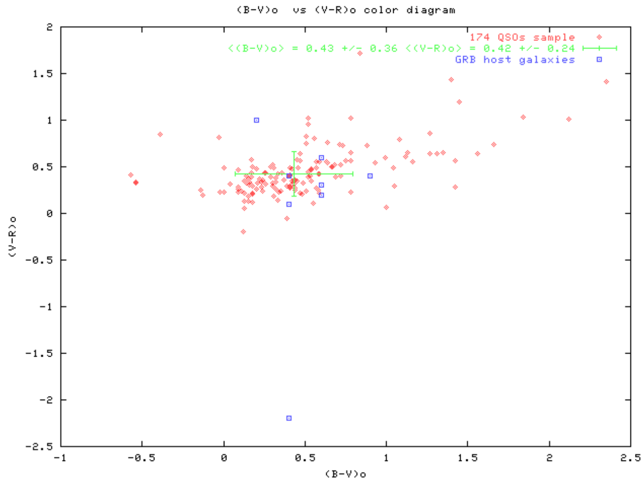

Figure 7.1: The $(B-V)_0$ vs $(V-R)_0$ color diagram of GRB HGs with respect to the QSO distribution (see Section 4 for better explanation)

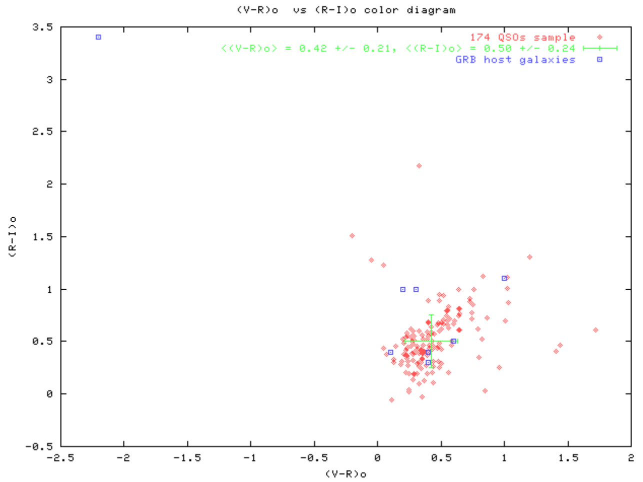

Figure 7.2: The $(V-R)_0$ vs $(R-I)_0$ color diagram of GRB HGs with respect to the QSO distribution (see Section 4 for better explanation)

GRB	z	B	V	R	I	K	Angular size [']
970228	0.695	26.4	25.8	25.2	24.7	22.6	0.8
970508	0.835	25.9	25.3	25.1	24.1	22.7	0.6
971214	3.418	26.8	26.6	25.6	24.5	22.4	0.4
980326				29.3		22.9	
980329				28		22.8	
980519				28	24.5	22.5	0.5
980613	1.097	25.1	24.2	23.8	23.4	21.7	2
980703	0.966	23.4	23	22.6	22.3	19.6	0.6
981220		24.6	24.2	26.4	23	19	0.7
990123	1.6	25	24.6	24.5	24.1	21.7	1
991208	0.706	25.2	24.6	24.3	23.3	21.7	0.1
000301C	2.034			28		23	

Table 7.1: Colors of host galaxies of GRBs (Chary et al. 1999)

7.2.2 Discussion and conclusion

There are only 8 HGs available in the $(B-V)_0$ vs $(V-R)_0$ and a different set of the same number of 8 $(U-B)_0$ vs $(B-V)_0$ color diagrams. This sample is too small to say that HG are correlated with either OAs or AGNs although the deviation of the sample (excluding the most excentric HG) from the OAs mean values are not too high. Most of them are bluer than an average galaxy (assuming galaxy as a average of the cluster of stars). This is in an agreement with the idea that the GRBs are associated with star-forming regions. I will discuss possible explanation and other hints for correlation between GRBs and star-forming regions in the following section. It also means that a small fraction of historical OAs possibly found e.g. (Vrba et al. 1994, Motch, Hudec & Christian 1990) in anonymous host galaxies could be related to GRB phenomenon but with high uncertainty.

7.3 Do GRBs originate in star-forming regions?

There are several pieces of evidence that GRBs are intimately linked with the deaths of massive stars. For long-burst afterglows localized so far, the host galaxies show signs of the ongoing star-formation activity necessary for the presence of young massive progenitor stars and a dense ISM:

- **Iron lines:** The presence of an iron lines feature was found (Piro et al. 2000).
- **Offsets:** Location of GRB in their host galaxies, at todays resolution is up to tens of pc at low redshift z = 0.1 so understanding of the local GRB environment waits for Next Generation Space Telescope (NGST). The popular idea that GRBs are linked with cataclysmic collapse of massive stars would imply that GRB in inner and outer parts of HG could be intrinsically different (Bloom, Kulkarni, & Djorgovski 2001). GRBs occur close to the birth sites of their short-lived progenitors and so their

evolution is likely to be affected only by local properties of the HG. Collapsars are expected to occur where massive stars are formed, in molecular clouds and H II regions, whereas merging binaries can merge a few to hundreds of kiloparsecs from their birthsite. Modeling of the location of merging binaries suggests that $\sim 1/3 - 1/2$ of all GRBs should occur > 10 kpc in projection from the centers of their host galaxies.

Bursts located closer to the center of their parent galaxies have smaller isotropic equivalent energies (or broader jets), and so progenitors in the inner and outer galactic locations may be intrinsically different. This could be the outcome of abundance gradients in the host galaxy (Ramirez-Ruiz, Lazzati & Blain 2002).

Models in which GRBs are produced during the collapse of massive stars must lead to a correlation of GRBs with star-forming regions. In the model of merging binary relativistic stars GRBs can occur far from formation regions of massive starts due to two kicks which deal a blow to the pair after a supernova explosion in the binary. The relatively small offsets of the centers of HGs and inside the star-forming regions argues against neutron star mergers, however the optical extinction is 10–100 times smaller than expected from the high column densities. This could be interpreted as an evidence for dust destruction along the LOS to a burst.

Burst	**z**	$E_{51,iso}$	**err**	R_0 **(kpc)**	**err**	$r_0(b)$	**err**	**Host** R^m
970228	0.695	22.4	2.50	3.266	0.259	1.37	0.25	24.6
970508	0.835	6.33	0.82	0.09	0.09	0.03	0.03	25.8
970828	0.958	249	21.7	4.05	4.33	1.63	1.80	24.5
971214	3.418	185	51.6	1.1	0.56	0.43	0.23	25.6
980613	1.100	5.67	1.0	0.78	0.67	1.37	1.57	26.1
980703	0.966	121	16.0	0.96	0.54	0.62	0.39	22.8
990123	1.600	3280	512	6.11	0.03	2.09	0.63	23.9
990506	1.300	874	144	2.680	4.144	2.47	3.96	25.0
990510	1.619	168	27.1	0.60	0.08	0.44	0.15	28.5
990705	0.850	270	20.2	7.17	0.78	0.79	0.06	22.8
990712	0.433	5.27	0.67	0.30	0.49	0.20	0.32	24.4
991208	0.706	147	19.8	1.51	0.75	0.60	0.35	24.4
991216	1.020	564	79.3	3.11	0.28	1.27	0.40	24.9
000301C	2.033	46.4	6.2	0.62	0.06	0.44	0.14	27.8
00041	1.119	297	99.0	0.20	0.56	0.07	0.19	23.9
010222	1.476	712	83.0	1.23	1.30	0.79	0.83	>24.0

Table 7.2: The HGs of GRBs. $E_{51,iso}$ is the isotropic, K-corrected equivalent energies (20-2000 keV), R_0 is the projected physical off set and r_0 the host-normalized offset (offset/half-light radius) (Bloom et al. 2001).

The GRB distribution differs from radial distribution of all types of SN. The SN distribution can be fitted by an exponential decline in density with a constant coefficient and agrees well with the surface-brightness distribution in the disks of spiral galaxies (Tsvetkov et al. 2000).

- **Strong OII emission** Host galaxies show signs of ongoing star formation necessary for the presence of young, massive progenitor stars. I expect OB

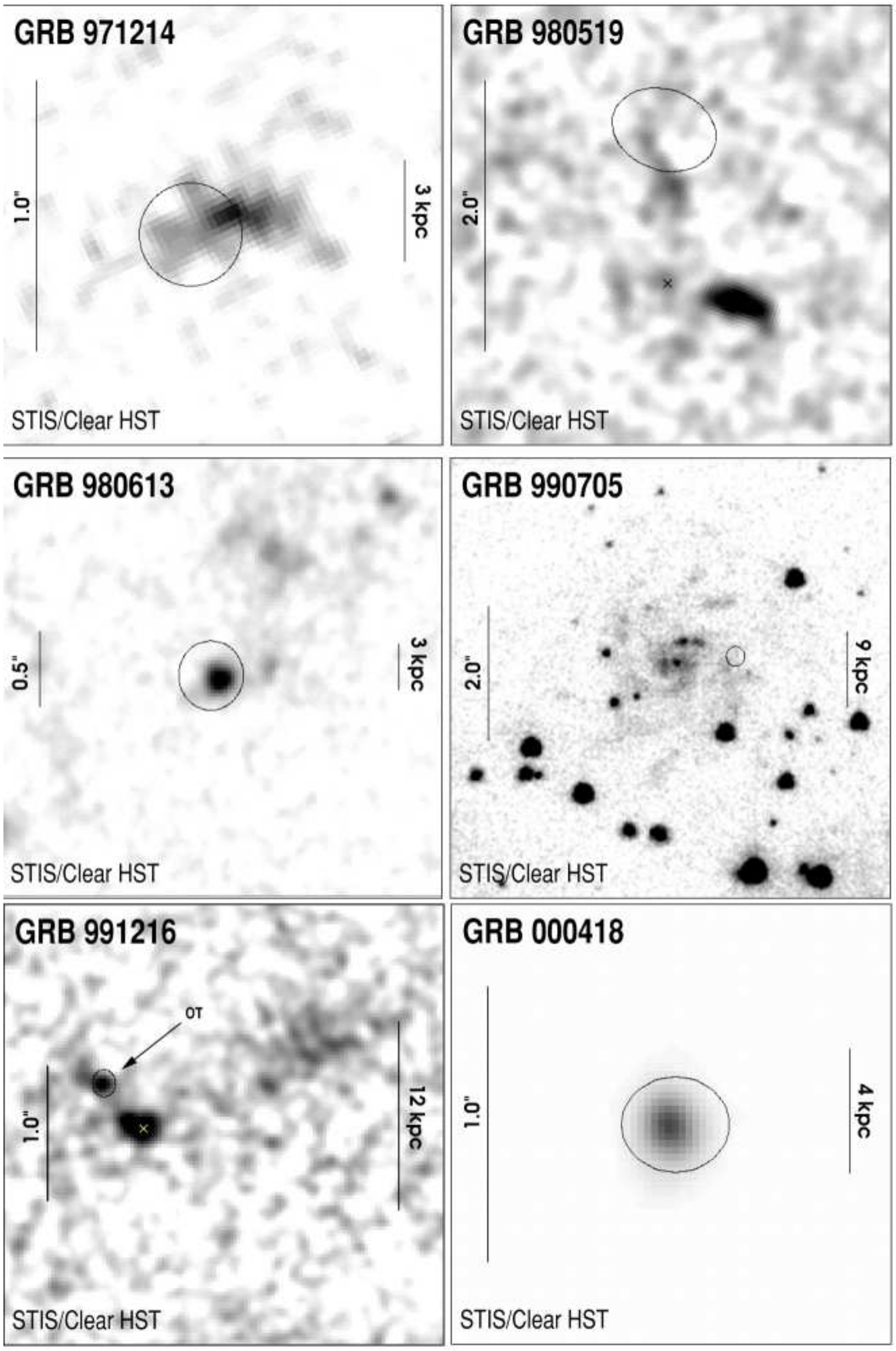

Figure 7.3: Examples of assumed GRB locations (error boxes) in their host galaxies (BLOOM ET AL. 2001)

association and H II shells correlations similarly to the local star-forming regions. High mass stars as O, B live for a short period (10^6 yrs). The same states for HII shells that were created by excitation of these massive and hot stars. The evidence for such an association of the [O II] 3727 doublet and high flux ratio of [Ne III] 3869 to [O II] (higher in the case of star-forming activity) was observed. The [Ne III] requires photoionization by massive stars in hot H II regions.

- **Underlying SN:** A sub-sample of light curves of the OAs of GRBs can be explained by adding the SN light curve to the fit, but no SN was observed. These GRB with a SN association are e.g. GRB 980425 (sn1998bw), GRB 980326, GRB 970228 appears to be overtaken by a light curve akin to that of SN 1998bw, similar associations show GRB 990712, GRB 980703, GRB 000418, GRB 991208, GRB 990510, GRB 000911. All of the nearest GRBs with measured redshifts show various degrees of evidence for a supernova in their AG. It could imply that there is at least a subclass of GRBs related to SN, that a SN doesn't manifest in the way of general expectation and that the cannonball model of GRB γ-emission and of afterglows which assumes in definition an underlying SN explosion could be correct.

- **Morphology:** The morphology of redshifted galaxies is well demonstrated in the Hubble Deep Field-North (Corbin et al. 2001). High redshifted galaxies appear to be more irregular at observed blue wavelength than at red because $z > 1$ galaxies have their rest-frame UV light, which os dominated by star formation redshifted to visible band. In addition extinction in the UV is much stronger than in visible, amplifying the irregular distribution of UV light. In the contrast, the rest frame visible light which is dominated by main sequence stars is redshifted into the K 2.2μm band.

GRB	**Galaxy type**
970228	Disk?
970508	Elliptical
971214	Irregular
980326	-
980329	-
980519	Interacting?
980613	Interacting
980703	Unresolved
981220	AGN?
990123	Irregular
991208	Interacting?
000301C	-

Table 7.3: Host galaxies morphology, (CDS Strasbourg web site)

- **High column densities:** The column densities in galactic-like clouds which are supposed to be universal and sufficiently high to make bursts dark at optical wavelengths, the sublimation of dust by the prompt burst emission or by the optical flash and fragmentation of dust by the burst and afterglow radiation can leave a comparable number of optically detected bursts - the bursts which are sufficiently near the Earth-facing side of the cloud and/or in sufficiently small clouds.

(Galama & Wijers 2000, Reichart & Price 2002) consider equilibrium of diffuse clouds uniformly magnetized, isothermal and non-rotating (only with small corrections $c_1 = 0.53$ and $c_2 = 0.60$ from these assumptions.) Clouds of $R > R_m$ are unstable to gravitational collapse if

$$\frac{GM^2}{R_m^4} = \frac{25/p_m}{1-(M_c/M)^{2/3}}$$

here

$$M = 4\pi\rho R_m^3$$

is he mass of the cloud, $\rho = \mu_H m_H n_H$, $\mu_H = 1.87$ is the mean molecular weight per hydrogen atom,

$$p_m = \frac{3.15c_2(kT/\mu)^4}{G^3M^2[1-(M_c/M)^{2/3}]^3}$$

T is the temperature of the cloud, $\mu = 1.44$ is the mean molecular weight,

$$M_c = \frac{0.023(c_1B)^3}{G^{3/2}\rho^2} \simeq 10^4\left(\frac{B}{1\mu\mathrm{G}}\right)^3\left(\frac{n_H}{1\mathrm{cm}^{-3}}\right)^{-2}M_\odot$$

where B is the magnetic field within the cloud. Typical values are 10 and 100 K, $B = 3\mu$G or $T = 30$ K and $B = 1$ or 10μ G. The most galactic clouds in Galactic ISM have temperature of 10K $< T <$ 10 K and $B = 3\nu$G.

Using X-ray to optical absorption ratio they found an evidence that column densities in GRBs environment are in a range 10^{22}–10^{23} cm^{-2} which is right around the average of giant molecular clouds and they estimated the cloud size to be $10-30$ pc, implying masses of $\geq 10^5 M_\odot$.

- **Dark bursts:** They show a strong absorption of UV and optical emission of the flash and afterglow of a GRB, unless the optical peak flash has a peak isotropic luminosity $L_{peak} \geq 10^{49}$ erg s^{-1}, otherwise the dust will radiates as a black body on rest-frame wavelength of about 8 μm (Venemans & Blain 2001). This means that the lack of observation a prompt optical transient is OK, as well as dark bursts.

  While nearly 90% of GRBs observed in the X-ray by BeppoSAX showed XA about 60% of them have not manifested OAs. This could be due to the absoption at the source location but only if the hard X-ray emission doesn't destroy the dust responsible for absorption in the optical band. If the dust is efficiently destroyed it could imply that a class of GRBs with X-ray but with no detectable optical afterglow may be of different nature. Dark bursts are the well-localized bursts with no OT despite deep and rapid searches. The "dark bursts" is e.g. GRB 970828. A possible explanation is that the burst is obscurred by dust in their HG or bad geometry arrangement in the host.

An IR afterglow without an optical counterpart would prove the correctness of this assumption. But there is no direct evidence for a such event. The other way out is that the fireball model is wrong or the shock blast wave reversing into the ejecting material and believed to cause synchrotron emission of an optical afterglow fails to rise.

Also a very red afterglow of GRB 000418 as a further evidence for dust extinction in a GRB host galaxy was observed (Klose et al. 2000) with $(R-K)_0 \sim 4^m$.

To convert column density into dust absorption I adopt the dust to gas ratio from (Predehl & Schmitt (1995))

$$A_V = \frac{N_H}{1.79 \times 10^{21} \mathrm{cm}^{-2}}$$

The problem is that the wavelength is stretched by redshift $\lambda = \lambda_{obs}/(1+z)$. (Lazzati et al. 2000) assume an average redshift of afterglows $z = 1$ and got

$$A_R(z=1) = 1.31 A_V$$

Note that about 60% to 80% of prompt and well-localized GRBs have AGs fainter than 24 mag 18 hrs after the burst. The other possibile explanations of dark bursts avoiding a dusty environment are:

- Dark bursts are intrinsically different.
- The absence of detectable optical flux accompanying strong X-ray emission in the 2-10 keV BeppoSAX energy band may simply be due to the strong redshift dependence of dust obscuring at optical wavelength in comparsion to the X-rays, i.e. $\tau_{opt}/\tau_{x-ray} \propto (1+z)^4$ (Ramirez-Ruiz et al. 2001).
- BeppoSAX instrument selection.
- A large fraction of GRB occur at $z \gg 5$ and so are optically invisible due to Lyman α absorption by intervening systems. But so high redshift is unlikely in so many cases.

7.3.1 Discussion and conclusion

Caveats

Although the long play-list of indirect pieces of evidence there are still caveats and misconceptions in the question of the GRBs star-forming regions correlation:

- **Recurrence:** The suggested association of GRBs and SFRs allows to consider the possible recurrence of the GRB triggers in the sense of triggers occurring in the same SFR i.e. in the same galaxy but at different times. I expect more deaths of massive stars, moreover GRBs are supposed to act as star-forming activity triggers. This may explain the possible recurrent OTs observed on astronomical archival plates at positions close to the positions of known GRBs (Vrba et al. 1994, Motch, Hudec and Christian 1990).

- **Selection effect:** However if GRBs originate in dusty environment we should observe the whole range of extinction due to the selective effect. This doesn't correspond to observational data, there are only nearly unextinct or highly redden afterglows. A dust destruction mechanism can be responsible for this.

Galaxy evolution

I suggest a new approach to the GRB vs star-forming region correlation. Let try to guess the evolution of galaxies and search for star-forming regions of close galaxies in local universe with respect to that there was a time period in their evolution when they could have been the hosts of GRBs (galaxies in latter phase of evolution that have passed the star-formation activity in the past). Observations using HST deep field could be made aiming to check GRBs host galaxies and compare them. A galaxy evolution should be considered. The problem is that the majority of GRB HGs of earlier times pre-spiral galaxies are irregular or even merging and a prediction of their evolution is problematic.

Tracing down the SFR history of galaxies through their chemical properties (CONTINI ET AL. 2001) as clues for star-burst activity could be a way out. Emission lines from HII regions have long been the primary means of chemical diagnostic in local galaxies, but this method has only recently been applied to galaxies at cosmological distances. A solution could be in studying a ratio of N/O against a O/H ratio.

7.3.2 Gamma-ray burst remnants

Introduction

Another valuable source of information about the GRBs is a studying of GRB remnants (GRBR). What will be left after an apocalyptic explosion? What is the nature of GRBRs and how could we observe them? The generalization of the theory of supernova remnants is needed.

Shells around SNe and GRBs

The ISM is heated by the propagating shock wave and the radiation and starts cooling. How to distinguish GRBR from other emitting regions such SNR (CHEVALIER & LI 1999, CHEVALIER & FRANSSON 2001), HII regions, etc. also with high [OIII] or a ratio of [OII] to Hβ.

The interstellar turbulence plays a role only after slowing to 10 km s^{-1}. For a uniform medium of density $n_1 \sim 1$ cm^{-3} and an energy $\sim 10^{54}$ ergs deposited in the gas, this will happen at radius

$$R_{kpc} \sim 0.7 E_{54}^{0.32} n_1^{-0.36}$$

or in terms of elapsed time at

$$t \sim 2.1 \times 10^7 E_{54}^{0.32} n_1^{-0.36} \mathrm{yr}$$

Combining this timescale with GRB rate per galaxy we get that there should be $\sim 10^1$ GRBRs at given time in every galaxy. Maybe it has something to do with HI supershells in spiral galaxies derived from the 21 cm surveys but larger

≥ 1 kpc than typical post-SN shells. But there are more common explanation of HI supershells by OB association winds or multiple SN explosions (Loeb and Perna 1998).

X-ray and UV components of the afterglow radiation create an ionized bubble of radius ~ 100 pc $n_1^{-1/3}$ in the surrounding galaxy, where n_1 is the ambient density. Cooling times are typically very long

$$t_{cool} \sim 10^5 (T/10^5 K)/(n_e/1\ cm^{-3})\mathrm{yr}$$

at a temperature T and an electron density n_e. If GRBs occur in galaxies then their rate is estimated to be $\sim 10^6 f_b$ yr^{-1} per galaxy, where $f_b \leq 1$ is the unknown beaming factor.

Discussion and conclusion

I would suggest that the way to distinguish between these possibilities could be in spectrography, since there should be recombination lines in higher ionization energies associated to gamma-ray and X-ray emission not common in OB association or SNe.

However there are several serious points of complication that would erase the asymmetry:

- **Transversal evolution:** Even if a GRB explosion is initially beamed, the asymmetry of the blast wave in the ISM will be erased after long enough time period (lower boundary for $\Gamma \sim 1$)

  $$t_{iso} \sim 10^4 \times \left(\frac{E_{52}}{n_1}\right)^{1/3} \mathrm{yr}$$

  However the blast wave of non-relativistic ejecta still would moderate the initial asymmetry as soon as it decelerates to subsonic speed.

- **Inhomogeneous ISM:** External anisotropies of ISM also play a crucial role. (Ehlerová, Efremov & Palouš 1999) showed that pressure and density gradient in the galactic disk plays a crucial role in creating asymmetric prolonged shells. Smaller shells with radii $\sim 200 - 400$ pc with smaller energies are often explained as a consequence of the collective action of stellar winds and supernova explosion, originating from hot OB star associations.

  After the shell has expanded to a size comparable to the scale height of the galactic disk its upper part accelerates and become Rayleigh-Taylor unstable and "blow up". It escapes from the interior to exterior (to the halo). The shell then fragments. Surviving filamentary pieces are called "galactic worms".

- **Bubble merging:** Also a bubble merging adds an additional hardly predictable effect.

- **Galactic rotation:** The galactic rotation effect will be disruptive and will deform the shell through centrifugal forces.

Thus observing shapes of bubble shell remnants could not identify the presents of a GRB in the past for a certainty. Additional data from new era satellites Next Generation Space Telescope and Swift will be very valuable. The late phase of the blast wave expanding into ISM would result in a cool HI shell expanding at a velocity

$$V_{sh} = 4.5 \text{ kms}^{-1} E_{54}^{0.71} n_1^{-0.80} R^{-2.2}$$

in an ISM ambient gas of $n_1 \sim 1\ cm^{-3}$, comparable to that in spiral galaxies, E is the initial energy and R the shell radius. The material is expected to decelerate down to 10 km s^{-1} at a radius

$$R_{kpc} = 0.7 E_{54}^{0.32} n_1^{-0.36}$$

after a time of

$$t = 0.31 R/V_{sh} = 21 E_{54}^{0.32} n_1^{-0.36} \text{ millionyears}$$

If I assume GRBs to be non-evolving population and neglecting all the caveats I expect an asymmetric shell from a GRB once per $\sim$ 40 million years per L_* galaxy and a mean lifetime of this GRB remnant of $\sim$ 10 million years. It implies $\sim$ 1 observable remnant per galaxy. If GRBs are beamed they illuminate only a fraction of the sky given by $f_b = 1 - \cos\theta$ where θ is the beaming angle, the rate should be higher by this factor and isotropic energy equivalently lower.

A direct count measurement of GRB remnants per galaxy in the local Universe could determines the values of f_b and the efficiency of the explosion ϵ defined as $E_{54} \sim 10 \times (\frac{\epsilon}{1\%})^{-1}$.

But things are not as bad as seemed. The identification could be made by investigating the inner parts of the shell. The difference between HI shells created in connection to GRBs and HI shells formed around OB associations is that there is no stellar cluster inside a supershell or inside an arc of young OB stars in GRBR neither there is an evidence of HVC (High Velocity Clouds) and/or neighboring galaxies. Moreover there is no hot gas inside the shell, even in the case of a young supershell (Ehlerová & Palouš 2001).

Chapter 8

Dust destruction

8.1 Introduction

Why do we see an optical afterglow only in a fraction of GRBs? The most natural explanation of it is because they are obscured by dust in their host galaxy, the second less likely explanation is that there is no ISM dense enough to produce an afterglow on a very large scales. I don't believe in the latter because already philosophers are in an agreement with astrophysics and say that there is more something than nothing (void).

There are more than 52 detected well localized GRBs when a deep search for OT could have been done while good weather conditions. Only 27 out of them were found. It gives that the rest 48% is hidden.

In the previous chapter I have discussed that I wonder why the majority of bursts OAs shows a low extinction and that there is only a small variability in reddening of OAs. If I assume a random depth of GRB in the ISM in the star-forming region a plenty of reddening should be observed with continuous distribution. This could be explained through a dust destruction along the LOS in the host galaxy. The dust can be destroyed by hard UV and X-ray radiation where the cross-section for photons to interact with dust grains is the largest. There is however a lot of GRBs with XAs as detected by BeppoSAX and RXTE (Greiner web site).

The dust destruction is considered along the LOS thus the mechanism is independent of any GRB collimation or beaming.

8.2 GRB X-ray emission

I will consider the destruction by X-rays only. The X-ray emission of the long bursts is divided into two parts: a short 1–100 s pulse coinciding with gamma-ray burst itself and a longer, smooth decline X-ray afterglow. Shorter afterglows (< 1 s) drop below the BeppoSAX resolution. During the burst the X-ray flux in the 0.3–10 keV is strong and hard with spectral index α between -1 and 1. The maximum of the emitted X-ray energy of the burst could be above 100 keV. Then it decays and the XA is observed with a typical slope of the power-law spectral index $p \sim 2.3$.

The peak X-ray flux occurring in the X-ray afterglow of a GRB is about $\sim 10^{-6} - 10^{-7}$ ergs cm^{-2} s^{-1}. At the time of the trigger ($t = 0$) the X-ray emission could be even stronger.

8.3 Dust destruction mechanism

The fundamental interaction between X-ray and dust grains is the K-shell photoionization of medium-Z elements. Dust grains can absorb optical or UV photons through a variety of continuous opacity mechanisms. X-rays (rest frame 0.3 – 10 keV) are primarily absorbed by K shell ionization of medium-Z elements such as C, Si, O, Mg and either K-shell or L-shell photoionization of Fe.

When K-shell photoionization occurs, a fast electron is created with an energy equal to the difference between the absorbed photon energy and the ionization threshold for the relevant shell. Then the atom relaxes by either Auger ionization (which results in a second fast electron with energy slightly less than the initial ionization threshold) or fluorescence. For medium-Z elements the Auger ionization dominates. As these fast electrons travel through the grain, they lose energy by Coulomb scattering. It produces a cascade which slows down quickly, only a very energetic electron (300 keV – 1 MeV) gets far (Draine & Hao 2001)

$$R \simeq 0.03\rho^{-0.85} E_{keV}^{1.5}\ \mu\mathrm{m}$$

where ρ is a density in g cm^{-3}. Thus for a grain of size of $\sim 0.1\ \mu$m and ISM only electrons of energy ≥ 1 keV or produced close to the grain surface ca escape. Electron Coulomb scattering also breaks chemical bonds, weakening the crystal structure of the grain.

Two principles are responsible for the dust destruction: the grain heating and the grain charging (Fruchter et al. 2001).

8.3.1 Heating and sublimation

The immediate result of massive X-ray photoionization is the heating of an individual grain at rate

$$G \sim 3{\times}10^{-3}\frac{T_h(x_K,\alpha,N)}{2+\alpha}\frac{E_{51}\sigma_{-19}n_{23}}{D_{100pc}^2}\frac{a_{0.1}^3}{t_{10}}x_K^{1-\alpha}[1-(1+x_{min}/x_{keV})^{-(2+\alpha)}]ergs^{-1}$$

where the grain is assumed to be optically thin to the X-rays. E_{51} is the total energy radiated in X-rays $4\pi\epsilon E_\epsilon/d\Omega$ evaluated at $\epsilon_0 = 1$ keV and $dE/d\Omega$ is the energy radiated per unit energy per solid angle. σ_{-19} is the K-shell edge cross section, n_{23} atomic density in the grain, x photon energy, $a_{0.1}$ grain size in 0.1μm, t_{10} characteristic time, D_{100} distance GRB to the dust, α spectral energy index $E_\epsilon = e^{-\alpha}$, N hydrogen atom column density along the LOS, x_{min} minimum energy of electrons able to escape from grain. T_h describes the transparency of ISM (between the burst and the dust) to X-rays.

For saving the space let define modified fluence

$$A \equiv \sigma_{-19}n_{23}E_{51}D_{100}^{-2}$$

$\sigma_{-19}n_{23} \sim 1$, the exact value depends on chemical composition (O, Si, Mg ~ 2, graphite ~ 17).

Two processes balance the heating: cooling and sublimation. The rate of radiation cooling per grain is $4\pi a^2 \times \pi \int Q_a B_\lambda d\lambda$, where Q_a is the absorption efficiency of the grain and B_λ Planck function. For small grains ($\leq 1\mu$m) a formula for the cooling rate (WAXMAN & DRAINE 2000) could be used

$$G \sim 3.1 \times 10^{-3} a_{0.1}^3 T_3^5 \Phi \text{ ergs s}^{-1}$$

A material dependent factor $\Phi \simeq 0.3$ for silicates and $\Phi \simeq 3$ for graphite.

The sublimation rate is thus rewritten as

$$\frac{da}{dt} = -n^{-1/3} \nu_0 \exp\left(-\frac{H}{kT}\right)$$

where ν_0 is the characteristic frequency and H is the binding energy per atom ($\nu_0 = 2 \times 10^{14} s^{-1}$ and $H = 1.1 \times 10^{-11}$ ergs for graphite, $\nu_0 = 10^{15} s^{-1}$ and $H = 0.94 \times 10^{-11} erg$ for silicates). We estimate graphite for all carbon grains. The sublimation is sensitive to the temperature.

Neglecting fluctuations due to absorption of individual energetic photons (important in very small grains), the grain temperature is determined by the heat balance equation (FRUCHTER ET AL. 2001)

$$\begin{aligned}\frac{dE_{therma}}{dt} = 3 \times 10^{-3} \frac{T_h A}{(2+\alpha) t_{10}} a_{0.1}^3 x^{1-\alpha} \\ \times [1 - (1 + x_{min}/x)^{-(2+\alpha)}] \\ -3.1 \times 10^{-3} a_{0.1}^3 T_3^5 \Phi \\ -2.7 \times 10^{10} a_{0.1}^2 n_{23}^{2/3} \nu_{15} H_{-11} \\ \times \exp(-72.5 H_{-11}/T_3) \text{ ergs s}^{-1}\end{aligned}$$

where the three terms on the right side correspond to the X-ray heating, radiative cooling and sublimation cooling. E_{therma} is the total thermal energy in the grain, T temperature. The radiation dominates at low temperature, sublimation at high. The temperature which divides these two regimes is

$$T_{eq} = 1000 \left[\frac{A T_h x^{1-\alpha}}{(2+\alpha)\Phi t_{10}}\right]^{1/5} \text{K}$$

where $|da/dt| > a/t$ for grain size a and X-ray emission duration t the grain is destroyed by sublimation during the burst. It appears approximately for

$$T_{eq} \geq T_{sub} = \frac{2360 H_{-11}}{1 - 0.033 \ln(a_{0.1} n_{23}^{1/3} \nu_{15}^{-1} t_{10}^{-1})} \text{K}$$

When T_{sub} is the critical temperature for sublimation. When comparing it to the previous equation it is clear that the flux is $\propto A/t_{10}$ and must be greater than A to completely sublimate most grains.

8.3.2 Charging and electrostatic shattering

An electron that escaped the grain leaves a positive charge behind. Even if the X-ray flux is too weak to evaporate grains along the LOS the grain could be thorn apart by electrostatic stresses greater than the tensile strength of the grains (WAXMAN & DRAIN 2000).

The rate of charging is the rate of photoionizations by photons of an energy high enough to escape the grain. I neglect the effect of Auger mechanism when a next electron is created.

$$R_{ion} \simeq 2.2 \times 10^6 \frac{AT_i(x_{min}, \alpha, N)}{3+\alpha} \frac{a_{0.1}^3}{t_{10}} x^{-\alpha} \times \left(\frac{1+x_{min}}{x}\right)^{-(3+\alpha)}$$

The T_i is almost like T_h but is proportional to the number of absorbed photons whereas the T_h is proportional to the energy of absorbed photons.

The grain temperature depends on the X-ray flux but the grain charge depends on the X-ray photon fluence (only 1 ultra energetic electron is useless).

The recombination rate is

$$R_{rec} \simeq 23 n_e a_{0.1} T_4^{-1/2} \left(\frac{Z_{grain}}{10^5}\right) \text{ s}^{-1}$$

However $R_{rec} \ll R_{ion}$.

The electric stress S created by the potential depends on the shape of the grains, as well as on the mobility of charges within the grain. Sharp corners will be loci of particularly large stress. The first order estimation is

$$S \equiv \frac{E^2}{4\pi} \sim \frac{(Z_{grain}e)^2}{4\pi a^4} = 1.8 \times 10^{10} \left(\frac{Z_{grain}}{10^5}\right)^2 a_{0.1}^{-4} \text{dyne cm}^{-2}$$

The grain with unflaved crystal structure could have tensile strength $S_{crit} \sim 10^{11}$ dyne cm^{-2}, less perfect and porous structures much smaller. (FRUCHTER ET AL. 2001) estimates that the grain survives only if

$$S_{crit} \geq 2 \times 10^{11} a_{0.1}^{-2/3} \text{dynecm}^{-2}$$

When charging is limited by electrostatic potential, the eventual charge if the grain is

$$Z_{grain} \simeq \begin{cases} [8 \times 10^{21} (1.4^{-5})^{-alpha} (\frac{\alpha+4}{\alpha+3}) AT_i a_{0.1}^{\alpha+6} x^3]^{1/(4+\alpha)} & \text{general } \alpha \\ 3.2 \times 10^5 (AT_i)^{1/4} a_{0.1}^{3/2} x^{3/2} & \alpha = 0 \\ 2.3 \times 10^5 (AT_i)^{1/5} a_{0.1}^{7} / 5 x^{3/5} & \alpha = 1 \end{cases}$$

The final stress is

$$S \simeq \begin{cases} 1.9 \times 10^{11} q_1(\alpha) (AT_i)^{2/(\alpha+4)} a_0^{-(4+2\alpha)/(4+\alpha)} x^{6/(\alpha+4)} & \text{general } \alpha \\ 1.9 \times 10^{11} (AT_i)^{1/2} a_{0.1}^{-1} x^{3/2} & \alpha = 0 \\ 1.0 \times 10^{11} (AT_i)^{2/5} a_{0.1}^{-6/5} x^{6/5} & \alpha = 1 \end{cases} \quad \text{dyne cm}^{-2}$$

where $q_1(\alpha) = [0.24^\alpha (3/4)^{(\alpha+4)/4} (\alpha+4)/(\alpha+3)]^{2/(\alpha+4)}$, $q_1(0) = 1$.

The transparency factors can be evaluated as

$$T_h \simeq \begin{cases} 1 & x_c < x \\ (x/x_c)^{2+\alpha-\delta} & \alpha = 1 \\ 0 & x_c > x + x_{min} \end{cases}$$

and

$$T_i \simeq \begin{cases} 1 & x_c < x + x_{min} \\ ((x_{min}+x)/x_c)^{3+\alpha-\delta} & x_c > x + x_{min} \end{cases}$$

if the soft X-ray opacity for photons of energy $0.5 \le x \le 5$ keV scales as $\propto x^{-3+\delta}$ where $\delta \simeq 0.4 - 0.6$ depends on the ionization state. x_c is the energy below which the ISM is optically thick but above which is the ISM transparent for X-rays.

The typical total column densities are $\sim 10^{21}$ cm^{-2}, however compact star-forming regions are 100 times denser. If the gas is neutral then the random lines of sight passing through giant molecular clouds or star-forming regions might have up to $x_c \simeq 3.4$.

8.4 The length of destroyed path

The maximum distance for dust evaporation by X-ray heating fulfill the condition

$$D_{100pc} \le 0.11 \times \left(\frac{CT_h x^{1-\alpha}}{(2+\alpha)\Phi t_{10} H_{-11}^5} \left(1 - 0.0326 \frac{a_{0.1} n_{23}^{1/3}}{\nu_{15} t_{10}} \right)^5 \right)^{1/2}$$

where

$$C \equiv E_{51}\sigma_{-19}n_{23} = D_{100pc}^2 A$$

So long the logarithm on the right hand side is small it can be simplified to

$$D_{100pc} \le 0.11 \left(\frac{CT_h x^{1-\alpha}}{(2+\alpha)\Phi t_{10} H_{-11}^5} \right) \left(\frac{a_{0.1} n_{23}^{1/3}}{\nu_{15} t_{10}} \right)^{-0.0815}$$

The characteristic $E_{51} \sim 1 - 10$, $t_{10} \sim 3 - 5$. Thus destruction distances in the range of $5 - 20$ pc are reasonable for this mechanism.

For X-ray charging the destruction distance is the smaller one of two cases: energy requirement for an electron to escape the grain is dominated by internal energy losses or by the electrostatic potential. An assumption made by (Fruchter et al 2001, Waxman & Drain 2000) is

$$D_{100pc} \le 1.2 \left(\frac{3}{3+\alpha} \right)^{1/2} 4^{-\alpha/2} \sqrt{CT_i} S_{crit,10}^{-1/4} a_{0.1}^{-1/2-\alpha/3} x^{3/2}$$

and for the case where electrostatic potential determines the minimum photon energy for charging they found

$$D_{100pc} \le 19 q_2(\alpha) \sqrt{CT_i} S_{crit,10}^{-1-\alpha/4} a_{0.1}^{-1-\alpha/2} x^{3/2}$$

where

$$q_2(\alpha) = 1.02^{\alpha}[(3/4)^{1+\alpha/4}(\alpha+4)/(\alpha+3)]^{1/2}$$

(WAXMAN & DRAINE 2000) obtained a destruction radius of

$$D_{100pc} \simeq 0.12\sqrt{\frac{L_{49}(1+0.1a_{0.1})}{a_{0.1}}}$$

8.5 Discussion and conclusion

The dust may be destroyed up to ~ 100 pc. This dust destruction can permit us to see the UV/optical afterglow even when the burst is deep within the dust region. The destruction depends on the size and on the composition of the grains. It may be possible to observe the amount and wavelength-dependence of the extinction change during the first minutes of the afterglow.

When the typical size of the molecular cloud in a star-forming regions is of $10-100$ pc it is obvious that reddening of only $A_V = 1.3$ (BURTON ET AL. 1992) as derived from the color indices (ŠIMON ET EL. 2001) is clearly understood through the dust destruction mechanism. The GRBs within the dense star-forming region could effectively destroy the dust of $n_{23} \sim 1-3$, thus only the bursts occurring from the cloud center to the boundary of ISM opposed from us could be hidden ($\sim 50\%$). This is in an agreement with the observational data. The existence of bubbles, shells and galactic disk worm tunnels (as mentioned in the previous chapter) make the direct prediction hard. Statistically more relevant is the variability in X-ray spectral index α that determines how much dust grains will be destroyed along the LOS. The variability of α is comparable to the variability of the intrinsic reddening of OAs.

In a case of multiphotometrical data from times very soon after the burst there could be an evidence for beaming as a case of ISM turbulence. The empty space after the swept and vaporized dust will be refilled by surrounding matter in the time proportional to the turbulence velocity. In the case of a very narrow jet this effect could be measurable. Thus the observation of the OAs in the later time of $t = t_0 + 10$ days would help to decide whether is this idea a right step. This sort of measurement will be available after the start of the INTEGRAL mission.

The calculation shown here is only a rough assumption to the reality. More effects (and non linear equations) should be included, e.g. absorption on molecules, atom and ions of different elements, line absorption (very important for e.g. H_2), the shape and the composition of the grains, solving the equation of the radiative transfer etc. The problem is too complex even for numerical modeling and more than 50 empirical parameters and parameters from quantum mechanics have to be included. The final solution is very sensitive on the exact values of the entire parameters. Thus the direct comparing of X-ray and optical absorption is extremely difficult and problematic.

Chapter 9

Gamma-ray bursts and cosmology

9.1 Estimation of the redshift of gamma-ray bursts

9.1.1 Introduction

The great debate of the distance to GRBs has been solved after the BeppoSAX mission started. There are only two ways how to measure a redshift of GRB events: directly from finding an absorption line, a break or a cut-off in spectrum of the GRB afterglow or semi-directly from spectrum of the host galaxy of the burst. There are 26 bursts with a known (or at least roughly estimated) redshift only of the total more than $\sim$ 2800 GRB detected. All these bursts are of the long-duration subclass.

9.1.2 Variability - luminosity - redshift correlation

I have suggested Cepheid-like empirical measurement of redshift vs time variability of GRB light curve correlation. Variability of the burst transformed from an observer frame and I would have examined the "spikiness" (variability) V_f and isotropic-equivalent peak luminosity L trying to find an empirical relation

$$logV_f(L) = \log V_{median} + b + m(\log L - \log L_{median})$$

where m the slope and b the intercept of the line.

This method was later probed by (Ramirez-Ruiz 2001) at a sample of GRBs from the 4B BATSE catalogue. This estimation is highly dependent on a method used in determining the variability. Since its publishing there were several modification of that where peak separation, peak width or peek steepness were used as the variability measure. Redshifts known from previous "classical" spectral analysis are used as a calibration of the model. The correctness of this method is hard to prove because of a very small sub-set of GRBs with apriori known redshift. The estimated deviation is more than 40%. I suggest further to test it on the sample of bursts with known redshifts, exclude a pair of them and try to fit the correlation. If the result is in agreement with the redshifts of the excluded bursts it can be considered as an evidence.

9.2 Cosmology Toolkit

As GRBs originate at high z at early stages of the Universe their reveal useful information about the distribution of intergalactic medium ionized by UV emission from GRB explosion from the first generation stars.

9.2.1 Gravitational lensing and microlensing in GRBs afterglows

The gravitational lensing, in which multiple image of astronomical sources can be produced as light is deflected around intervening massive objects due to the curved space-time geometry, has been recognized as a theoretical possibility since 1930s and as an observable fact since the early 1980s.

An object of mass M and radius R in LOS would even in Newtonian assumption bend the path of the light ray by an angle $\theta = \frac{4GM}{c^2R}$ or in non Euclidean geometry

$$\beta D_s = \frac{D_s}{D_d}\xi - \frac{2r_s}{\xi}D_s$$

where $r_s = \frac{2GM}{c^2}$ is the Schwarzschild radius of the deflector. In general at cosmological distance $D_{ds} \neq D_s - D_d$, α β are small $\theta D_d = \xi$ implies

$$\beta = \theta - \frac{2r_s D_{ds}}{D_d D_s}\theta^{-1}$$

while defining $\alpha_0 = \sqrt{\frac{2r_s D_{ds}}{D_d D_s}}$ we get $\xi_0 = \alpha_0 D_d$ and than quadratic equation

$$\theta^2 - \beta\theta - \alpha_0^2 = 0$$

has two roots, two possible locations of images whose angular separation would be $\delta\theta = \sqrt{4\alpha_0^2 + \beta^2}$. These images called Einstein rings are indeed observed.

The gravitational lensing of distant sources by intervening individual object, typically in the mass range from $10^{-4}M_\odot$ to $10^6 M_\odot$ such as a less massive star, a Jupiter size planet or a brown dwarf crossing the LOS that causes a rise in luminosity is called microlensing. That lasts for a few days to months.

The microlensing could help in weightening the entire Universe and so to probe the famous dark matter distribution. GRBs set to cosmological distances provides a tool for doing this.

A spherical GRB fireball appears on the sky as a thin ring that exhibits superluminal expansion at a speed γ_c, where γ is the Lorentz factor of the GRB shock.

The simplest microlensing model can be described by three parameters R_0, b, and W.

R_0 is the ring radius at $t = 1$ day in units of the Einstein radius of the lens. At other times the ring radius evolves as

$$R_S(t) = R_0 t^{5/8}$$

where $R_0 = \rho_0/r_E$ and

$$\rho_0 = 4 \times 10^{16} \left(\frac{E_{53}}{n_1}\right)^{1/8} (1 + z_S)^{-5/8}\, cm$$

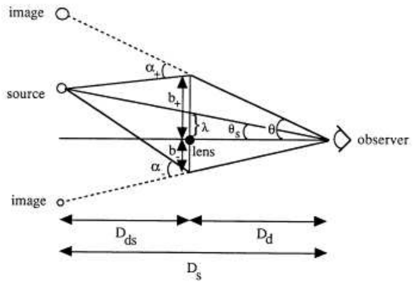

Figure 9.1: The gravitational lensing geometry (Kembhavi & Narlikar 1999)

where the factor involving the source redshift z is due to the cosmic time dilation. The Einstein radius of a lens of mass M_{lens}

$$r_E = \left(\frac{4GM_{lens}}{c^2}D\right)^{1/2} = 7.7 \times 10^{16}\left(\frac{M_{lens}}{1M_{\odot}}\right)^{1/2}\left(\frac{D}{10^{28}cm}\right)^{1/2} cm$$

where $D = (D_s D_{ds})/D_l$, b is the lens separation on the sky (impact parameter) in units of the Einstein angle $\theta_E = r_E/D_s$. If $R_s \ll b$ the source is point-like and is magnified by a time-independent factor. The maximum in the magnification curve is reached when $R_s \approx b$; the timing of this maximum can be used to fix the ratio R_0/b.

W is the brightness-weighted width of the ring divided by its radius. The width determines the height and the duration of the magnification event. The larger the width is, the smaller the height is and the broader the duration is. It's only an estimation with uncertainity of $\sim 10\%$ in optical or IR.

Because the gravitation affects light at all wavelengths an achromatic fluctuation in the light curve of GRB 0000301C occurred well before the power-law break, and so we assume that during the microlensing event the jet still behaves as a part of a spherical fireball.

Gravitational microlensing offers a way to study the structure of high-redshifted sources on micro-arcseconds scales. The declining light curve of the OA of GRB 000301C showed a rapid variability with one particularly bright feature at about $t - t_0 = 3.8$ days. This event was interpreted as gravitational microlensing (Koopmans & Wambsganss 2000). A posterior probability of a such microlensing for GRB 000301C at redshift $z = 2.04$ with an amplitude $\Delta m \geq 0.95$mag (as observed) is 0.7% (2.7%) in standard flat Λ-dominated cosmology model with $\Omega_m = 0.3$ and a fraction of dark matter $f_* = 0.2$ (1.0).

Note that this is the probability of microlensing in GRB afterglows if all compact objects in the universe are associated with observable galaxies. It is much smaller than the probabilty assuming other forms of the dark matter (e.g. so-called WIMPs - Weakly interacting mass particles).

As light travels a different path and due to a relativistic time dilation in a strong gravitational field the time delay between two detectable images is expected:

$$\delta t = \frac{R_S(1 + z_{lens})}{c}\left(\frac{f-1}{\sqrt{f}} - \ln f\right)$$

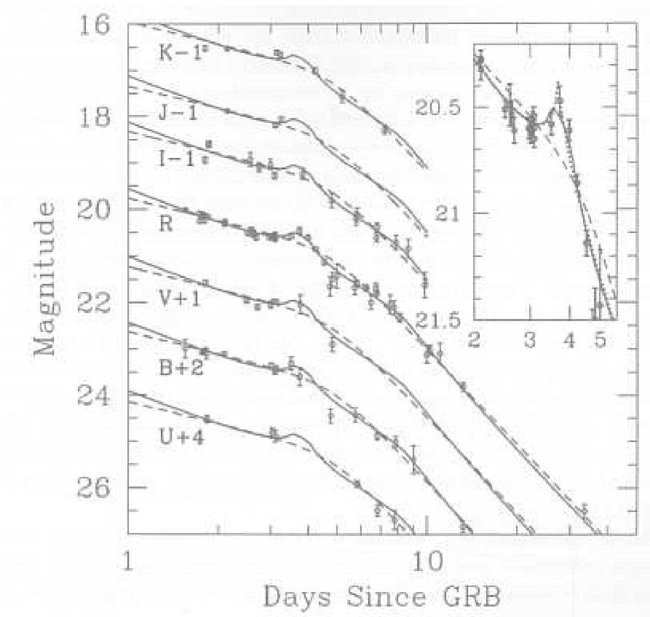

Figure 9.2: The multi-spectral light curve of GRB 000301C - the hottest candidate for the microlensing effect (Koopmans & Wambsganss 2000)

where f is the brightness ratio of the two images, z_{lens} the redshift of the lens and R_S the Schwarzschild radius ~ 3 km$(\frac{M}{M_\odot})$.

A point-like mass lens gives for the median value of the time delay $\delta t = 50\ \mathrm{s} \times (M/M_\odot)$ (Loeb & Perna 1998).

Searching for gravitational lensing in GRB light curves of the bursts from the 4B BATSE catalogue should be made in further work.

9.2.2 Lyman α forest

Quasars have been since their discovery used as a lighthouses probing Universe at high z Universe with z up to 6. Their spectra show strong metal emission lines because of rich medium. It suggests that in cores of galaxies there were supernovae and massive stars before the AGN activity.

If GRBs originate from the remnants of massive stars (such as neutron stars or black holes) then they exist at least out to the same redshifts as quasars. Hence, GRBs promise to be as useful as quasars in probing high-redshift universe. Not much is known about redshift interval $6-30$, when the first generation of galaxies condensed out of the primordial gas left over from the Big Bang. The observation of microwave background anisotropies indicate that a cosmic gas became neutral at $z \sim 1000$ and remained so at least down to $z \sim 30$.

Ly α resonance[1] in the spectrum of the highest redshift QSOs and galaxies indicates that intergalactic medium was reionized to more than 99.999% at redshift $z \sim 6$. This follows from the fact that the Ly α optical depth of the

[1] Ly α line occurs due to $2p \rightarrow 1s$ transition

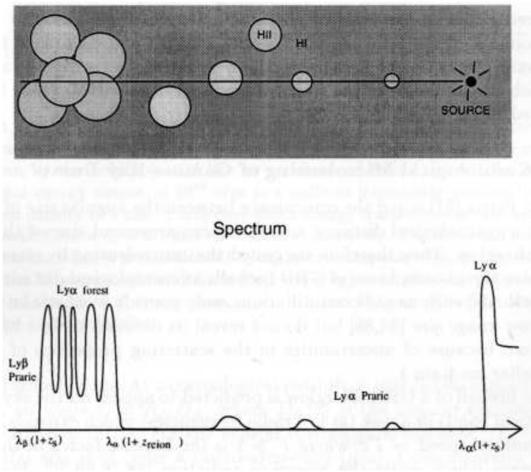

Figure 9.3: The Lyman forest sketch (LOEB 2001)

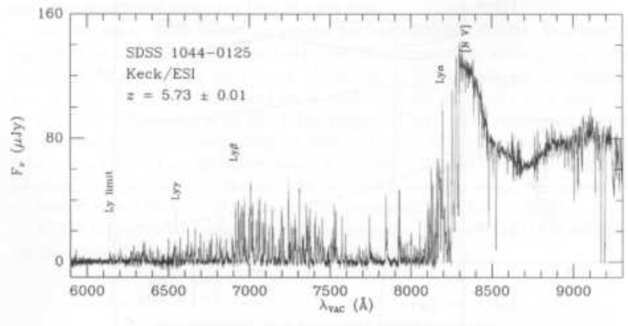

Figure 9.4: The spectrum of the QSO SDSS1044-0125 at z=5.73 (LOEB 2001)

IGM at $z \gg 1$ is

$$\tau_\alpha = \frac{\pi^2 f_\alpha \lambda_\alpha n_{HI}(z)}{m_e c H(z)} \approx 6.15 \times 10^5 x_{HI} \left(\frac{\Omega_b h}{0.03}\right) \left(\frac{\Omega_m}{0.3}\right)^{-1/2} \left(\frac{1+z}{10}\right)^{3/2}$$

where $H = 100h$ $\mathrm{kms^{-1}Mpc^{-1}}\Omega_m^{1/2}(1+z)^{3/2}$ is the Hubble parameter at source redshift z, $f_\alpha = 0.4162$ and $\lambda_\alpha = 1216A$ are the oscillator strength and the wavelength of Ly α transition (LOEB & PERNA 2000).

The UV spectrum of GRB afterglows can be used to probe the ionization and thermal state of the intergalactic gas during the epoch of reionization $z \sim 7-10$. Stretching the GRB light curves by cosmological redshift factor $(1+z)$ have to be considered. If GRBs result from compact stellar remnants (BH, NS) then the GRB rate may be higher at early cosmic times (GRB 980329 $z \sim 5$).

9.3 Gamma-ray burst rate

The dependence of the star forming rate on redshift z, the SFR plot, is conventionally determined by measurement in $H\alpha$ luminosity for $z < 0.2$ of galaxies or in UV for $z > 0.2$. However the amount and nature of ISM is unclear as the exact value of dust extinction. Also the stellar initial mass function IMF could be problematic to assume.

The coincidence between GRB 980425 and SN 1998bw and light curves of afterglows of e.g. GRB 980326 and GRB 970228 are consistent with SNe, for this reason it is believed that GRBs (at least those of long duration) track the star formation rate (SFR) in galaxies.

The GRB connection with deaths of massive stars means that the GRB rate should copy the already known star forming rate at lower redshift and eventually it is possible to estimate the rate in early stage of the universe at high redshift $z \geq 3$. The statistics of GRBs with known or constrained redshift is however poor. There are 22 such GRBs only.

Chapter 10

Conclusions

This work is an attempt to create a much more complete overview of the recent status of our understanding of GRBs as, at least to my knowledge, never done before. All the information on GRBs was split into hundreds sometimes very tiny pieces of information completely scattered in many journals and notices.

My attempt was not only to make a much more complete and up-to date overview but also to compare and to discuss various approaches and results suggested and published by various groups and to achieve a uniform view. This has included the comparison of the both theoretical models explaining the engine of GRBs, namely the fireball and the cannonball models. This was not, at least to my knowledge, done before.

I suggest new possible methods of observation which would eventually help to decide between the fireball and cannonball models.

According to my suggestions, the modeling of the accretion process at the GRB progenitors as well as of the search for the correlation between the hard X-ray radiation and the dust destruction could be possible with (unfortunately) non-public BeppoSAX data.

In correlations of GRBs with other extragalactic objects such as SNe, my new approach was to focus on physical approaches and analyses rather than on purely statistical methods used before. I suggest that this approach is much more relevant.

My study of colors of OAs of GRBs and those of QSOs and AGNs represents also a completely new approach with significant consequences for future optical searches including searches for orphan afterglows and also for physical understanding of faint blue objects found at positions of historical OTs detected on archival astronomical plates. I show that both more filters and time profiles of light curves are needed to distinguish reliably between a GRB OA and a QSO/AGN brightening.

I summarize pieces of evidence that GRBs originate in star-forming regions and I put several clues and implications which could be made in a further work. I put stress on the current effort of finding GRB remnants and on the observational evidence of such a correlation.

I discuss the dust destruction implications with respect to the behavior of color indices of OAs. The color analyses of OAs discussed in this work proved to be extremely important for establishing the physical nature of the environment of the sources. The study has indicated the importance for well organized and densely sampled optical observations of OAs in international color filters. Also the dense ond high quality optical data for later stages of the OAs light curves are extremely important since they can e.g. put constraints on the beaming (assuming dust destruction scenario and dust turbulence).

The dust destruction model is in agreement with the observational results of colors of OAs. More and better observational data are however required to find more evidence and to reveal more physical details. There is however still the possible alternative explanation of the clustering of color indices of OAs namely that the objects are not located in dense environments.

In the future it will be very interesting and valuable to carefully re-analyse the GRBs gravitational lensing and microlensing with respect to much better set of instruments on planned INTEGRAL and first of all Swift GRBs satellites. Searching for hidden dark matter along the path from the source of a GRB to us will be one of the aims of such study. Remember that 90% of the matter in the Universe is hidden but only a negligible fraction (if any) is closer than 1 kpc. The current assumption of probability of lensing seems to be understimated.

Also the studying of GRBs' remnants in the local Universe could bring a better understanding to GRBs, as well as better theoretical background for asymmetric SN explosions.

A qualitatively new results are expected from nearly finished gravitational waves detectors such are LIGO (LIGO WEB SITE)and LISA (LISA WEB SITE). This could prove or eliminate some of the suggested GRB progenitors.

The analyses of GRBs and related matter as described here are related to the Grant of the Grant Agency of the Academy of Sciences of the Czech Republic (No. IAA3003206), to the Grant of the Grant Agency of the Czech Republic No. 205/0145/99, and to the Project of the Ministry of the Education and Youth of the Czech Republic KONTAKT ES002. The work at the CNR Bologna described in chapter 6 was also supported by the collaborative project of the CNR and Academy of Sciences of the Czech Republic "Investigation of Gamma Ray Bursts".

Bibliography

Balberg and Shapiro 2001, ApJ, 556, 944-957
Barger et al. 2001, AJ 121, 662
Bethe, H.A. 1993, ApJ 419, 197
Blandford, R. D. and McKee, C. F. 1976, Physics of Fluids, 19, 1130
Blandford, R. D. and Znajek, R. 1977 MNRAS 179, 433
Bloom, J.S. 1998, ApJL 493, L27
Bloom, J.S. et al. 1999, Nature, 401, 453
Bloom, J.S., Kulkarni, S.R. and Djorgovski, S.G. 2001, astro-ph/0010176
Burton, W.B., Elmegreen, B.G., Genzel, R. 1992, The galactic interstellar medium, Springer-Verlag 1992
Chary, R., Becklin, E.E. and Armus, L. 1999, ApJ 566, 229
Cappellaro, E. and Turatto, M. 2000, Mem. Soc. Astron. Ital., 71, 411-427
Chevalier, R.A. and Li, Z.-Y. 1999, ApJ 520, L29
Chevalier, R.A. and Fransson, C. 2001, astro-ph/0110060
Contini, T. et al. 2001, astro-ph/0109396
Corbin, M., Urban, A., Stobie, E., Thompson, R. and Scheider, G. 2001 ApJ 551, 23
Costa, E. et al. 1997, IAUC, 6572, 273
Dado, S., Dar, A. and De Rjula, A. 2001, astro-ph/0107367
Dado, S., Dar, A. and De Rjula, A. 2002, astro-ph/0203315
Dalal, N., Griest, K. and Pruet, J. 2002, ApJ 564, 209-215
Dar, A., De Rujula, A. 2000a, astro-ph/0008474
Dar, A., De Rujula, A. 2000b, astro-ph/0012227
Djorgovski, S.G. et al. 2001, astro-ph/0106574
Draine and Lei Hao 2001, astro-ph/0108243
Ehlerová, S., Efremov, Yu.N. and Palouš, J. 1999, astro-ph/9908044, A&A 350, 457
Ehlerová, S. and Palouš, J. 2001, astro-ph/0105530
ESA 2000, The fourth Integral Workshop Sep 2000, Exploring gamma-ray universe
Fishman, G.J. 2000, astro-ph/0002168
Fishman, G.J. and Meegan, C.A. 1995, ARA&A 33, 415
Frail, D.A. et al. 1997, ApJL 483, L91
Frail, D.A., Kulkarni, S.R., Sari, R., Djorgovski, S.G., Bloom, J.S., Galama, T.J., Reichart, D.E., Berger, E., Harrison, F.A., Price, P.A., Yost, S.A., Dieckers, A., Goodrich, R.W. and Chaffee, F. 2001, ApJ 562, L55-L58
Fruchter, A.S., Krolik, J.H. and Rhoads, J.E. 2001, astro-ph/0106343, ApJ 563, 597

Gal-Yam, A. et al. 2002, astro-ph/0202354
Galama, T.J. 1998 Nature 395, 670, astro-ph/9806175
Galama, T.J. 1999, Ph.D. Thesis, Gamma-ray burst afterglows
Galama, T.J. and Wijers, R.A.M.J 2000, astro-ph/0009367
Gorosabel, J. 1999, Ph.D. thesis, GRB: The search for correlation
Gorosabel, J. 2001, astro-ph/0110007
Granot, J., Piran, T. and Sari, R. 1999, ApJ 513, 679
Granot, J., Piran, T. and Sari, R. 2000 ApJ 534, L163-L166
Greiner, J. 1999, Astronomy and Astrophysics Supplement, v.138, p.441-442
Groot, P.J. et al. 1997, IAUC, 6584, 1
Halpern et al. 2000, Science, Volume 290, Issue 5493, pp. 955-958
Hawking, S. 1976, Phys. Rev. D14, 2460
Hoflich. P, Khokhlov, A. and Wang, L. 2000, ApJ, 537, 810
Hornschemeier et al. 2001, ApJ 554, 742
Horváth, I. 1998, ApJ 508, 757
Hudec, R. et al. 1990, AA 235, 174
Hudec, R. 1999, AASuppl. 138, 593
Hudec, R., Hudcová, V. and Hroch, F. 1999, AASuppl. 138, 475
Hudec, R., Hroch, F. and Rezek, T. 1999, A&ASuppl. 138, 473
Hurley et al. 1999, ApJ 515, 497
Kembhavi , A.K. and Narlikar, J.V. 1999, Quasars and acitve galactic nuclei An introduction, Cambridge Univ. Press 1999
Kippen, R.M. et al. 1999, ApJ 515, 497
Klebesadel, R.W., Strong, I.B. and Olson, R.A. 1973, ApJ 182, L85
Klose, S. et al. 2000, astro-ph/0007201
Koopmans, L.V.E and Wambsganss, J. 2000, astro-ph/0011029
Kouveliotou, C. et al. 1993, ApJL 413, L101
Kouveliotou, C. et al. 1998, Nature, 393, 235-237
Kulkarni, S.R. 2000, astro-ph/0002168
Lamb, D.Q. 2001, American Astronomical Society Meeting 198, #35.11
Lamb, D.Q. and Reichart, D.E. 2000, ApJ, 538, 1
Lazzati, D., Covino, S. and G. Ghisellini 2000, astro-ph/0011443
Liebendoerfer et al. 2001, Physical Review D, vol. 63, Issue 10, id. 103004
Lee, M.G. 2000, astro-ph/0008285
Lehmann et al. 2001, A&A 371, 833
Levinson, A., Ofek, E., Waxman, E. and Gal-Yam, A. 2002, astro-ph/0203262
Loeb, A. 2001, astro-ph/0108432, astro-ph/0106455
Loeb, A. and Perna, R. 1998, ApJ 495, 597
Loeb, A. and Perna, R. 2000, ApJ 503:L35-L37
Longair, M.S. 1992, High energy astrophysics, Cambridge Univ. Press, 1992
Masetti, N. et al. 2000, A&A 364, L54-L61
Mazets, E. et al. 1997, astro-ph/9705128
Mészáros, A., Balasz, L.G, Horvath, I. and Vavrek, R. 2000, astro-ph/0003284
Mészáros, P. 1998, Bulletin of the American Astronomical Society, 30, 877
Mészáros, P. and Rees, M.J. 1993, ApJ 405, 278
Mászáros, P. and Rees, M.J. 1997, ApJ 476, 232
Mészáros, P. 2001, Science, 291, 79, astro-ph/0102225
Mezzacappa, A. 2000, Mem. Soc. Astron. Ital., 71, 515-537
Mirabel, I.F. 2000, astro-ph/0005591
Motch, Hudec and Christian 1990, A&A 235, 185

Mukherjee, S. et al. 1998, ApJ 508, 314
Norris, J. et al. 1995, Apj 439, 542
Paczyński, B. 1998, ApJ 494, L45
Paczyński, B. 1999, astro-ph/9909048
Peebles, J.E. 1997, Principles of Physical Cosmology, Princeton Univ Press, 1997
Perna, R., Raymond, J. and Loeb, A. 2000, ApJ 533:658-669, 2000
Phinney, E.S. 1991, ApJ 380, L17-L21
Piran, T. and Granot J. 2001, astro-ph/0107009
Piran, T. 1999, Phys. Rep. 314, 575, astro-ph/9810256, astro-ph/9907392
Piro et al. 2000, Science, 290, 955
Predehl and Schmitt 1995 A&A V. 293 p. 889
Press, W.H., Teukolsky, S.A., Vetterling, W.T., Flannery, B.P., Numerical recipes in C, Camdridge Univ. Press 1993
Ramirez-Ruiz, E., Fenimore, E.E. and Trentham, N. 2000, astro-ph/0010588
Ramireze-Ruiz, E., Trentham, N. and Blain, A.W. 2001, astro-ph/0103239
Ramirez-Ruiz, E., Lazzati, D. and Blain, A.W. 2002, ApJ 565: L9-L12
Rees, M.J. 1997, astro-ph/9701162
Reichart, D.E. and Price, P.A. 2002, ApJ 565, 174
Rhoads, J.E. 1997, ApJL 487, L1
Rhoads, J.E. 1999, ApJ, 525, 737
Rhoads, J.E. and Fruchter 2000, GCN 586
Rhoads, J.E. 2001, ApJ, 557, 943-948
Saha, A. et al. 1997, Conference Paper, Space Telescope Science Institute Series, The Extragalactic Distance Scale (Cambridge University Press)
Sari, R. and Piran, T. 1999a, A&AS 138, 537
Sari, R. and Piran, T. 1999b, ApJ 520, 641
Sari, R., Piran, T. and Narayan, R. 1996 ApJ 473, 204
Sari, R., Piran, T. and Narayan, R. 1998, ApJL, 497, L17
Sari, R., Piran, T. and Halpern, J.P. 1999, ApJL, 519, L17
Schmidt, B. 2000, IAUC, 7516, 1
Schmidt, M. 1968, ApJ 151, 393
Schmidt, M. 2001, ApJ, 552, 36-41
Stanek et al. 1999, ApJ 522, L39-L42
Schreier et al. 2001, ApJ 560, 127
Soderberg, A., Ramirez-Ruiz, E. 2002, astro-ph/0203241
Šimon et al. 2001, astro-ph/0108416, Astronomy and Astrophysics, 377, 450
Tsvetkov, D.Yu., Blinikov, S.I. and Pavlyuk, N.N. 2000, Astronomy Letters, 27, 411
van Paradijs et al. 1997 et al., Nature, 386, 686
Venemans, B.P. and Blain, A.W. 2001, astro-ph/0104169
Veron-Cetty, M.-P. and Veron, P. 1996, ESO Scientific Report, A Catalogue of quasars and active nuclei
Veron-Cetty, M.-P. and Veron, P. 2001, A&A 374, 92
Vrba, F. et al. 1994, ApJ, 424, 68
Vrba, F. et al. 1999, ApJ, 511, 298-303
Vietri, M. 1995, ApJ 453, 883
Vietri, M. and Stella, L. 1998, ApJL, 507, L45
Vietri, M. and Stella, L. 1999, The ApJ 527, L43-L46
Wallerstein et al. 1997, Rev. Modern Phys., 69, 995-1084 (1997)

Waxman, E., Frail, D.A. and Kulkarni, S. R. 1998, ApJ 497, 288
Waxman, E. & Draine, B.T. 2000, ApJ 537, 796
Waxman, E., Kulkarni, S.R. and Frail, D.A. 1998, ApJ 497, 288
Weiler and Panagia 1978, A&A 70, 419
Weinberg, S. 1972, Gravitation and Cosmology : Principles and Applications of the General Theory of Relativity, John Wiley & Sons 1972
Wheeler, J.C., Hflich, P. and Wang, L. 1999, astro-ph/9904047
Woosley & MacFayden 1999, ApJ, 524, 262

Gamma-ray bursts on the web

`http://lascaux.asu.cas.cz` BART web page
`http://www.batse.msfc.nasa.gov/batse` BATSE web site
`http://www.ifa.au.dk/ hst/grb_hosts/intro.html` Host Galaxies of GRBs - Bloom web site
`http://cdsweb.u-strasbg.fr` CDS Strasbourg web site
`http://chandra.harvard.edu` Chandra X-ray Observatory Center
`http://gcn.gsfc.nasa.gov/gcn/gcn3_archive.html` GCN Circulars Archive
`http://www.aip.de/ jcg/grbgen.html` Greiner GRB web site
`http://space.mit.edu/HETE` HETE-2 page
`http://stci.edu` Hubble space telescope
`http://cfa-www.harvard.edu/cfa/ps/cbat.html` IAU: Central Bureau for Astronomical Telegrams
`http://cfa-www.harvard.edu/iau/lists/Supernovae.html` IAU SN catalogue
`http://astro.estec.esa.nl/SA-general/Projects/Integral/` INTEGRAL mission web site
`http://ssl.berkeley.edu/ipn3/` IPN web site
`http://www.src.le.ac.uk/lobster/lobster.html` The Lobster Eye X-Ray Telescope web site
`http://www.ligo.caltech.edu/` LIGO detector
`http://lisa.jpl.nasa.gov/` LISA detector
`http://rsd-www.nrl.navy.mil/7212/montes/sne.html` List of SN pages
`http://ngst.gsfc.nasa.gov/` Next Generation Space Telescope
`http://merlino.pd.astro.it/ supern/snean.txt` Padova/Asiago SN catalogue
`htpp://heasarc.gsfc.nasa.gov/docs/xte/xte_1st.html` RXTE web site
`http://www.sai.msu.su/sn` SAI SN Research Group
`http://www.sciencemag.org` Science web site
`http://www.swift.psu.edu/` Swift satellite
`http://heasarc.gsfc.nasa.gov/W3Browse/all/veron2001.html` Veron 2001 QSOs and AGNs catalogue
`http://sci.esa.int/home/xeus/index.cfm` XEUS web site
`http://xmm.vilspa.esa.es/` XMM Newton satellite